FABRICATION AND EVALUATION OF PORCINE CHOLECYSTIC EXTRACELLULAR MATRIX SCAFFOLD FOR CARDIAC TISSUE ENGINEERING

RESHMA S.

Ph.D. THESIS

2020

SREE CHITRA TIRUNAL INSTITUTE

FOR MEDICAL SCIENCES AND TECHNOLOGY

THIRUVANANTHAPURAM

FABRICATION AND EVALUATION OF PORCINE CHOLECYSTIC EXTRACELLULAR MATRIX SCAFFOLD FOR CARDIAC TISSUE ENGINEERING

A THESIS PRESENTED BY

RESHMA S.

TO

SREE CHITRA TIRUNAL INSTITUTE

FOR MEDICAL SCIENCES AND TECHNOLOGY

THIRUVANANTHAPURAM

IN PARTIAL FULFILMENT OF THE REQUIREMENTS

FOR THE AWARD OF

DOCTOR OF PHILOSOPHY

2020

DECLARATION

I, Reshma S., hereby certify that I had personally carried out the work depicted in the thesis titled: ***"Fabrication and evaluation of porcine cholecystic extracellular matrix scaffold for cardiac tissue engineering"*** except where due acknowledgement has been made in the text. No part of the thesis has been submitted for the award of any other degree or diploma prior to this date.

Date: *Reshma S.*

Reg. No: 2014/PHD/17

SREE CHITRA TIRUNAL INSTITUTE FOR MEDICAL SCIENCES & TECHNOLOGY, TRIVANDRUM
Thiruvananthapuram – 695011, INDIA
(An Institute of National Importance under Govt. of India)
Phone-(91)0471-2520282 Fax-(91)0471-2341814
Email: tvanilkumar@sctimst.ac.in Web site – www.sctimst.ac.in

CERTIFICATE

This is to certify that **Ms. Reshma S.**, in the Division of Experimental Pathology of this institute has fulfilled the requirements prescribed for the Ph. D. degree of the Sree Chitra Tirunal Institute for Medical Sciences and Technology, ***"Fabrication and evaluation of porcine cholecystic extracellular matrix scaffold for cardiac tissue engineering"*** Thiruvananthapuram. The thesis entitled, was carried out under my direct supervision. No part of the thesis was submitted for the award of any degree or diploma prior to this date.

* Clearance was obtained from the Institutional Animal Ethics Committee and Institutional Committee for Stem Cell Research and Therapy for carrying out the study.

Thiruvananthapuram

Dr. TV Anilkumar, MVSc, PhD, FRCPath

(Research Supervisor)

Scientist G & Head
Division of Experimental Pathology
BMT wing, SCTIMST
Thiruvananthapuram

The thesis entitled

FABRICATION AND EVALUATION OF PORCINE CHOLECYSTIC EXTRACELLULAR MATRIX SCAFFOLD FOR CARDIAC TISSUE ENGINEERING

Submitted by

RESHMA S.

for the degree of

Doctor of Philosophy

of

SREE CHITRA TIRUNAL INSTITUTE
FOR
MEDICAL SCIENCES AND TECHNOLOGY
THIRUVANANTHAPURAM

is evaluated and approved by

16/12/2020

Dr. T. V. Anilkumar
(Research Supervisor)

Examiner

Dedicated to my family,

teachers & friends…

ACKNOWLEDGEMENTS

I would like to express my deepest gratitude and respect to my research supervisor Dr. T. V. Anilkumar, for his wise guidance and continuous encouragement throughout the course of this thesis. I thank him for his innovative ideas, critical analysis, detailed discussions and encouragement during the entire study. I am very much fortunate to have a great teacher as my PhD guide.

I am extremely grateful to my doctoral advisory committee, Dr.R. Renuka Nair, Dr. T. V. Kumary, Dr. Prabha D. Nair and Dr. R. S. Jayasree for their suggestions, comments and support right from the beginning of the work.

I convey my thanks to the Director, SCTIMST and the Head, BMT Wing, SCTIMST for all the facilities provided during the course of my work.

I wish to thank the Director, RGCB for providing the facilities to perform electrocardiography and echocardiography.

I am thankful to the Registrar, the Dean, the Associate Dean (Ph. D.), staffs of academic division, staffs of accounts, library, Computer division, Stores and purchase- BMT Wing for their help.

I am greatly indebted to the Department of Science and Technology, INSPIRE, Govt. of India for the PhD fellowship and Department of Biotechnology, Govt. of India for the international travel fellowship.

I express my whole hearted gratitude to Dr. Praveen K. S., who was constant support and motivator throughout my research work. He lend a hand in collaborating with RCGB for the completion of animal studies. He trained me for some of the experiments, shared his reagents and equipments for my study. He was always ready to help me whenever I approached him. His project staff, Ms. Aswathy M. R. also needs special mention. She helped me in cell culture studies and western blot. I thank her for the sincere dedication and friendship.

I am extremely thankful to Dr. Sachin J. Shenoy who performed the animal surgery and care. His patience and dedication was a great inspiration for me. I also thank Dr. V. S. Harikrishnan, Mr. Sarath, Mr. Manoj, Mr. Sunil and all members, Division of Laboratory Animal Science for their help during animal experiments.

I am thankful to Mr. Lijikumar G., Medical Illustration for taking quality images of the animal surgery.

I would like extend my regards to Dr. Mukund A. Prabhu, Department of Cardiology, SCTIMST for interpreting the electrocardiography and echocardiography data.

I thank Dr. Santhosh Kumar, Dr. Surya Ramachandran Dr. Vikas Kumar, Mr. Jithin, RGCB for electrocardiography and echocardiography analysis.

I wish to convey my thanks to Dr. Sujatha, Mr. Rishad, NIIST for 4-Point probe measurments.

I thank Dr. Anilkumar P. R. and Mr. Vinod for helping me in Fluorescent microscopy, Dr. Balu V. Gopal for training tissue culture, Dr. Kalliyanana Krishnan, Dr. Vibha for Dynamic light scattering, Dr. Rekha M. R. for Dynamic light scattering and her lab members Dr. Priya, Dr. Caroline, Ms Dhanya, Ms Rajalekshmi, Ms. Nayana and Ms. Annie for their friendship.

I also thank Dr. Roy Joseph, Dr. Radha Kumari, Mr. Willi Paul for Thermogravimetry and Luminiscent imaging, Dr. Anoop Kumar and his lab members for Nanodrop facility, all members of Bioceramic laboratory helping me in SEM, TEM and OES-ICP analysis, Er. Leena Mr. Rajesh for Profilometry, Dr. Anugya Bhat for flow cytometry, Dr. Sabareeswaran and lab members for Tissue processor and Nikon microscope, Dr. Prabha D. Nair and her lab members for UV Vis spectrophotometer, Fluorescent microscope & Plate Reader.

I am extremely thankful to the members of the Division of Experimental Pathology: Dr Geetha C.S., Dr. Akhila Rajan, Dr. Deepa R., Dr. Jaseer Muhamed, Ms. Jimna Mohamed Ameer, Dr. Karthika S, Dr. Lekshmi Chandran, Dr. Purnima C., Ms. Manjula P. M., Ms Reshmi Raj, Mr. Pratheesh K.V., for their help, support, encouragement and friendship.

Thanks to all my friends inside and outside SCTIMST for their help and friendship. Special mention to my best friend and well-wisher Ms. Chinchu M. Raj for her prayers and support.

I owe my family a debt of gratitude for all their support over the years. I extend my heartfelt regards to my beloved grandmother, father, mother, brother and in laws for their constant encouragement, prayers, love and care. I would also like to express

love to my niece, Dheksha. Heartfelt thanks to my husband Mr. Mahesh V. R. for his help, patience, encouragement and love. I greatly value his contribution in completing my thesis. My thesis acknowledgement would be incomplete without thanking my little daughter, Mydhili, whose smiling face always made me cheerful and enthusiastic.

I bow before Almighty God for showering blessings and giving me the strength, knowledge, health and opportunity to undertake this research study and to persevere and complete it satisfactorily.

Reshma S.

TABLE OF CONTENTS

LIST OF FIGURES

LIST OF TABLES

ABBREVIATIONS

AuNP	Gold nanoparticles
BSA	Bovine serum albumin
C-ECM AuNP	Gold nanoparticle incorporated C-ECM
C-ECM	Cholecystic extracellular matrix
CK	Creatine kinase
CK-MB	Creatine kinase muscle/brain
Dmaj	Major cell diameter
DMEM	Dulbecco’s Modified Eagle's Medium
Dmin	Minor cell diameter
ECG	Electrocardiography
ECHO	Echocardiography
ECM	Extracellular matrix
EDC	Ethyl-3-(3-dimethylaminopropyl)-carbodiimide
EF	Ejection fraction
ESEM	Environmental scanning electron microscopy
FBS	Fetal Bovine Serum
FDA	Fluorescein diacetate
FS	Fractional shorteing
FTIR	Fourier transform infrared spectroscopy
$HAuCl_4$	Tetrachloroauric acid
HE	Haematoxylin and eosin
HRP	Horse radish peroxidase
IVSs	End-systolic septum thickness
IVSd	End-diastolic septum thickness
LVIDd	Left ventricular end diastolic internal diameter
LVIDs	Left ventricular internal dimension at end systole
LVPWd	Left ventricular end-diastolic posterior wall thickness
LVPWs	Left ventricular posterior wall thickness at end systole
MI	Myocardial infarction
MT	Masson’s trichrome

MTT	(3-(4,5-dimethylthiazol-2-yl)-2,5)-diphenyltetrazolium
$Na_3C_6H_5O_7$	Tri sodium citrate
NBF	Neutral buffered formalin
NHS	N-hydroxysuccinimide
OES-ICP	Optical Emission Spectroscopy with Inductively Coupled Plasma
PBS	Phosphate buffered saline
PI	Propidium iodide
PVDF	Polyvinylidene difluoride
rBMSCs	Rat bone marrow mesenchymal stem cells
SDS-PAGE	Sodium dodecyl sulfate polyacrylamide gel electrophoresis
TBST	Tris Buffer Saline -Tween
TNBS	Picryl sulfonic acid or 2,4,6-Trinitrobenzenesulfonic acid
Trop T	Troponin T

SYNOPSIS

Coronary heart disease is referred to as a condition that includes constricted or blocked blood vessels leading to ischemia/hypoxia resulting in infarction or heart attack. About 50% of the deaths due to cardiovascular diseases were contributed by coronary heart disease. All the treatment strategies for heart diseases have been focused on guarding the diseased heart from progression to heart failure. Revascularization by thrombolysis, cardiac intervention, and bypass surgery help to improve blood supply and can rescue the injured myocardium. In contrast to these cardioprotective therapies that target ischemia in the failing heart, only limited therapies are available for preventing end-stage heart failure. Thus, biomaterials have gained attention in cardiac repair, for their ability to serve as a matrix to improve cell survival and behaviour, as well as to act as a reservoir for sustained local delivery of therapeutic factors. The use of animal-derived biological tissues as scaffolds for cardiac tissue engineering has been sought by several research groups. Indeed, CorMatrix® made of porcine small intestinal submucosa has gained popularity in the cardiovascular field, but the limited market availability and high cost diminished its usage in India.

Porcine cholecystic extracellular matrix (C-ECM) is a relatively new collagen-rich biomaterial with a mesh-like architecture. It was originally intended as a buttress material for staple line reinforcement. Later, the research works conducted using C-ECM proved that the material has excellent skin wound healing property in rabbits, rats and dogs. Extensive refinement in the method of preparation of C-ECM from porcine cholecyst without the use of any harsh chemicals or enzymes commonly used for decellularisation resulted in an extracellular matrix scaffold suitable for various tissue engineering applications. In this background, this study hypothesized that C-ECM prepared by a non-enzymatic/detergent method is a suitable scaffold for fabricating cardiac-patch. The study also deals with the modification of C-ECM with gold nanoparticles to enhance the conductive property of the material. To test the hypothesis, the pristine scaffold and a modified form of the scaffold fabricated from C-ECM incorporated with gold nanoparticles (C-ECM AuNP) were used as potential cardiac-patches. Both *in vitro* and *in vivo* effects of the scaffolds were evaluated. The

data collected will be presented in the proposed thesis with six chapters.

The first chapter will be the introduction which includes the background and the objectives of the study. The main objectives are the following:

I. Evaluation of the properties of porcine cholecystic extracellular matrix scaffold and its suitable modifications for cardiac tissue engineering
II. Differentiation of rat cardiomyoblast cell line H9c2 and rat bone marrow mesenchymal stem cells to cardiomyocyte-like cells
III. Functional evaluation of the cardiac patches in a rat model of non-fatal myocardial infarction

The second chapter will be a review of literature that elaborates relevant and related research outcomes in the area of cardiac tissue engineering with brief information about the heart, embryology, anatomy and physiology.

The third chapter will be the materials and methods section which describes the methodologies adopted for acquiring the results. The first part of the section includes preliminary tests for evaluating the cytocompatibility of C-ECM, such as direct contact test, live dead staining and (3-(4,5-dimethylthiazol-2-yl)-2,5)-diphenyltetrazolium (MTT) assay. The *in vivo* effect of the C-ECM was evaluated in a suitable animal model for myocardial infarction. The animal model was established by surgical ligation of the left anterior descending coronary artery and the C-ECM was implanted as an epicardial graft. The following section deals with the method for the modification of C-ECM to enhance conductivity. For that gold nanoparticles were synthesised and characterised by the following methods such as UV-Vis spectrophotometry, transmission electron microscopy, and dynamic light scattering. After incorporation of gold nanoparticles to the C-ECM, it was characterised by surface profilometry, scanning electron microscopy, energy-dispersive x-ray spectroscopy, 4-point probe method for conductivity, 2,4,6-trinitrobenzene sulfonic acid assay for estimation of free amino groups, Fourier-transform infrared spectroscopy for determination of functional groups, thermogravimetric analysis for thermal stability and degradation assay. Biological characterisation of the C-ECM AuNP was achieved by direct contact test, live dead staining and MTT assay.

The next section deals with the differentiation of cardiomyoblast cells H9c2 and rat bone marrow-derived mesenchymal stem cells (rBMSCs) to cardiomyocyte-like cells. The differentiation of H9c2 cells to cardiomyocyte-like cells in the presence of retinoic acid was studied using phase contrast microscopy, cytoskeleton staining and western blot for cardiac proteins such as troponin T, myo D and connexin 43. Rat bone marrow-derived mesenchymal stem cells were isolated and characterised using phase contrast microscopy, immunostaining for positive marker, flow cytometry and multilineage differentiation. Similarly, the differentiation of rBMSCs was studied by phase contrast microscopy and western blot for cardiac proteins.

For the functional evaluation of the cardiac patches, the C-ECM and C-ECM AuNP scaffolds were implanted in a rat model of myocardial infarction as epicardial grafts and evaluated by serum biochemistry, electrocardiography, echocardiography, and histology. Histological evaluation was carried out by haematoxylin and eosin staining, Masson's trichrome staining, picro sirius red staining, Herovici's staining and immunohistochemistry for CD4 (helper T lymphocytes), CD8 (cytotoxic T lymphocytes), CD68 (macrophages), α-smooth muscle actin (smooth muscle cells and myofibroblasts), CD31 (endothelial cells), proliferating cell nuclear antigen (proliferating cells) and connexin 43 (cardiomyocytes). Morphometry was used for the quantification of various parameters like right ventricular area, left ventricular area, interventricular septal area, infarct area, diameter of cardiomyocytes, number of cardiomyocytes and the number of positively stained cells from immunohistochemistry.

The fourth chapter will elaborate on the results of the study. From the preliminary studies conducted on the pristine C-ECM, it was observed that C-ECM provided a suitable substrate for the growth of H9c2 cells. Further, an animal model for MI was established and the C-ECM was implanted as an epicardial graft. Moreover, the conjugation of functionalised gold nanoparticles to porcine C-ECM was possible and the modified C-ECM AuNP was a potential conductive biomaterial for cardiac tissue engineering. H9c2 cells and rBMSCs were cultured and differentiated to cardiomyocyte-like cells, established with the expression of cardiac proteins like trop T, myo D, connexin 43. The results of the *in vivo* evaluation of C-ECM and C-ECM AuNP in MI model indicated reduction in the deposition of total collagen in the grafted

animals. Also, there was relative abundance of degradable reticular type III over type I collagen as quantified from Herovici's stained sections. Immunohistochemistry for proliferating cell nuclear antigen indicated increased cell proliferation in the presence of both the grafts. Enhanced angiogenesis was observed in the grafted animals by immunohistochemistry for α- smooth muscle actin and CD31. A favourable graft acceptance reaction was observed after immunohistochemistry for CD4 and CD8.

The fifth chapter will be a discussion of the results that explains the implications of the study. The study indicated that the porcine C-ECM and the C-ECM AuNP are suitable scaffolds for cardiac tissue engineering application as evidenced by the *in vitro* and *in vivo* experiments.

The sixth chapter will be the summary and conclusion. In short, with the incorporation of gold nanoparticles to C-ECM, conductivity was improved making it suitable for cardiac tissue engineering. Both these scaffolds were found to be compatible with H9c2 cells and rBMSCs. When porcine C-ECM and C-ECM AuNP were used as an epicardial graft in a rat model of MI, there was reduction in cardiac fibrosis by the delayed deposition of type I collagen, increased angiogenesis and enhanced cell proliferation were observed. It was revealed that C-ECM and C-ECM AuNP scaffolds can mitigate cardiac remodelling process. As an epicardial graft, C-ECM and C-ECM AuNP can be used as an adjunct to any current treatment strategies. Thus, the porcine cholecystic extracellular matrix prepared by the non-enzymatic/detergent method is a potential biomaterial for fabricating cardiac patches.

1. INTRODUCTION

The heart is the first organ to start functioning in humans at about three weeks of gestation and it is also the last organ remaining functional, until death (Radisic, 2015). It is a continuously working muscular pump, contracting on average 80 times per minute to push 6000-7500 liters of blood through body tissues daily (Tzahor & Poss, 2017). The heart functions by pumping blood out from the left chambers to all the tissues through arteries and blood containing waste products are taken back to the right chambers through veins. This strenuous activity is controlled by specialized cells in the heart muscle named cardiomyocytes having the ability to contract in response to electrical stimulation. Mammalian cardiomyocytes exit the cell-cycle to make the heart the most stable organ, with a rare chance of cardiac tumor, but relentlessly disturbs the repair process after muscle injury (Mohamed *et al*, 2018; Sadek & Olson, 2020). Due to the limited regenerative capacity of mammalian cardiomyocytes, the repair process leads to scar formation and the irreversible events finally result in cardiac failure.

Cardiovascular diseases (CVDs) are the leading cause of deaths occurring globally. About 17.9 million people died from CVDs in 2019, which contributed to 31% of all global deaths. CVDs include coronary heart disease, stroke, hypertensive heart disease, inflammatory heart disease and rheumatic heart disease. Among these deaths, nearly 7.4 million were due to coronary heart disease (*Cardiovascular diseases (CVDs, WHO 2017*). It is generally referred to as conditions that include constriction or blockage of blood vessels leading to myocardial infarction or heart attack, angina or stroke (*Heart disease - Symptoms and causes - Mayo Clinic*). The blockage of the artery is mainly due to atherosclerosis, accumulation of cholesterol or any fatty deposits.

All the current treatment strategies focus on protecting the heart from progression to heart failure. Revascularization by thrombolysis, cardiac intervention, and bypass surgery help to improve blood supply and can rescue the injured myocardium. Pharmacological approaches that slow or reverse cardiac remodelling, such as angiotensin-converting enzyme inhibitors, angiotensin receptor–neprilysin

inhibitors, β- blockers, and mineralocorticoid- receptor antagonists, have decreased heart failure mortality. In contrast to these cardioprotective therapies that target the remodelling process in the failing heart, limited therapies are available for the advanced remodelled heart at end-stage heart failure. Mechanical support therapies, such as left ventricular assist devices (LVADs) and cardiac resynchronization therapy, show beneficial outcomes in patients with end-stage heart failure, but for them, cardiac function can be re-established by heart transplantation which is the gold standard in cardiac treatment (Wilhelm 2015). But then, there are many limitations including the lack of donors, the problem of rejection, cardiac allograft vasculopathy, chronic kidney disease, graft dysfunction, infection and malignancies (Alba *et al*, 2016). So there is a huge demand for other strategies to reduce the risk of ischemic heart diseases by promising technologies. With the evidence of the transient regenerative capacity of the neonatal mouse heart, studies have been focused on the reactivation of pre-existing cardiomyocytes for proliferation after cardiac injury or activation of resident stem cell population which can give rise to new cardiomyocytes (He & Zhou, 2017). First-generation cell-based therapies involved the use of non-cardiac cells such as skeletal myoblasts, bone marrow-derived cells and mesenchymal stem cells. But the long-term follow-up studies did not show beneficial and consistent clinical results. Thus, other therapies were explored including the use of cardiac stem cells, pluripotent stem cells, secretory factors, growth factors, microRNAs, exosomes, direct reprogramming of various cells into cardiomyocytes, targeting fibrotic response or stimulating endogenous cardiac repair process (Hashimoto *et al*, 2018).

Biomaterials have been used in cardiac repair for their ability to serve as a matrix to improve cell survival and behaviour, as well as to protect the therapeutic factors from degradation and to act as a reservoir for its sustained local delivery. Biomaterial based delivery systems thus provide a scaffold to improve the therapeutic effects of both cellular and non-cellular approaches. With the principles of tissue engineering, myocardial patches, sheets and 3D heart tissues mimicking the native heart structure has been designed. Engineered heart tissues can be directly transplanted to the damaged heart and have been shown to improve therapeutic outcomes (Hashimoto *et al*, 2018). Natural and synthetic scaffolds are used for cardiac tissue

engineering, including their hydrogel forms with cells for easy delivery to the damaged site (Reis *et al*, 2016). Indeed, hydrogels prepared from collagen, gelatin, Matrigel, alginate, fibrin, poly(2-hydroxyethyl methacrylate), poly(N-isopropylacrylamide) and poly(ethylene glycol) have a lot of contemporary medical use (Camci-Unal *et al*, 2014).

In addition, conductive biomaterials are emerging as a promising strategy to repair infarcted myocardium and to improve cardiac function. Electrical conduction is important for the heart muscles to contract. Therefore, engineered cardiac tissues with conductive materials are gaining more attention in the field of cardiac tissue engineering. Scaffolds developed using conductive biomaterials may restore the electrophysiological function of a damaged heart. Some of the conductive materials used are carbon-based nanomaterials (graphene) (Saravanan *et al*, 2018) and carbon nanotubes (CNTs) (Kitsara *et al*, 2017), metal derived materials (gold nanoparticle) (Nair *et al*, 2017) and conductive polymers (polyaniline, polythiophene and polypyrrole) (Ye & Qiu, 2017).

Porcine cholecystic extracellular matrix (C-ECM) is a relatively new biomaterial with a mesh-like architecture prepared from gall bladder (Burugapalli *et al*, 2007) intended as a buttress material for staple line reinforcement (Burugapalli *et al*, 2008) abounding in collagen and growth factors such as VEGF and bFGF (Anilkumar *et al*, 2014). A refined method for the preparation of C-ECM by a non-detergent/ non-enzymatic method with controlled crosslinking (Mony & Anilkumar, 2019) was proposed. This xenogeneic biomaterial has excellent wound healing property in rabbits (Revi *et al*, 2013) and dogs (Karthika *et al*, 2018). Recent studies on the subcutaneous implantation of C-ECM have shown lesser immunogenicity and higher graft acceptance reaction compared to other grafts from xenogeneic origin (Muhamed *et al*., 2015 a, Muhamed *et al*., 2015 b & Muhamed *et al*., 2017). It has been used as a urinary bladder repair graft (Kajbafzadeh *et al*, 2014), corneal graft (Anoop *et al*., 2017) and hernia repair graft (Balakrishnan-nair *et al*, 2018). Recently, the sheet form of C-ECM was comminuted to powder forms to increase the flexibility in terms of delivery (Raj *et al*, 2018).

With this background, this thesis hypothesises that the porcine cholecyst derived extracellular matrix is a suitable scaffold for fabricating cardiac-patch. To test the hypothesis, a modified form of the scaffold fabricated from C-ECM incorporated with gold nanoparticles was used as cardiac-patches and compared its biomaterial properties with the pristine scaffold. Both *in vitro* and *in vivo* properties were evaluated.

The specific objectives of the study were the following:

1. Evaluation of the properties of porcine cholecystic extracellular matrix scaffold and its suitable modifications for cardiac tissue engineering
2. Differentiation of rat cardiomyoblast cell line H9c2 and rat bone marrow mesenchymal stem cells to cardiomyocyte-like cells
3. Functional evaluation of the cardiac patches in a rat model of non-fatal myocardial infarction

2. REVIEW OF LITERATURE

2.1 Cardiac embryology

The cardiovascular system is the first system to develop due to the increased metabolic demands by the growing embryo. The heart starts its function around day 21 or 22, just three weeks after fertilization. During the initial period of development, simple diffusion of necessary nutrients through the placenta was sufficient but later on becomes scarce to supply oxygen and nutrients. The formation of structures and changes in spatial configuration in proper timing determines the complex interplay of molecular signalling during cardiac development. Congenital heart diseases develop when there is any genetic or environmental intervention with this process (Mathew & Bordoni, 2019).

Around 18 days after fertilization, the heart forms from an embryonic tissue called mesoderm. The development starts near the head of the embryo in a region known as the cardiogenic area. The cardiogenic area commences to form two strands called the cardiogenic cords in response to the chemical signals from the underlying endoderm. A lumen rapidly develops within them and are referred to as endocardial tubes. They migrate together and fuse to form a single primitive heart tube. The primitive heart tube forms five different regions such as truncus arteriosus, bulbus cordis, primitive ventricle, primitive atrium and the sinus venosus. The above mentioned five regions develop into recognizable structures in a fully developed heart. The truncus arteriosus will divide and forms the ascending aorta and pulmonary trunk. The bulbus cordis matures into the right ventricle. From the primitive ventricle, the left ventricle is formed, the anterior portions of the right and left atria are formed from the primitive atrium. Subsequently, the sinus venosus develops into the posterior part of the right atrium, the sinoatrial node and the coronary sinus.

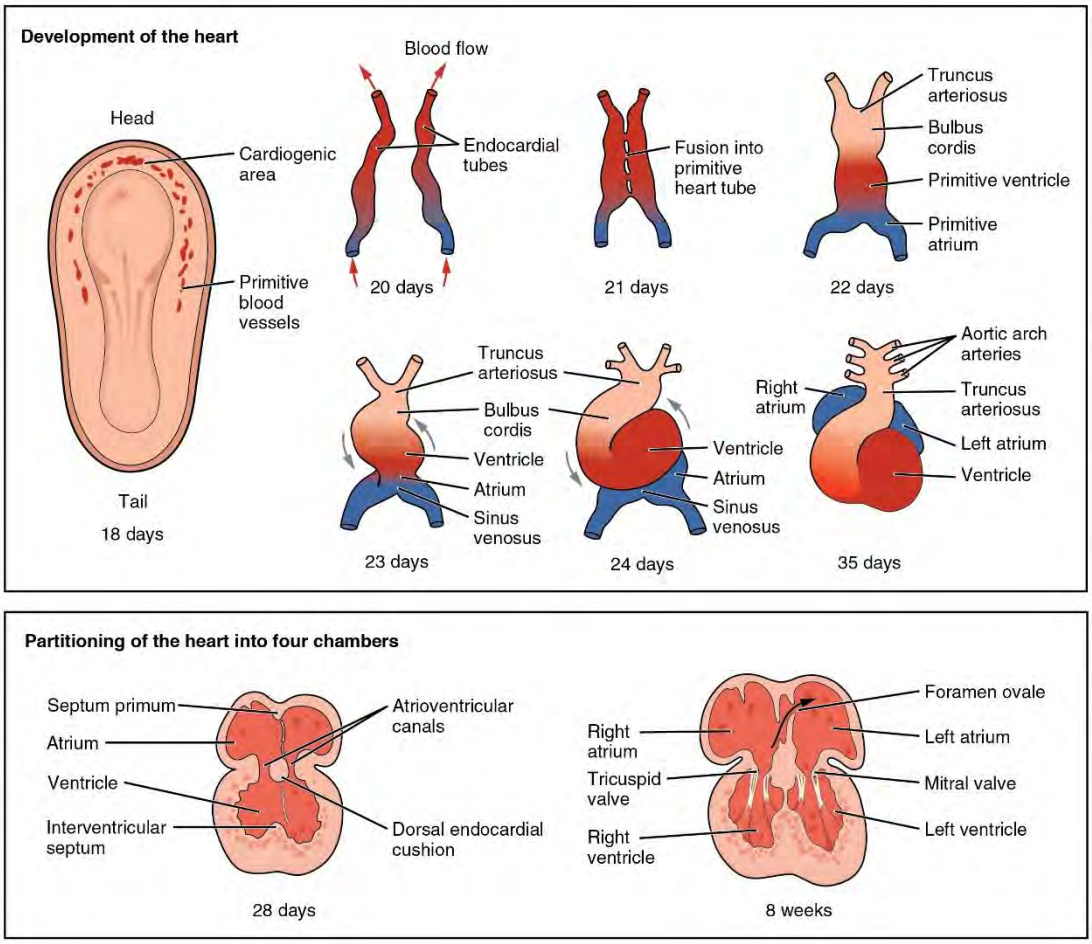

Figure 1: Human heart development. This diagram shows the schematic representation of the development of the human heart and the partitioning to form heart chambers (Adapted from Development of the Heart – Anatomy and Physiology by Rice University)

As soon as the primitive heart tube elongates, it starts to fold within the pericardium, resembling an 'S' shape, which positions the chambers and major vessels in place. Further, the development of septa, valves, and remodelling of the actual chambers takes place. Finally, the partitioning of the atria and ventricles by the interatrial septum, interventricular septum and atrioventricular septum takes place by the end of the fifth week.

2.2 Anatomy and physiology of heart

The human heart is situated within the thoracic cavity, between the lungs behind the sternum and above the diaphragm. The heart is separated from the other mediastinal structures by a tough membrane known as the pericardium and sits in the space called the pericardial cavity. The shape of the heart is similar to a pinecone, slightly broad at the base and tapering to the apex. The size of the heart is approximately the size of our fist and the weight ranges from 250 to 300 grams in females and about 300 to 350 grams in males. There are four chambers in the human heart, the upper chambers, the right atrium and the left atrium acts as receiving chambers and contracts to push blood into the lower chambers, the right ventricle and the left ventricle. The primary pumping chambers are the ventricles that pump blood to the lungs or to the rest of the body. The pulmonary circuits and systemic circuits are the two interlinked routes in human circulation. The pulmonary circuit transports deoxygenated blood away from the right ventricle to the lungs and return oxygenated blood to the left atrium and ventricle while the systemic circuit transports oxygenated blood to almost all the tissues of the body and returns deoxygenated blood and carbon dioxide to the heart. (Betts *et al*, 2017)

2.3 Regenerative capacity of the heart

The mammalian heart has limited regenerative capacity due to the presence of terminally differentiated cardiomyocytes (Sadek & Olson, 2020). These cardiomyocytes are quiescent while those from axolotls, newts, frogs and zebrafish, retain lifelong ability to proliferate (Hashimoto *et al*, 2018). It has been found that cardiomyocytes renew around 1% of the cells per year at the age 20 which reduces to 0.3% at 75 years of age (Arnal-Pastor *et al*, 2013). Therefore, the key limitation to cardiac regeneration is likely the poor ability of adult mammalian cardiomyocytes to enter the cell cycle and divide. On the other hand, cardiomyocytes in the fetal heart are mononucleated and can proliferate but after shortly birth, DNA replication occurs without cytokinesis or karyokinesis and they become mono-nucleated cells with polyploidy nucleus. It is rare for a cardiomyocyte to enter the cell cycle after this post-natal switch (Kikuchi & Poss, 2012).

The heart has two unique features: first, it functions as a syncytium and the second, it has the exceptional ability to generate and sense electrical impulses. These two are the major challenges faced by investigators working on the regeneration of the heart. In short, the laboratory-generated cardiac cells must be programmed to orchestrate with resident cardiac cells so that they function synchronously making use of the electrical conduction system. Thus, the regenerated heart must possess its own electrical conduction system, which is required to the heartbeat (Forough *et al*, 2011).

Two main concepts have been practiced to generate cardiomyocytes for cardiac regeneration either through activation of resident cardiac stem cells or the revival of pre-existing cardiomyocytes after cardiac injury (He & Zhou, 2017). The belief that the adult heart is a post-mitotic organ and cannot renew by itself has been challenged by some recent studies. The reports that human cardiac stem cells/ progenitor cells can renew despite with gradual decrease in number with age. These cells include resident side population cells, c-kit-positive cells, Sc-1-positive cells, cardiosphere cells, Is1-positive cells but their numbers are too minimal to replace an injury and difficult to expand in the lab (Wen *et al*, 2012). The proliferative capacity of adult cardiomyocytes has been modulated with molecular tools. Cell cycle activity of cardiomyocytes have been shown to increase with forced expression of cyclin B1-CDC2, and knockdown of p21/p27 (Senyo *et al*, 2014). In another approach, miRNAs were used to downregulate the insulin-like growth factor-1 pathway which contributes to cardiac hypertrophy. Some of the examples includes miR-199a and miR-590 which have the ability to induce cardiomyocyte proliferation in animal models (Chaudhuri *et al*, 2017).

2.4 Pathophysiology of myocardial infarction

The presence of acute myocardial injury evidenced by elevated cardiac biomarkers in the setting of evidence of acute myocardial ischemia is the clinical definition of myocardial infarction (Thygesen *et al*, 2018). Myocardial infarction is also defined as the necrosis of the cardiomyocyte with an increase and/or a decrease in plasma cardiac troponin (cTn). This is in accordance with the "Third Universal Definition of myocardial infarction (MI)" published in October 2012 by the global Myocardial

Infarction Task Force recommended by the European Society of Cardiology, the American College of Cardiology Foundation, the American Heart Association, and the World Heart Federation. Cardiac troponin measurement should be higher than the 99th percentile normal reference limit during any signs of MI, significant ECG ST-segment/T-wave changes/block in left bundle branch, the development of Q waves in ECG, loss of viable myocardium or abnormality in regional wall motion detected by any imaging method, detection of an intracoronary thrombus by angiography or autopsy (Reddy *et al*, 2015).

2.4.1 Clinical classification

MI can be classified into various types depending on pathological, clinical and prognostic differences, along with different treatment strategies: (1) Spontaneous myocardial infarction, MI type 1 (2) Myocardial infarction secondary to an ischemic imbalance, MI type 2 (3) Myocardial infarction resulting in death when biomarker values are unavailable, MI type 3 (4) and (5) Myocardial infarction associated with revascularization procedures, MI types 4 and 5 (Thygesen *et al*, 2012).

2.4.2 Biomarker detection

Elevation in the blood levels of sensitive and specific cardiac biomarkers such as cTn, high-sensitivity (hs)–cTn assays are recommended for routine clinical use or the MB fraction of creatine kinase (CKMB) determines myocardial injury (Thygesen *et al*, 2012). Troponin isoforms such as cardiac Troponin-I (cTnI) and cardiac Troponin-T (cTnT) are regulatory myofibrillar proteins, which are the preferred biomarkers for cardiac damage from myocardial infarction. Besides this clinical application, some researchers have also used the presence of troponins, to indicate the differentiation of cardiomyocytes (Forough *et al*, 2011). Troponin values may remain elevated for 14 days or more subsequent to the onset of cardiomyocyte necrosis. The best substitute to cTn assay is CKMB which is measured by mass assay. For both troponins and CKMB, increased values are determined as a value exceeding the 99th percentile of a normal reference population (upper reference limit) which is designated as the decision level for the diagnosis of MI (Thygesen *et al*, 2012). An increase in cTn values reveals injury to myocardial cells but does not specify the underlying pathophysiological mechanisms (Thygesen *et al*, 2018).

2.4.3 Other methods for the detection of MI

Electrocardiogram (ECG) is an important part of the diagnosis of patients with suspected MI and should be acquired and interpreted within 10 min after the patient presentation. The presence of severe or evolving changes in the ST–T waveforms and Q waves possibly allow the clinician, to assess the amount of myocardium at risk, to time the MI, to find the infarct-related artery as well as prognosis and to establish a therapeutic strategy. A greater degree of myocardial ischemia is associated with more intense ST-segment shift or T wave inversion. Cardiac arrhythmias, intraventricular and atrioventricular conduction delays and loss of precordial R wave amplitude are some of the signs associated with MI. In short, changes in the PR segment, the QRS complex, the ST segment or the T wave determines the ECG abnormalities associated with myocardial infarction (Reddy *et al*, 2015; Thygesen *et al*, 2012).

Echocardiography is also used for the assessment of cardiac structure and function, specifically myocardial thickness, thickening and wall motion. Echocardiographic contrast agents can improve visualization of the endocardial border and can be used to assess myocardial perfusion and microvascular obstruction (Thygesen *et al*, 2012).

Radionuclide imaging is another technique which allows the imaging of viable myocytes with the use of SPECT tracers thallium 201, technetium-99m MIBI and tetrofosmin, and the PET tracers F-2 fluorodeoxyglucose (FDG) and rubidium 82. This is the only commonly available method for measuring cardiomyocyte viability directly but the relatively low resolution of the images confines them for detecting the smallest areas of MI (Thygesen *et al*, 2012, 2018).

Magnetic resonance imaging provides an accurate assessment of myocardial function and is almost similar to echocardiography. With the use of paramagnetic contrast agents, assessment of myocardial perfusion and the increase in extracellular space associated with the fibrosis of prior MI can be detected (Thygesen *et al*, 2012).

Computed tomography (CT) is used in conditions where the necrotic myocardium is detected as a focal area of reduced LV myocardial enhancement, but further imaging demonstrated increased enhancement, as with late gadolinium imaging by MRI. Contrast-enhanced CT is not used routinely used but performed in

suspected pulmonary embolism and aortic dissection conditions with clinical features that overlap with those of acute MI (Thygesen *et al*, 2018).

2.4.4 Pathological characteristics

In pathology, MI is defined as myocardial cell damage as a result of continued lack of blood supply. Depending on the existence of collateral circulation or discontinuous coronary arterial occlusion, the sensitivity of the cardiomyocytes to ischemia, preconditioning, and demand for oxygen and nutrients differ. Histological cell death is not immediate after the ischemia, it takes about 20 min, or even less in some animal models. For the complete necrosis of cardiomyocytes at the infarct site, it requires at least 2–4 h, or longer, depending on the availability of oxygen or the extent of the damage. The whole process resulting in a healed infarction typically takes about 5–6 weeks (Thygesen *et al*, 2012).

2.4.5 Left ventricular remodelling

Myocardial infarction is the injury and is escorted by a wound healing process of the damaged area. It involves a series of events resulting in the substitution of damaged cardiac muscle by a scar and a makeover in the functional ventricle (Stefanon *et al*, 2013). The process by which the size, shape, and function of the ventricle are controlled by mechanical, neuro-hormonal and genetic factors is defined as left ventricular remodelling (St. John Sutton & Sharpe, 2000).

The loss of functional muscle leads to a rapid increase in loading conditions that induce the remodelling process involving the infarcted border zone and remote non-infarcted myocardium. A cascade of intracellular signalling processes is triggered that initiates and modulates the reparative process leading to dilatation, hypertrophy, and scar formation. This remodelling may remain for weeks or months until the expanding forces are compensated by the tensile strength of the collagen scar formed. Myocytes, extracellular matrix and the capillary microcirculation are the three integral components of the myocardium that maintains the contractile unit assembly. These three components provide important insights into the remodelling process and are the basis for future therapeutic strategies. Myocytes are terminally differentiated and develop tension by shortening. The extracellular matrix consisting of type I and type III collagen acts as a stress-tolerant, viscoelastic scaffold that couple myocytes and

retains the spatial relations between the myofilaments and their capillary microcirculation. During MI, macrophages, monocytes, and neutrophils migrates to the infarct zone and activates neuro-hormonal and intracellular signalling, which localizes the inflammatory response to the infarct zone. Left ventricular remodelling has been divided into an early stage that starts within 72 hours after infarct and a late-stage that starts beyond 72 hours after an infarct. The early-stage involves infarct zone expansion leading to ventricular rupture or aneurysm. Late remodelling involves the left ventricle and is associated with dilatation, ventricular shape distortion, and hypertrophy of the ventricular wall (St. John Sutton & Sharpe, 2000).

Myofibroblasts are the cells responsible for collagen synthesis, which starts in response to different stimuli such as the mechanical stress, vasoactive factors (angiotensin II) and growth factors (transforming growth factorβ,). They act directly or through the activation of connective tissue growth factor (CTGF). The degradation of collagen is mediated by a family of zinc-containing endoproteinases known as matrix metalloproteinases (MMPs). The level of these enzymes increases after MI in response to inflammatory cytokines and TGF-β but generally found in low levels in the heart. Endogenous inhibitors of MMP (TIMPs) also modulate the MMP activity. Crosslinking of fibrillar collagen by the action of lysyl oxidase (LOX) is another important step in collagen synthesis. LOX is an extracellular enzyme that provides the tensile strength and mechanical properties to the collagen fibres. Remarkably, increased ventricular stiffness and reduced compliance are contributed by collagen crosslinks. TGF-β, CTGF and pro-inflammatory cytokines control LOX production in the heart and play a role in ventricular stiffness (Stefanon *et al*, 2013).

Type III and type I collagen deposition occurs predominantly in the infarct zone. By day 2, type III collagen mRNA rises and remains elevated for 3 weeks. On the other hand, type I collagen mRNA increases by day 4 and may remain prominent for up to 3 months. By day 7, collagen is detectable microscopically and then increases gradually. By 28 days, the necrotic myocytes will be replaced completely by fibrous tissue. As the scar tissue balances the distending and restraining forces, collagen formation is down-regulated and the myofibroblasts undergo apoptosis (St. John Sutton & Sharpe, 2000).

An adaptive response during post-infarction remodelling is myocyte hypertrophy that balances the increased load, attenuates progressive dilatation, and stabilizes contractile function. It is initiated by neuro-hormonal mechanism of activation leading to myocardial stretch, the activation of the local tissue renin-angiotensin system (RAS), and paracrine/autocrine factors (St. John Sutton & Sharpe, 2000). The increased workload executed by MI can elicit a hypertrophic response in the remote region of MI depending on the infarct size, type (subendocardial or transmural), location (septal vs. anterior, lateral or posterior walls), reperfusion type (full reperfusion, no reperfusion or reperfused with areas of no-reflow), degree of non-ischemic infarct extension, preload and afterload, health status (obesity, diabetes, hypertension), and other factors (such as state of inflammatory activation) (French & Kramer, 2007).

2.5 Cardiac tissue engineering

Langer and Vacanti in the early 90s proposed tissue engineering (TE) as "an interdisciplinary field which applies the principles of engineering and life sciences toward the development of biological substitutes that reinstate, preserve, or increase tissue function" (Langer & Vacanti, 1993). TE was officially founded at a National Science Foundation meeting in 1987 by Y. C. Fung, tailed by the first tissue engineering workshop at Lake Tahoe in 1988 (Ma & Vunjak-Novakovic, 2016). The concept of cardiac tissue engineering is to develop highly reliable mimics of human tissue for demonstrating physiology and pathology or to repair the damaged cardiac muscle. For this, careful selection of the source of cardiomyocytes, development of biomaterials that support the growth, proliferation and differentiation of these cells with an appropriate feature of electromechanical stimulation is recommended (Radisic, 2015).

2.5.1 Scaffolds

A wide range of biomaterials have been used for tissue engineering of different tissues including bone, tendon, cartilage, skin, etc., but the ability to exploit natural or synthetic scaffolds for cardiac tissue engineering has proven to be more challenging than any of the above-mentioned tissues (Schwach & Passier, 2019). A biomaterial as

unique as the heart will be the most appropriate biomaterial for cardiac tissue engineering, having highly flexible, elastic and capable of withstanding millions of contraction cycles, while supporting the cells *in vitro* and *in vivo* (Radisic, 2015). An ideal scaffold should provide a 3-dimensional environment for cells to attach, interact, transmit load and conduct signals. It should also induce alignment, provide appropriate stiffness to generate the physiological force and enzymatically degrade over time to be replaced by extracellular matrix proteins secreted by the cells (Vunjak Novakovic *et al*, 2014). It should match the mechanical properties of the myocardium. Young's modulus of adult human myocardium ranges from 10-20 kPa at the start of the diastole to 200- 500 kPa at the end of the diastole (Huyer *et al*, 2015).

In cardiac tissue engineering, two types of materials: cardiac-patches and hydrogels are being used. Collagen, gelatin, laminin, Matrigel, hyaluronic acid, alginate, and chitosan are typical natural hydrogels and the synthetic counterpart includes poly (2-hydroxyethyl methacrylate) (PHEMA), poly (N isopropylacrylamide) (PNIPAAM) and poly (ethylene glycol) (PEG) (Camci-Unal *et al*, 2014). Compared to the synthetic ones, natural biomaterials are widely preferred due to the similarity in their structure with the native molecules which minimizes the chance of immune rejection (Li & Guan, 2011).

An important characteristic of the heart muscle is electrical conductivity which has emerged as a key factor in designing biomaterials for cardiac application. Engineered heart tissues developed using electrically conductive biomaterials with biomimetic topographical signals have received wide attention. Electrically conductive biomaterials are known to restore the electrophysiological function of the heart (Ye & Qiu, 2017). Some examples of conductive biomaterials include carbon-based nanomaterials such as graphene (Saravanan *et al*, 2018) and carbon nanotubes (Ren *et al*, 2017), metal derived materials such as gold nanoparticle (Nair *et al*, 2017) and conductive polymers such as polyaniline (Kapnisi *et al*, 2018), polythiophene (Chan *et al*, 2018) and polypyrrole (Kai *et al*, 2011).

2.5.1.1 Natural scaffolds

Most of the natural scaffolds mimic endogenous tissues and organs which facilitate better tissue integration compared to other scaffolds. Even then, there are considerable

number of limitations in using these scaffolds for various tissue engineering applications. The limited availability, batch to batch variation, low shelf life, and high costs are important drawbacks. Also, there is difficulty in designing scaffolds from natural biomaterials (Schwach & Passier, 2019). Some of the natural biomaterials used for cardiac tissue repair are gelatin (Echave *et al*, 2017), collagen (Wu *et al*, 2019), Matrigel (Hirt *et al*, 2014), fibrin (Barsotti *et al*, 2011), hyaluronic acid (Bonafè *et al*, 2014), alginate (Liberski *et al*, 2016), decellularised matrices (Kc *et al, 2019* ; Moroni & Mirabella, 2014), etc.

2.5.1.2 Synthetic scaffolds

Synthetic scaffolds are made from a monomer, therefore their properties can be tailored to match desired characteristics. In addition to that, they are free from risks associated with animal origin scaffolds (Arnal-Pastor *et al*, 2013). Some of the synthetic scaffolds used for cardiac application are poly-esters (Dhingra *et al*, 2014), poly-lactones (Santoro *et al*, 2016), elastomers (Bat *et al*, 2014), polyethylene glycol (Grover *et al*, 2014)

2.5.2 Cells

Cell therapy has been extensively studied for long as an effective treatment for ischemic heart disease (Chen *et al*, 2015). Cells recovered using easy isolation procedure, having the ability to proliferate, non-immunogenic nature and capability to differentiate into functional cardiomyocytes are chosen as an ideal sources for engineering myocardial patch (Leor *et al*, 2005). Unfortunately, none of the cells currently satisfies all these. Autologous cells are difficult to obtain and expand but free of immune reaction. On the other hand, allogenic cells are easily available and preferred even with associated immune reactions (Leor *et al*, 2005). The preferred cells for myocardial repair include non-cardiomyocytes, cardiac-derived cells and pluripotent stem cells (Hashimoto *et al*, 2018).

2.5.2.1 Non-cardiac cells

The first generation cell-based therapies involved transplantation of non-cardiac cells as researchers could not obtain a sufficient number of functional cardiomyocytes to replace the cells lost during myocardial infarction (Hashimoto *et al*, 2018). Skeletal

myoblasts, bone marrow-derived cells and mesenchymal stem cells have been the initial source for cell-based therapies in treating myocardial infarction.

First studies using a cell-based strategy for ischemic heart disease doubted on skeletal myoblasts, depending on its ability to regenerate skeletal muscle through the proliferation of quiescent satellite cells located under the basal lamina (Chen *et al*, 2015). The advantages include ease of expansion *ex vivo* and the availability of autologous source. Preclinical studies demonstrated its potential for intra-myocardial injection for improving LV function. Numerous clinical trials including MAGIC (Behfar *et al*, 2014) and MARVEL (Hastings *et al*, 2015) have revealed a lack of efficacy. Moreover, studies also showed that the injected cells do not integrate electromechanically with the surrounding myocardium due to the lack of connexin 43 expression by these cells. Considering the lack of significant clinical improvement and their potential arrhythmogenic hazards, skeletal myoblasts have fallen out of favour as a therapeutic candidate (Chen *et al*, 2015).

The next set of cells used for cardiac therapy were unselected bone-marrow derived mononuclear cells which have been used as a therapeutic option for heart diseases (Chen *et al*, 2015). Clinical trials, such as the BOOST trial and the REPAIR-AMI trial revealed some beneficial effects in acute MI patients with improved ejection fraction but further larger clinical trials did not reproduce the same results. Thus, no definite conclusion was obtained (Hashimoto *et al*, 2018).

Further, trials were focused on the use of mesenchymal stem cells (MSC) which are non-immunogenic, isolated from bone marrow or adipose tissue. It has been observed that under specific culture conditions (presence of the DNA methyltransferase inhibitor 5-azacytidine) and after injection into healthy or infarcted myocardium in animals, MSCs differentiate to cardiomyocyte-like cells. It may also improve regional wall motion and prevent the remodelling process of the myocardium. It is observed that MSCs have the ability to secrete cytokines which promote angiogenesis and improve the blood flow (Wollert & Drexler, 2005).

2.5.2.2 Cardiac-derived cells

Cardiac stem cells are resident heart cells that are clonogenic, multipotent and have the ability to self-renew. They can differentiate into three major cardiac cell types such

as cardiomyocytes, smooth muscle cells, and endothelial cells (Hastings *et al*, 2015). Interestingly, these cells can be clonally expanded from human myocardial biopsies. Studies reported that intra-myocardial injection of these cells stimulates cardiomyocyte and vascular cell growth (Wollert & Drexler, 2005). Three cell-surface markers have been expressed by these cells: MDR-1 (multi-drug resistant protein), C-kit (the receptor for stem cell factor), and Sca-1 (Stem cell antigen 1). Only one cardiac stem cell per every 1000 myocytes was found residing in the atrium and the ventricular apex. Studies in animal models revealed that these cells restored, initiated myocardial repair and regeneration in response to injury (Leong *et al*, 2017).

Cardiospheres are 20-150 μm cellular spheres with a mixed population of cardiac stem cells, isolated from explants of heart biopsies. These consist of cardiac stem cells residing in the core and cardiac lineage committed cells and differentiated cells (vascular smooth muscle cells, endothelial cells) (Leong *et al*, 2017). With cardiosphere therapy after MI, the scar size and left ventricular volumes benefitted but left ventricular ejection fraction was not significantly increased (Hastings *et al*, 2015). In that context, another clinical trial RECONSTRUCT was planned to address the efficacy of autologous cardiospheres and the ALLSTAR study to examine the efficacy of allogenic CSC cardiospheres in acute MI (Behfar *et al*, 2014).

2.5.2.3 Pluripotent stem cells

A major drawback of the early clinical trials was the limited ability of the transplanted stem cells to differentiate into cardiomyocytes. Therefore, scientists were forced to generate functional cardiomyocytes *in vitro* and to transplant these cardiomyocytes to the injured heart.

The first cell source studied was embryonic stem cells (ESCs) derived from the inner cell mass at the blastocyst of early embryos. They are clonogenic, self- renewing, and pluripotent, can differentiate into all cell types of the three germ layers: endoderm, ectoderm, and mesoderm (Hashimoto *et al*, 2018). Human ESC derived cardiomyocytes show structural and functional properties of early-stage cardiomyocytes which can electrically couple with host cardiomyocytes. These cells can be expanded into infinite numbers but due to ethical, immunological and legal concerns, it is not in use currently (Wollert & Drexler, 2005).

Yamanaka and colleagues cleared the ethical issues of using ESCs when they stated that mouse and human fibroblasts could be reprogrammed to an ESC- like pluripotent state defined as induced pluripotent stem cells (iPSCs). These cells are forced to express four genes encoding transcription factors for OCT3/OCT4 (POU5F1), SOX2, KLF4 and MYC (OSKM factors). Yamanaka won the 2012 Nobel Prize in Physiology or Medicine for this discovery and offered iPSCs as a new cell-based approach for heart repair, enabling autologous or allogeneic transplantation and circumventing the ethical concerns associated with ESCs (Hashimoto *et al*, 2018).

Moreover, the addition of Flk1, Isl1 or Nkx2.5 to iPSCs has led to the formation of cardiac progenitor cells used in cardiac tissue engineering. Extensive studies have been performed in infarcted hearts of rats and pigs to understand the functionality of these cells (Chaudhuri *et al*, 2017).

Parthenogenetic stem cells are pluripotent stem cells that may avoid the disadvantages of human ESCs due to reduced immune rejection. Studies indicated integrated electrical coupling with host myocardium and improved cardiac function in a mouse model of myocardial infarction with the transplantation of mouse parthenogenetic stem cell-derived cardiomyocytes (Sun *et al*, 2014).

2.5.3 Growth factors

The development of effective therapy for increasing angiogenesis is one of the main goals of the therapies for myocardial infarction. In the early 1990s itself, intra-coronary administration of basic fibroblast growth factor protein improved heart function and increased the number of collateral blood vessels in dogs. Thus, current therapies have been focused on the direct delivery of growth factors or genes that encode for the synthesis of growth factors to the target tissues (Maulik & Thirunavukkarasu, 2008). The growth factors have a direct action on several cell functions such as adhesion, proliferation, migration, and others. When the coronary artery blood flow obstruction occurs, delivered growth factors induce angiogenesis and thereby improves the myocardial hypoxic condition, with the formation of new sprouts of blood vessels. This can further lead to improved cardiac function. They have the potential to induce positive remodelling of the extracellular matrix, the proliferation of adult cardiomyocytes, homing of cardiac stem cells, anti-apoptotic and/or angiogenic effect (Rebouças *et al*, 2016). Some examples of such growth factors used are vascular

endothelial growth factor, stromal cell-derived factor-I, recombinant human neuregulin-I (NRG-I), hepatocyte growth factor, insulin-like growth factor-I, and fibroblast growth factor-1/2/4 (Hastings *et al*, 2015).

Several growth factors have shown great therapeutic potential in clinical trials, and some have been approved for cardiac applications. Still, these factors are not widely used for cardiac repair. The reasons for the less acceptability are high cost, short half-life, low stability, fast destruction of the specific properties by the enzymes present in the body (Wang *et al*, 2017).

2.6 Strategies in cardiac tissue engineering

Cardiovascular tissue engineering is the most proliferative discipline in the field of tissue engineering with more than 9200 PubMed entries. The first report on tissue-engineered vasculature was published in 1986 followed by the engineered heart tissue (EHT) in 1994 from chicken embryonic heart cells in collagen I. Today almost 20 years later, this field is progressing towards first-in-man applications (Weinberger *et al*, 2017). This section presents some of the strategies in cardiac tissue engineering that have shown promising results *in vivo.*

2.6.1 Classical tissue engineering approach

In this approach, a tissue construct is developed by culturing desired cells into a scaffold *in vitro* with or without specialized culture conditions and implantation in an organism. It started with the use of isolated rat fetal cardiomyocytes for repairing injured myocardium. It was observed that the tissue construct facilitated neovascularization and survival of the fetal cardiomyocytes with improved heart function lacking contractility. Further studies were focused on the role of tensile strength provided by the scaffold or paracrine effects of the surviving cells in contributing to the improvement. To provide cell survival, several scaffold materials have been investigated with the incorporation of angiogenic and survival factors to scaffolds, co-culturing of cardiomyocytes with smooth muscle cells and endothelial cells (Tee *et al*, 2010). Scaffolds have been developed with physiocochemical properties similar to the native extracellular matrix, based on natural materials, such as collagen, chitosan or synthetic materials, such as poly-lactic acid or poly-glycolic

acid. The main advantage is the flexibility of these materials to be changed to any form or size as desired for the recipient (Gálvez-Montón *et al*, 2013).

2.6.2 Engineered heart tissue

Engineered heart tissues vary from classical scaffold-based tissue-engineered cardiac constructs since they are originally made from heart cells, liquid collagen I and Matrigel as well as growth supplements, reorganized in circular moulds and subjected to mechanical strain. This will lead to the development of cardiac organoids which shows contractile property and electrophysiological activity similar to the myocardium. Initial implantation experiments of the engineered heart tissue was performed in healthy rats which revealed survival, excellent vascularization and indications of terminal differentiation of the tissue grafts (Zimmermann *et al*, 2004, 2006).

2.6.3 Cell sheet/cell patch technology

A novel technology was developed by Shimizu *et al*, 2002 where contractile cardiac grafts were engineered without the use of scaffold materials by stacking mono-layered cell sheets. Neonatal cardiomyocytes were cultured on the surfaces coated with a temperature-responsive polymer (Poly-N- isopropylacrylamide), which is non-adhesive below 32°C. When the temperature was lowered, pulsatile cell sheets were detached with preserved cell junctions and adhesive proteins. These cell sheets were overlaid to form grafts where the extracellular matrix produced by cells enabled the cell sheets to stick together (Dengler & Radisic, 2007). The outcome of this approach is a scaffold-free, cell dense tissue comparable to compact myocardium. It was noticed that the limited diffusion of nutrients causes difficulty in sustaining the viability of the patch and for thick myocardial tissue constructs, vascularization strategies need to be employed for the success of the graft (Tee *et al*, 2010).

2.6.4 Biological cell assembly

In this approach, cells were suspended in hydrogel-based scaffolds instead of seeding cells into a three-dimensional porous scaffold. The hydrogel act as an environment for cells to migrate and assemble into contractile tissues either *in vitro* using gravity enforced techniques to form spheroid-like microtissues or *in vivo* using an

arteriovenous loop embedded chamber to vascularize the assembled CMs (Tee *et al*, 2010).

The hydrogel method is currently the most popular technology in cardiac tissue engineering due to its simple method, flexibility and viability of cardiac tissue developed. The basic requirements are cells, a hydrogel, a casting mould, and mechanic support. Initially, the liquid hydrogel is mixed with cells, it forms a gel. This gel traps the cells in a three-dimensional form that is provided by a casting mould. To provide mechanic support, casting mould is inserted to provide the mechanical load which is considered as one of the essential factors driving cardiac tissue development and maturation (Weinberger *et al*, 2017).

The main drawback of porous and fibrous scaffolds includes limited contractile force because of the inherent stiffness of the scaffold, partial biodegradation, and poor cell alignment. On the other hand, these hydrogels exhibit no mechanical or spatial restrictions (Dengler & Radisic, 2007).

2.6.5 Decellularised matrix

The use of biological tissues as scaffolds for cardiac tissue engineering has been sought by several research groups utilizing myocardium as well as from other organs. Xenogeneic and allogeneic cellular antigens induce an inflammatory response or an immune-mediated rejection of the tissue as they are recognized as foreign by the host upon implantation. Conversely, most of the ECM components are generally conserved among species and are abided well even by xenogeneic recipients (Gilbert *et al*, 2006). In 2008, decellularised rat hearts were seeded with cardiomyocytes and endothelial cells which retained contractile activity after four days in culture. Earlier in 2005, a decellularisation technique pioneered by the Badylak laboratory, removed all cellular components from a tissue, resulting in an intact, functional extracellular matrix (ECM) (Vunjak Novakovic *et al*, 2014).

Decellularisation is the process of removal of all cells and genetic material from tissue, without altering the structural, biochemical and mechanical properties. The selection of appropriate decellularisation methods is dependent on the ability to preserve the physical and biochemical properties of a specific tissue which includes the thickness, density and three-dimensional architecture. Various decellularisation

protocols have been described which involves a combination of physical, chemical and enzymatic methods.

Freeze–thaw processing, hydrostatic pressure and mechanical delamination of specific tissue layers are physical strategies for achieving decellularisation while the chemical methods include the use of weak acids such as peracetic acid, use of alkalies such as sodium hydroxide, hypotonic and hypertonic solutions, chelating agents (EDTA) and detergents such as sodium deoxycholate and sodium dodecyl sulphate. They mainly disrupt the cell membrane and removes cytosolic/genomic material. Alcohols like methanol and acetone are used for de-lipidisation. Proteases such as trypsin, dispase and thermolysin and nucleases such as RNase and DNase are also used to remove cell debris and nucleic acids from tissues (Hussey *et al*, 2018).

Generally, the mildest protocol that yields an acellular material with minimal loss of the structural and functional component of ECM is widely preferred. It is incongruous that any combination of the above-mentioned methods will eliminate 100% of all cell components from a tissue or organ. It relies on the method which removes visible cellular material resulting in an ECM scaffold that is nontoxic for implantation without any adverse inflammatory effects (Gilbert *et al*, 2006). For assessing the efficacy of removal of cellular components from tissues and organs, some benchmarks have been devised: after the decellularisation process the ECM must have only less than 50 ng of double-stranded DNA per mg dry weight of ECM, the DNA fragment length should be less than 200 bp DNA and there should not be visible nuclear material after staining with 4′,6-diamidino-2-phenylindole (DAPI). Moreover, the protein content remaining in the ECM should be assessed, mostly the structural proteins like collagen, fibronectin, laminin glycosaminoglycans (GAGs) and growth factors. Also, the mechanical properties: elastic modulus and tensile strength, should match the original tissue based on the end application of the biomaterial (Gilpin & Yang, 2017).

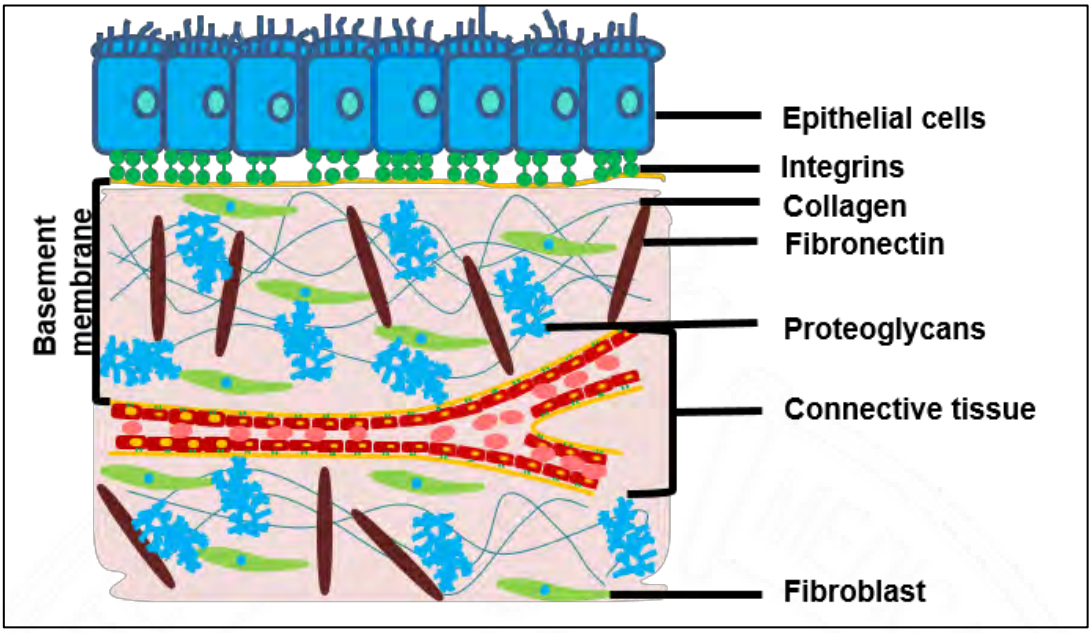

Figure 2: ECM organisation

ECM is composed of functional and structural proteins such as collagen, elastin, laminin, fibronectin, proteoglycans and many other glycoproteins (Fig. 2). It is known to play important role in many processes and cellular responses including proliferation, differentiation and migration. All these peculiar properties make it attractive as a suitable scaffold in cardiac tissue engineering techniques to recruit cells that replace the damaged myocardium. Extracellular matrix has been successfully isolated from a variety of tissues including cardiac valves, blood vessels, skin, nerves, skeletal muscle, tendons, ligaments, small intestinal submucosa, urinary bladder, liver and gall bladder (Gálvez-Montón *et al*, 2013; Anilkumar *et al*, 2014). ECM biomaterials modulate the tissue reaction by a process called constructive remodelling through which the host responds to the implanted ECM by angiogenesis, stem cell recruitment, innervation, antimicrobial activity and modulation of the innate immune response. The functional remodelling takes place through activation of anti-inflammatory M2 macrophage and T helper 2cell response associated with reduced local inflammation and crosstalk with stem and progenitor cells (Hussey *et al*, 2018).

Decellularised ECM scaffolds in the form of surgical mesh materials have been approved by the Food and Drug Administration for various clinical applications such as ventral hernia repair, musculoskeletal reconstruction, breast reconstruction,

oesophageal reconstruction, dura mater replacement, and cardiac repair (Hussey *et al*, 2018).

Mewhort *et al*, (2016) proposed an epicardial infarct repair method using a bio-inductive ECM biomaterial (CorMatrix™ ECM) to promote endogenous myocardial repair and functional recovery after myocardial infarction. A pre-clinical porcine model of coronary ischemia-reperfusion was used to assess the effects on regional functional recovery, safety, and the mechanism of action. In another proof-of-concept study, CorMatrix™ ECM biomaterial patch incorporated with basic growth factor–enhanced attenuated myocardial remodelling and improved cardiac performance after sub-acute myocardial infarction in a rat coronary ligation model (Mewhort *et al*, 2014).

In cardiac regeneration, ECM scaffolds have shown necessary signals to reduce cardiac fibroblast activation, thus preventing excessive scar expansion and thickening. Moreover, they may also stimulate endogenous mechanisms of repair and regeneration including angiogenesis, with the help of the inherent bio-inductive properties (Pattar *et al*, 2019). ECM from myocardium has been widely used in tissue engineering due to the combination of biochemical and mechanical cues retained from native myocardium that promotes cell attachment, proliferation and differentiation during recellularization (Kc *et al*, 2019). Acellular porcine cardiac ECM patches improved contractility, ventricular dimensions and cardiac remodelling in rat MI model by driving cardiac-progenitor dependent restoration (Sarig *et al*, 2016). Further, decellularised sheets of the human heart were used as a scaffold for *in vitro* culturing and *in vivo* delivery of cells for cardiac repair. These scaffolds have preserved protein content, similar mechanical strength compared to the heart muscle as well as conserved anisotropy and topography (Vunjak Novakovic *et al*, 2014). Due to the increasing list of biologic scaffolds used for tissue engineering or regenerative medicine applications with minimal adverse reactions compared to synthetic counterparts, there is an immense need for the development of better decellularisation protocols (Gilbert *et al*, 2006).

2.6.6 Vascularisation

The establishment of vasularisation is one of the key objectives of cardiac tissue engineering. Vasularisation within the scaffold allows continuous diffusion of

nutrients and oxygen towards the interior of the matrix which facilitates the migration and incorporation of cells into the damaged myocardium. Both *in vitro* and *in vivo* vascularization strategies have been employed. Researchers have incorporated growth factors such as vascular endothelial growth factor or basic fibroblast growth factor into the tissue construct to enhance vascular structure formation from the mesenchymal stem cells and/or endothelial progenitor cells or addition of cytokines to activate the recipient's endothelial progenitor cells following implantation. In a nutshell, the vasularisation approach promotes cellular infiltration and the formation of blood vessels (Gálvez-Montón *et al*, 2013).

Mammalian heart development is a complex and highly organized process. Therefore, to repair the human heart, a combination of multiple therapeutic approaches have to be adopted. Novel research discoveries and promising preclinical outcomes in the field of cardiac tissue engineering provides confidence in the development of effective regenerative therapies for the dying human heart. Yet, there are many disappointing results of previous clinical trials of cardiac regenerative therapies. So, we need to acknowledge and address the limitations of preclinical studies and the difficulties faced during clinical translation (Hashimoto *et al*, 2018). This field is still in its infancy, more intensive research has to be done to fill the gaps. Identification of an optimal cell source, the engineering of a scaffold that is compatible with the seeded cells and implantation site and an efficient vascularization strategy has to be carried out (Tee *et al*, 2010).

3. MATERIALS AND METHODS

3.1 Evaluation of the properties of C-ECM and its suitable modifications for cardiac tissue engineering

3.1.1 Materials

Tetrachloroauric acid (Sigma Aldrich), Tri-Sodium Citrate (Merck), L-cysteine hydrochloride monohydrate (Molychem), Ethyl-3-(3-dimethylaminopropyl)-carbodiimide (EDC) (Sigma Aldrich) and N-hydroxysuccinimide (NHS) (Molychem), Formalin (Molychem), Disodium hydrogen phosphate (Merck), Sodium dihydrogen phosphate (Merck) Ketamine Hydrochloride, Xylazine Hydrochloride, Isoflurane, Betadine, 7-0 Prolene suture (Centenial®), 3-0 Mersilk suture (Ethicon®), 3-0 Truglyde™ (Sutures India), Ceftriaxone, Meloxicam, Tetracycline, Centrifuge tubes, surgical scissors, forceps, curved forceps, cautery forceps, scalpel holder, needle holder, chest retractor, Paraffin wax with ceresin (Merck), Harris's haematoxylin (Sigma Aldrich, India), Eosin (Merck), Glacial acetic acid (Merck), 2-propanol (Merck), Xylene (Merck), Ammonia (Merck), Hydrochloric acid (Merck), Mounting medium (Leica).

H9c2 is subclone of the original clonal cell line obtained from embryonic BD1X heart tissue or myocardium of *Rattus norvegicus* purchased from National Centre for Cell Science, Maharashtra.

3.1.2 Preparation of C-ECM scaffold

Cholecyst/gall bladder was purchased from Meat Products of India Ltd, Edayar, Ernakulam, Kerala, India. The slaughtering of pigs (Large White Yorkshire) was carried out under strict veterinary supervision from selected animals free from zoonotic disease. The specimens without any gross lesions were transferred to a bottle containing 10% NBF and brought to the laboratory.

The isolation of the extracellular matrix from the cholecyst was initiated within 24 to 48 hours after collection. First, the cholecyst was washed with tap water for 1 hour to remove the excess NBF. The top and bottom portion of the gall bladder was removed and cut open to form a sheet. The thin layer of the extracellular matrix (ECM) was mechanically delaminated. The mucosa and muscle remnants were scraped off

from the isolated sheet to prepare the ECM sheet. All these procedures were carried out inside a fume hood (ESCO Ductless fume cabinet). The wet sheet was pre-freezed at -80°C (SANYO) and lyophilized (CHRIST–ALPHA 2-4LD plus^{TM}, Germany) for 16 hours to remove the water content. The dried sheets were sterilised by ethylene oxide and stored in desiccator for further use.

3.1.3 Evaluation of the biocompatibility of the scaffold

3.1.3.1 Culture and maintenance of H9c2 cells

Cells received from NCCS, Pune in T25 flasks were trypsinised and split into T75 flasks containing DMEM high glucose media with 10 % FBS. On the fourth day, cells were trypsinised and used for the following experiments.

3.1.3.2 Direct contact test

A direct contact test was performed to evaluate the cytotoxic effect of the scaffolds by assessing the morphology, detachment and lysis of cells when observed using an inverted phase contrast microscope (Olympus, Japan). 2.5×10^4 H9c2 cells/cm^2 were cultured in a 24 well plate and incubated for 3 days to become confluent while maintaining the culture conditions. The culture medium was then removed and scaffolds of size 4 mm were placed carefully on the cell monolayer. Sufficient culture medium was then added and cells together with scaffolds were incubated for further 24 hours. Cell viability after the direct contact test was also assessed by treating with a neutral red dye (1 mg/ml). The working solution was prepared in 1.8% NaCl solution in equal dilution. 500µl of the dye was added to each well and the cells were incubated for 10 min at 37°C, after which cells were washed two times with PBS solution. Images were taken under an inverted phase contrast microscope, Olympus, Japan. Experiments were conducted in triplicate.

3.1.3.3 Live-dead staining

The viability of the H9c2 cells seeded on the C-ECM scaffold was determined by FDA and PI staining. All the reagents were prepared freshly before use. The FDA stock solution was prepared in acetone (10 mg/ml) and10 µl of this stock solution was made up to 1 ml using serum-free media. 5×10^4 H9c2 cells were cultured on the scaffolds placed in a 24 well plate and incubated for 24 hours. Further, the cell-seeded scaffold

was treated with 500 µl FDA for 10 min, then 100 µl of PI was added and incubated for 30 seconds. The cells were examined under a fluorescence microscope Leica DMI 6000 B equipped with I3 (green) and N21 (red) filters. Triplicates were used for the analysis.

3.1.3.4 MTT assay

Cell viability on the scaffold was confirmed by performing the MTT (3-(4,5-Dimethylthiazol-2-Yl)-2,5-Diphenyltetrazolium Bromide) assay. 5×10^4 H9c2 cells were cultured on C-ECM scaffold placed in a 24 well plate and incubated in a CO_2 incubator for 3 days. Cells cultured on 24 well plates were taken as the control. After incubation, the medium was removed and 50 µl MTT reagent (0.5 mg/ml) was added and cells incubated for 3 h in a CO_2 incubator with 99% relative humidity, 5% CO_2 at a temperature of 37°C. After incubation, the MTT reagent was removed and 500 µl dimethyl sulphoxide was added. This was kept at room temperature for 2 h protected from light. The absorbance was measured at 570 nm using a multi-well plate reader (Biotech Synergy 4, USA). The cell viability was calculated as the ratio of the absorbance value of cell-seeded scaffolds to the absorbance value of control used, multiplied by 100.

3.1.4 Establishment of myocardial infarction model and implantation of C-ECM as an epicardial graft

3.1.4.1 Animal ethics

All animals were handled humanely, without making pain or distress and with due care for their welfare according to the regulations of the Committee for the Purpose of Control and Supervision of Experimental Animals (CPCSEA), Govt. of India. All the animal experiments were carried out after getting prior approval from the Institutional Animal Ethics Committee (IAEC) and performed under the approved institutional protocol. The B form number for this study is SCT/IAEC-198/NOVEMBER/2016/90.

3.1.4.2 Myocardial infarct model

To induce MI, rats underwent coronary artery ligation after tracheostomy under aseptic conditions. For the procedure, rats were anaesthetized by intramuscular injection of 80mg/kg of Ketamine Hydrochloride and 10mg/kg of Xylazine Hydrochloride. The

tracheostomy tube was placed by making a mid-ventral neck incision and retracting the muscle tissue to expose the trachea. It was then connected to a ventilator (Small animal ventilator R407) at 40 breaths per minute and 1.2 ml tidal volume per 100 g body weight under 1.5% Isoflurane anaesthesia. The sternum and the left costochondral junctions of 2nd to 5th ribs were exposed. A left parasternal thoracotomy was performed by dissecting the pectoralis muscle, the ribs at the costochondral junction and the pleura. Excess bleeding was prevented by cauterization. The retractor was placed among the sternal border and the rib cage between the 1st to 6th intercostal space. The pericardium was picked gently with an atraumatic forceps and incised to expose the heart. The left anterior descending artery was identified using a loupe amplification system and passed the needle of 7-0 Prolene suture underneath and ligated the artery (Fig. 3). Three knots were tied carefully and bleeding was controlled.

3.1.4.2 Treatment of MI with scaffolds

The infarct region was identified by visible blanching and cyanosis rapidly after ligation of the artery. A lyophilised sheet of the C-ECM scaffold was cut into the desired shape and placed over the blanched area, secured by suturing using 7-0 Prolene (n=3 per group). Another group with artery ligation without any graft placement served as the control. The chest retractor was removed and the rib cage was apposed with the sternum after keeping a chest tube (lumen diameter 2 mm). The muscle layer was also sutured to place with a 3-0 Truglyde™ (Absorbable surgical suture U.S.P, Sutures India) suture. Then, using a 3-0 Mersilk* (Non-absorbable surgical suture U.S.P, Ethicon®), the skin was closed and the chest tube was removed after suction of air from the thoracic cavity. Later, the tracheostomy tube was removed as the rats regained spontaneous breathing and the skin was closed using 3-0 Mersilk*. The rats were observed till a steady heart rate was attained and administered with Ceftriaxone (antibiotic, 20mg/kg) and Meloxicam (analgesic, 0.5mg/kg) for three days. After 2 weeks all the animals were euthanized and tissues were collected for histological evaluation.

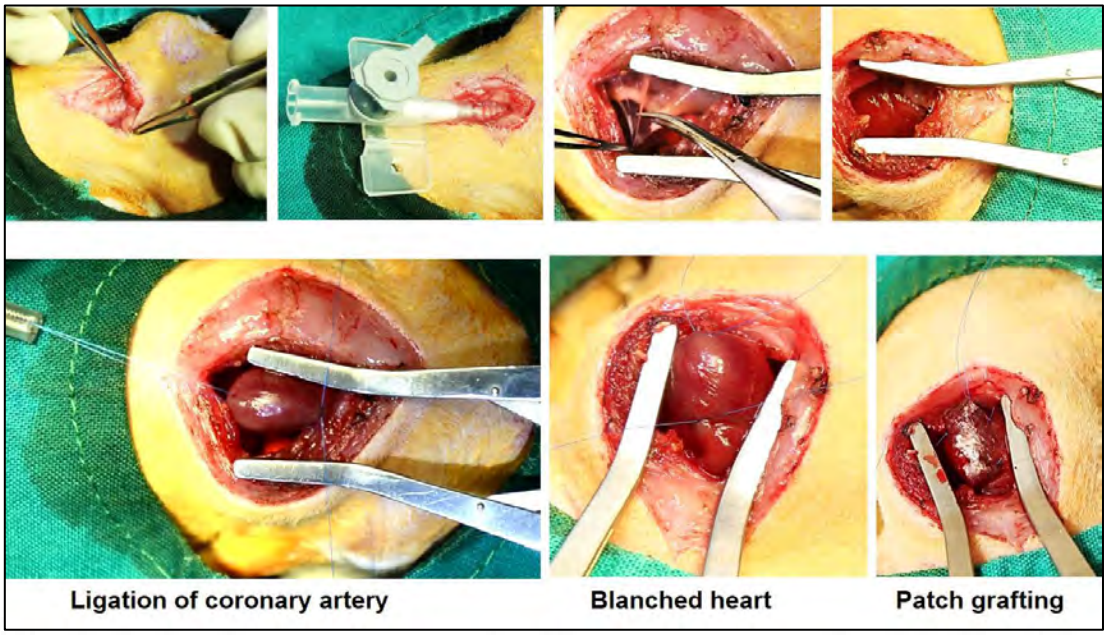

Figure 3: Establishment of myocardial infarction model and implantation of C-ECM as an epicardial graft

3.1.4.3 Clinical monitoring by estimation of cardiac biomarkers

Blood samples were collected from retro-orbital plexus of rats for serum analysis of cardiac biomarkers like CK, CK-MB and trop T at three time points: two days prior surgery (pre-surgery), 24 hours after surgery (post-surgery) and two weeks after surgery (terminal).

3.1.4.4 Histological evaluation

H&E staining is the most prominent stain used by pathologists to study the distribution of cells and tissue structure. For performing H&E staining, the sections were de-paraffinised in xylene and hydrated to water through descending grades of alcohol. Sections were treated in Harris's haematoxylin for 30 minutes, washed gently in water, differentiated in acid alcohol and blued in ammonia water. It was then treated in eosin stain for 2 min, washed gently in water, dehydrated through ascending grades of alcohol, cleared in xylene and mounted for microscopic evaluation (Drury, 1983). Images were captured using a BX51 microscope (Olympus Corporation, Japan).

3.1.5 Modification of C-ECM to enhance conductivity

3.1.5.1 Synthesis of gold nanoparticles (AuNPs)

AuNPs of 20 nm diameter were synthesized according to Turkevich's method (Turkevich *et al*, 1951). Tetrachloroauric acid solution (0.5mM) was boiled at 100℃ for 5 min with vigorous stirring. Trisodium Citrate (1%) was added, stirred for 5 minutes and cooled to room temperature. The synthesized AuNP was purified by centrifugation (Eppendorf centrifuge 5430R, Germany) at 7000 rpm for 20 minutes (Fig. 4). The pellet was suspended in Milli-Q water and filtered before storage in the dark at 4℃. Amine functionalisation of the gold nanoparticles was performed by adding a thiol compound, L-cysteine hydrochloride monohydrate. In this method, 1 mM solution (100µl) of L-cysteine hydrochloride monohydrate was added to 1 ml of the gold nanoparticle solution. After adding the thiol compound, the reaction mixture was incubated overnight at 4℃.

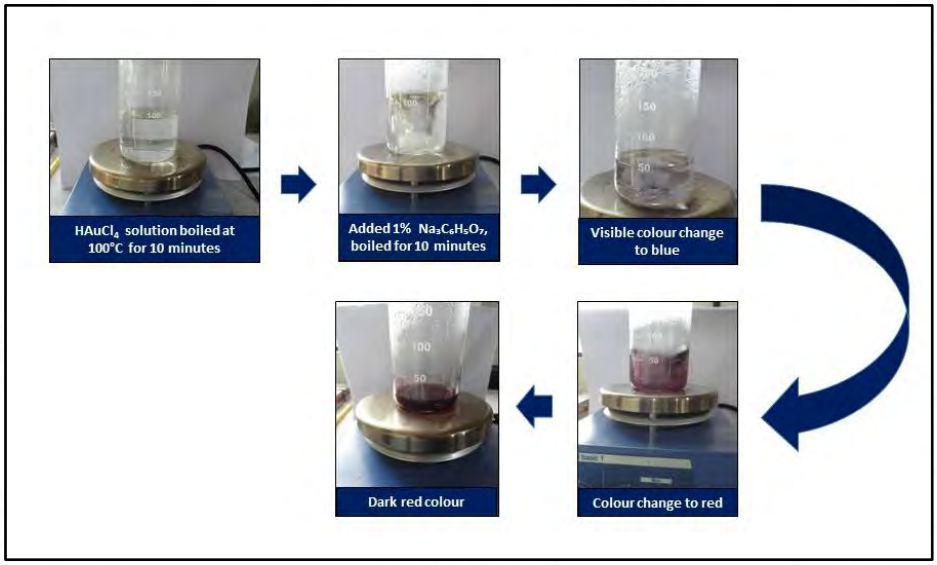

Figure 4: Schematic diagram for the preparation of gold nanoparticles

3.1.5.2 Characterisation of AuNPs

3.1.5.2.1 UV-Vis spectroscopy

The peak absorption wavelengths of the prepared gold nanoparticles were measured using a Varian Cary100.9.0 Spectrophotometer with the recommended 1 cm path length quartz cuvettes in the 400–800 nm wavelengths range. Absorbance

measurements in the visible range were used for evaluating the extent of functionalisation of the gold nanoparticles.

3.1.5.2.2 Transmission electron microscopy

The gold nanoparticle solutions with and without cysteine were adsorbed on the specimen grids after sonication and air-dried for 48 h. The samples were observed with a transmission electron microscope (Hitachi H-7650) at an accelerating voltage of 80 kV and the size measurements were performed using Image J software.

3.1.5.2.3 Dynamic light scattering

The stability of the gold nanoparticles after amine functionalisation was ascertained using a Malvern Zetasizer NanoZSVer.2.3 instrument. The measurements were made by diluting the samples with Milli-Q water in the ratio of 1:10 followed by sonication for 30 min at 25◦C. The zeta potentials were measured in triplicate using quartz cuvettes with a scattering angle of 173◦at a temperature of 25◦C and expressed as an average of 30 runs.

3.1.5.2 Preparation and characterisation of the gold nanoparticle modified scaffold

The scaffolds prepared by the method referred to in section **3.1.2** were used for the modification. The sheets were cut into discs of 15 mm diameter, packed, sterilized by ethylene oxide treatment and stored at room temperature until use. The binding of amine functionalised gold nanoparticles to the C-ECM scaffold was accomplished by using 1-Ethyl-3-(3-dimethyl aminopropyl)-carbodiimide (EDC) (Sigma Aldrich) and N-hydroxysuccinimide (NHS) (Molychem) chemistry. The reaction was characterised by the formation of covalent bonds between primary amines of gold nanoparticles and activated carboxylic groups of collagen in the C-ECM. Briefly, the scaffolds were immersed in a filtered solution of EDC (2 mM) and Sulfo-NHS (5 mM) in phosphate-buffered saline (PBS) for 15 min for the activation of carboxylic groups. Amine functionalised gold nanoparticles were then added in varying volumes (100, 500 and 1000 µl) to the reaction mixture and incubated with shaking for 24 hours. After the incubation, the crosslinking solution was removed and the scaffolds were washed with PBS for the next 48 hours. The scaffolds were air-dried and used for further characterisation. The resulting nanocomposite scaffold was designated as C-ECM AuNP.

3.1.5.2.1 Conductivity measurement

The conductivity of the scaffolds having a thickness in the range 0.1 to 0.2 mm and a diameter of 15mm were measured at 25 °C using a four-point probe system, Keithley in which two pairs of contacts are used to measure the conductivity. Voltage was kept constant throughout the experiment. Resistivity was calculated using the equation:

$$\rho = \frac{\pi * thickness\ of\ sample}{ln2 * conductance}$$

The inverse of the obtained resistivity value is taken as the conductivity of the sample.

3.1.5.2.2 Estimation of free amino groups

TNBS assay is a sensitive method used to quantitate free amino groups in a sample. For that, 10 mg of the scaffolds (C-ECM and C-ECM AuNP) were weighed out and incubated in 125 µl 0.1M $NaHCO_3$ buffer (pH 8-8.5) for 1 hour at room temperature followed by the addition of freshly prepared 0.05% TNBS solution at 40°C for 2 hours. Then, 375 µl 6 M HCl solution was added and incubated at 60°C for 90 min. The reaction mixture was diluted with distilled water and absorbance was measured at 340 nm (Biochrome, ASYS UVM 340, UK). The absorbance was correlated with free amino groups of 0.1 mg/mL glycine solution which was used to plot the standard curve.

3.1.5.2.3 FTIR spectroscopy

FTIR spectra of C-ECM and C-ECM AuNP were recorded in the range of 400–2000 cm^1 using a Nicolet 5700 FTIR Spectrophotometer (Nicolet Inc, Madison, USA) with a Diamond Attenuated Total Reflectance (ATR) accessory.

3.1.5.2.4 ESEM

The surface morphology of the pristine scaffold and the gold nanoparticle conjugated porcine C-ECM were investigated using an environmental scanning electron microscope (ESEM FEI, Quanta 200, USA) with an accelerating voltage of 15 kV. Samples were sputter-coated with gold before observation. The elemental identification of the scaffolds was studied using energy-dispersive X-ray spectroscopy (EDS) for the analysis of the characteristic X-rays emitted from the samples.

3.1.5.2.5 Surface profile measurement

Line profile measurement of the scaffolds was carried out using Talysurf CLI 1000, Taylor Hobson, UK for estimating the surface parameters Ra, Rq and Rp based on

measurement of 1mm scan length at 0.5µm spacing. Six line scans were averaged to get the mean roughness parameters.

3.1.5.2.6 Thermogravimetric analysis (TGA)

TGA was performed using the SDTQ600, simultaneous DTA–TGA system (TA Instruments Inc. Japan) according to the test method derived from ASTM E-1131-08. 5 mg of the sample was taken in a platinum cup and heated under an atmosphere of nitrogen at a heating rate of 10˚C per minute from room temperature to 600˚C with Calcined alumina used as reference material.

3.1.5.2.7 Enzymatic degradation assay

Enzymatic degradation of the scaffold was performed by the collagenase assay. Here, 1mg of the scaffold was weighed out and added 200µl of 0.1 M Tris (hydroxyethyl)aminomethane buffer with 0.25M$CaCl_2$, pH 7.4 for 1h at 37℃. Collagenase (600 units/ml) prepared in Tris-$CaCl_2$ buffer was added and incubated for various time points: 24h, 48h and 72h with constant shaking at 160 rpm at 37℃. After the predetermined incubation period, 100 µl supernatant was taken and added 2% Ninhydrin solution, boiled (Julabo TW 20, Germany) for 10 minutes. Twenty microliters of the final solution were diluted with distilled water and made up to 400 µl and read the optical density at 570nm.

3.1.6 Evaluation of the biocompatibility of the scaffold

3.1.6.1 Direct contact test

The cytocompatibility of H9c2 cells on the gold nanoparticle modified C-ECM AuNP scaffold was carried out as in section 3.1.3.2.

3.1.6.2 Live-dead staining

H9c2 cells were seeded on C-ECM AuNP scaffolds and the live-dead staining was performed as in section 3.1.3.3.

3.1.6.3 Cell viability

Cell viability of the scaffolds was confirmed by performing the MTT assay using the H9c2 cells seeded on scaffold for 3 days as in section 3.1.3.4.

3.2 Differentiation of rat cardiomyoblast cell line H9c2 and rat bone marrow mesenchymal stem cells to cardiomyocyte-like cells

3.2.1 Differentiation of rat cardiomyoblast cell line H9c2 to cardiomyocyte-like cells

3.2.1.1 Materials

DMEM High glucose (Sigma Aldrich), Bovine Serum Albumin (Himedia), Triton X 100, FBS (Gibco). Penicillin/Streptomycin 100 X (Himedia), TrypLE Express (Gibco), Paraformaldehyde (Merck), Retinoic acid (Sigma Aldrich), FITC conjugated phalloidin (P5282, Sigma), Hoechst (Invitrogen), Acrylamide (GE Healthcare, Sweden), Bis-acrylamide (GE Healthcare, Sweden), Trizma base (GE Healthcare, Sweden), Sodium dodecyl sulphate (GE Healthcare, Sweden), Ammonium persulphate (GE Healthcare, Sweden), TEMED (GE Healthcare, Sweden), β-mercaptoethanol (GE Healthcare, Sweden), Glycerol (Merck), Bromophenol blue (GE Healthcare, Sweden), Tris (GE Healthcare, Sweden), Glycine (GE Healthcare, Sweden), PVDF membrane (Bio Rad USA), Ponceau S solution (Sigma Aldrich), non–fat milk, Bovine serum albumin (Merck), Troponin T antibody (Developmental Studies Hybridoma Bank), Myo D (Abcam), Connexin 43 (Abcam), β-actin (Abcam), culture flasks (Himedia), 24 well plate, 6 well plate (Nunclon), Cell strainer 100µm (Himedia), MTT (Invitrogen).

H9c2 is a subclone of the original clonal cell line obtained from embryonic BD1X heart tissue or myocardium of *Rattus norvegicus* purchased from the National Centre for Cell Science, Maharashtra.

3.2.1.2 Differentiation of H9c2 to cardiomyocyte-like cells

Differentiation of H9c2 to cardiomyocyte-like cells was initiated by reducing the percentage of serum in the media followed by retinoic acid supplementation. H9c2 cells were plated at a density of 1*10^5 with normal serum (10%) conditions for one day to attain 80 % confluency. The addition of retinoic acid (1µM) to media containing 1% serum was performed daily for 5 days. All-trans-retinoic acid was prepared in DMSO and stored at -20°C protected from light to avoid degradation. The

differentiated cells were observed under a Phase contrast microscope (Olympus, Japan) for the change in morphology.

3.2.1.3 Phalloidin staining

H9c2 cells were seeded in chambered cover glass (Thermo Scientific™ Nunc™ Lab-Tek™) at a density of 5×10^4 cells per well and differentiated using retinoic acid for 5 days. For staining, the medium was removed and washed with PBS (1X) for 3 times. The cells were fixed with 3.7% paraformaldehyde for 30 minutes. Again washed with PBS thrice. Cells were permeabilised with 0.1%Triton X-100 for 5 minutes and washed with PBS. Cells were stained with 5µg/ml (1:100 dilution) phalloidin-FITC for 40 minutes at room temperature in dark. Washed with PBS thrice and Hoechst (Stock: 10mg/ml, working solution 1:2000) was added and incubated for 5 minutes at room temperature in dark. Images were captured using a fluorescence microscope (Leica, Germany).

3.2.1.5 Western blotting

H9c2 cells were seeded in T 25 flasks containing DMEM media with 10% serum till attaining confluency. Other than the control flask, the media was changed to differentiation media and replaced every day for 5 days. Then, the media was removed, washed with PBS and trypsinised. The contents were centrifuged at 5000 rpm for 20 minutes at 4°C. The pellet was resuspended in 1 ml PBS and again centrifuged at 5000 rpm for 20 minutes at 4°C. PBS was removed and added phospholysis buffer (1% NP40, 10% glycerol, 137mM sodium chloride, 20mM Tris HCl-pH 7.4, 1µg/ml aprotinin, 11µg/ml leupeptin, 20mM sodium fluoride, 1mM sodium pyrophosphate, 1mM sodium orthovanadate, 1% Triton X-100 and 5mM phenylmethylsulfonyl fluoride based on the pellet size. This was incubated in ice for 45 minutes with intermittent shaking. Following that, the contents were centrifuged at 10000 rpm for 20 minutes at 4°C. The supernatant was carefully taken and stored at -80°C until used. Bradford method was used to determine the protein concentration and bovine serum albumin was taken as the standard. After denaturation for 5 min at 95°C in protein sample buffer supplemented with β-mercaptoethanol, equivalent amounts of total protein (50 µg) were separated by electrophoresis in 12% SDS-PAGE at 70 V

and electrophoretically transferred to a PVDF membrane at 100 V. Ponceau S stain was used for the detection of bands and then Ponceau stain was removed by washing with Tris Buffer Saline -Tween (TBST). After blocking with 5% milk in TBST (20 mM Tris-HCl, pH 8; 150 mM NaCl and 0.1% Tween 20) for 20 minutes at room temperature. The membranes were incubated overnight at 4°C with the specific antibodies: mouse anti-rabbit troponin T2, cardiac type [RV-C2] (DSHB), anti-myoD1 antibody (Abcam), anti-connexin 43/ GJA1 antibody [CXN-6] (Abcam). Then the membranes were washed with TBST thrice. The blots were treated with HRP-conjugated anti-mouse secondary 1:1000 prepared in 0.5g BSA in TBST for 1 hour. The unbound secondary antibody was removed by washing with TBST thrice. Enhanced Chemiluminescence (ECL), a luminol based substrate was used to detect the antigen-antibody complex and imaged by a luminescent image analyser (LAS 4000 FUJI). The membrane was washed with TBST and re-probed with an anti-β actin antibody (Abcam) (1:1000) and was developed by the ECL method and imaged.

3.2.2 Differentiation of rat bone marrow-derived mesenchymal stem cells to cardiomyocyte-like cells

3.2.2.1 Isolation, culture and characterisation of rat bone marrow-derived mesenchymal stem cells (BMSCs)

3.2.2.1.1 Materials

DMEM high glucose (Sigma Aldrich), Bovine Serum Albumin (Himedia), Triton X 100, FBS (Gibco). Penicillin/Streptomycin 100 X (Himedia), TrypLE Express (Gibco), anti-CD90/Thy 1 antibody (FITC.MRC OX-7) FITC ab226, anti-CD 34 antibody [ICO-115] (Phycoerythrin) ab 187284, anti-CD45 antibody [MRC OX-1] (FITC) ab 33916, Endoglin/CD 105 MEM-226 FITC (NB 500-453), 5' Nucleotidase/CD 73 (45M3B4) PE (NBP2-25235PE), paraformaldehyde, dexamethasone (Sigma Aldrich), β-glycerophosphate disodium salt hydrate (Sigma Aldrich), L-ascorbate-2-phosphate sesquimagnesium salt hydrate (Sigma Aldrich), Alizarin red S (Sigma Aldrich), Insulin (Gibco, USA), Isobutyl methyl xanthine, Oil Red O (Sigma Aldrich), Isopropanol (Merck), Pyruvic acid sodium salt (Himedia), TGF-β3 (Gibco), Alcian blue 8GX for microscopy (Molychem), Glacial acetic acid

(Merck), Indomethacin (Sigma Aldrich), culture flasks (Himedia), 24 well plate, 6 well plate (Nunclon), Cell strainer 100µm (Himedia), MTT (Invitrogen)

3.2.2.1.2 Animal ethics

All animals were handled humanely with due care for their welfare. The care and management of the animals will comply with the regulations of the Committee for the Purpose of Control and Supervision of Experimental Animals (CPCSEA), Govt. of India. All the animal experiments were carried out after getting prior approval from the Institutional Animal Ethics Committee (IAEC) and performed under the approved institutional protocol. The IAEC number for this study is SCT/IAEC-196/November/2016/90.

3.2.2.1.3 Institutional Committee for Stem Cell Research

Bone marrow mesenchymal stem cells (MSCs) were isolated from Sprague Dawley rats. All the experiments with MSCs were carried out after getting the approval from the Institutional Committee for Stem Cell Research (IC-SCR). The approval number is SCT/IC-SCR/38/Mar/ 2017.

3.2.2.1.4 Isolation of rat bone marrow-derived mesenchymal stem cells

Mesenchymal stem cell isolation was carried out from femurs of young Sprague Dawley rats. Animals were killed by CO_2 inhalation and the hair was shaved from both the legs. After disinfecting with spirit, femurs were collected in PBS containing 1X antibiotic. In laminar flow, muscle tissues were removed and the femur was cleaned. The femur was then cut at an epiphysis level using a sterile bone cutter and bone marrow was flushed out with DMEM serum-free medium using a 1ml syringe. Then, it was mixed well by pipetting several times and strained using a 100mm cell strainer to remove any muscle debris. The cell suspension was centrifuged at 600 rcf for 10 min (Eppendorf centrifuge 5430R). The cell pellet was resuspended in 2 mL of DMEM containing 20% FBS. This cell suspension was seeded in a 75 cm^2 cell culture flask and incubated at 37 °C in a carbon dioxide incubator (Thermo Electron Corporation Forma Series II Water Jacketed CO_2 Incubator). The next day, the medium was changed to remove unattached cells and replenished with fresh DMEM containing

20% serum. Thereafter medium change was performed every 2nd day. Upon confluence, cells were trypsinised and seeded at a split ratio of 1:3.

Doubling time was calculated by seeding 1*10^4 cells in a 12 well plate containing DMEM medium with 20% serum. The total number of cells in the wells at the third, fifth and seventh days of incubation were counted using a haemocytometer after trypsinisation followed by centrifugation (Eppendorf centrifuge 5430R) at 600 rcf for 10 minutes. The equation used for the calculation is as follows:

$$Doubling\ time = t \times log\ 2/\log(Nt - No),$$

where t is the time in hours, Nt is the cell count at the time 't' and No is the initial cell count.

3.2.2.1.5 Characterisation of rat bone marrow-derived mesenchymal stem cells

Mesenchymal stem cells isolated were characterized for the presence of stem cell markers by flow cytometry and immunostaining. The differentiation potential of the mesenchymal stem cells was evaluated by multilineage differentiation to adipocytes, osteocytes and chondrocytes. According to the Mesenchymal and Tissue Stem Cell Committee of the International Society for Cellular Therapy, the minimal criteria to define MSC are the following. MSC must be plastic-adherent, must express positive markers, lack expression of negative markers and must differentiate to osteoblasts, adipocytes and chondroblasts *in vitro*.

3.2.2.1.5.1 Expression of markers by flow cytometry

Bone marrow mesenchymal stem cells were cultured on 75cm^2 culture flasks and harvested by adding TrypLE Express. The cells were gently detached from the dish and passed through a cell strainer of pore size 100µm to get a single cell suspension. Then centrifuged at 400g for 5min to get the cell pellet. The pellet was resuspended in 1ml 1X PBS and counted. After counting, the cells were fixed in 3.7% paraformaldehyde in 1X PBS for 30 minutes and pelleted by centrifugation at 400g for 10 minutes. Cells were washed with 1X PBS for 5 minutes. The non-specific binding of antibodies was blocked by incubating cells in 1% Bovine serum albumin in 1X PBS for 10 minutes. Then cells were incubated with conjugated primary antibodies for 45 minutes in dark followed by centrifugation at 400g for 10 minutes. The pellet was

resuspended in 300µl of 1X PBS and centrifuged at 400g for 5 minutes. Flow cytometry analysis (BD FACSAria II) was carried out after resuspending the pellet in 1X PBS.

3.2.2.1.5.2 Expression of markers by immunostaining

This technique is used to detect the distribution and localization of proteins within individual cells by using specific antibodies to identify the target protein. BMSCs were cultured in a chambered cover glass system with a density of $1x10^4$ cells per well for two days. On the third day, cells were fixed with 3.7% Paraformaldehyde for 30 minutes and washed thrice with 1X PBS. The non-specific binding of antibodies was prevented by the addition of 1% BSA in PBS for 10 minutes. Then primary antibodies were added and incubated at 4°C in a humidified chamber overnight. On the next day, PBS wash was given thrice and added Hoechst (1:2000) and incubated for 10 minutes at room temperature in dark. It was again washed with PBS three times and fixed with a coverslip. Imaging was done using a confocal microscope (Olympus).

3.2.2.1.5.3 Multilineage differentiation of rBMSCs

Mesenchymal stem cells are multipotent having the ability to differentiate into cells of bone, cartilage and fat cells. To study the multilineage differentiation potential, 3×10^5 cells at passage 3 were seeded on to 6 well plates with DMEM and 20% FBS. After attaining confluence, the medium was changed to adipogenic, chondrogenic and osteogenic media after every two days and cultured for 21 days.

For adipogenic differentiation, the cells were cultured in DMEM containing 20% FBS, 10 µg/ml Insulin, 500 µM Isobutyl methylxanthine, I00 µM Indomethacin and 1 µM Dexamethasone (prepared in absolute ethanol). For osteogenic differentiation, the cells were cultured in DMEM with 20% FBS, 100 nM Dexamethasone, 10 mM β-glycerophosphate and 0.05mM L-Ascorbate-2-phosphate. For chondrogenic differentiation, the cells were cultured in DMEM with 20% FBS, 1mM Sodium pyruvate, 100nM Dexamethasone, 37.5 µg/ml L-Ascorbate-2-phosphate and 10ng/ml Tissue growth factor-beta 3. After 21 days of culture, the media was removed and the differentiated cells were fixed with 3.7% paraformaldehyde. The differentiated adipocytes were stained with Oil Red O, osteoblasts with Alizarin Red and

chondrocytes with Alcian blue and imaged using phase contrast microscope (Olympus, Japan).

3.2.2.1.5.3.1 Staining for adipocytes

The stock solution (0.5%) of Oil Red O was prepared in Isopropanol by gentle mixing. Then the working solution was prepared by mixing 3 parts of the stock solution with 2 parts of distilled water, kept for 10 minutes and filtered. This was prepared 15 minutes before use. For staining the cultured cells, the media was removed and washed the cells gently with PBS twice. The cells were fixed with 3.7% paraformaldehyde for 30 minutes and washed with PBS twice. Added 60% Isopropanol to the cells and kept for 5 minutes. Further, the cells were incubated in the Oil Red O working solution for 20 minutes. After that, cells were washed with distilled water about 2-3 times, then observed under phase contrast microscope (Olympus, Japan).

3.2.2.1.5.3.2 Staining for osteoblasts

Alizarin red staining solution (2%) was prepared in distilled water and the pH was adjusted to 4.1- 4.3 with 10% Ammonium hydroxide. Initially, the cell culture media was removed, washed with PBS and fixed with 3.7% paraformaldehyde for 30 minutes. After incubation, the cells were washed with PBS and stained with Alizarin red solution for 45 minutes in dark. The staining solution was removed, rinsed with distilled water and imaged under phase contrast microscope (Olympus, Japan).

3.2.2.1.5.3.3 Staining for chondrocytes

Alcian blue (1%) solution was prepared in 0.1N HCl. The media was removed from cells, washed with PBS and fixed with 3.7% paraformaldehyde for 30 minutes. It was removed and washed thrice with PBS. Alcian blue stain was added and incubated for 1 hour. It was then rinsed with 0.1 N HCl and again with PBS, images were captured using phase contrast microscope (Olympus, Japan).

3.2.2.2 Cytocompatibility evaluation

Direct contact test was conducted to evaluate the compatibility of the scaffolds and isolated mesenchymal stem cells. The experiment was carried out as described in section 3.1.3.2.

3.2.2.3 Differentiation of rBMSC to cardiomyocyte-like cells

3.2.2.3.1 Culture conditions

BMSCs were cultured with 20% serum-supplemented DMEM with high glucose and 0.1 % anti-microbial and anti-mycotic solution.

3.2.2.3.2 Morphological evaluation

BMSCs at passage 3 were used for the differentiation experiment. Cells at a density of $5x10^4$ were seeded in a 24 well plate and allowed to become 80 % confluency under 20% serum and DMEM media conditions. Then, 10µM Azacytidine was prepared, added to cells and incubated for 24 hours. The differentiation media was changed to DMEM media and cultured for 7 days with media change on every second day. The change in morphology was assessed using phase contrast microscope (Olympus, Japan).

3.2.2.3.3 Western blotting

Whole protein was extracted from control and 7 day differentiated cells using phospholysis buffer. Similar to the procedure in section 3.2.1.6, 50µg of protein sample was separated by electrophoresis in 12% SDS-polyacrylamide gels at 70 V and electrophoretically transferred to a polyvinylidene difluoride membrane at 100 V. The was blocked in 5% non-fat milk in TBST incubated with primary antibodies: Mouse anti-Rabbit Troponin T2 cardiac type [RV-C2] (DSHB), Anti-MyoD1 antibody (Abcam), Anti-Connexin 43/ GJA1 antibody [CXN-6] (Abcam) (1:1000) at 4°C overnight. After incubation, the membrane was washed 3 times with TBST and incubated with appropriate secondary antibody. The presence of protein bands of expression of Cardiac troponin T, Myo D, Connexin-43 and β-actin were imaged using a luminescent image analyser (LAS 4000 FUJI).

3.3 Functional evaluation of cardiac-patches in a rat model of non-fatal myocardial infarction

3.3.1 Materials

Ketamine Hydrochloride, Xylazine Hydrochloride, Isoflurane, Betadine, 7-0 Prolene suture, 3-0 Mersilk suture, 3-0 Vicryl suture, Ceftriaxone, Meloxicam, Tetracycline, Centrifuge tubes, surgical scissors, forceps, curved forceps, cautery forceps, scalpel holder, needle holder, chest retractor, Formalin (Molychem), Disodium hydrogen phosphate (Merck), Sodium dihydrogen phosphate (Merck), Paraffin wax with ceresin (Merck), Harris's haematoxylin (Sigma Aldrich, India), Eosin (Merck), Direct red 80 (Sigma Aldrich), Acid fuchsin (Sigma Aldrich), Phosphomolybdic acid (Merck), Aniline blue (Sigma Aldrich), Picric acid (Merck), Glacial acetic acid (Merck), Ethyl alcohol, (Himedia), Ferric chloride (Molychem), 2-propanol (Merck), Xylene (Merck), Ammonia (Merck), Hydrochloric acid (Merck), Mounting medium (Leica),

3.3.2 Animal ethics

All animals were handled humanely, without making pain or distress and with due care for their welfare. The care and management of the animals will comply with the regulations of the Committee for the Purpose of Control and Supervision of Experimental Animals (CPCSEA), Govt. of India. All the animal experiments were carried out after getting prior approval from Institutional Animal Ethics Committee (IAEC) and performed under the approved institutional protocol. The B form number for this study is SCT/IAEC-291/JANUARY/2019/99.

3.3.3 Myocardial infarct model

Same as in section **3.1.4.2.** There were three groups for the study: Control, C-ECM and C-ECM AuNP.

3.3.4 Treatment of MI with scaffolds

Same as in section **3.1.4.3.**

3.3.5 Clinical monitoring

3.3.5.1 Estimation of cardiac biomarkers

Blood samples were collected from the retro-orbital plexus of rats for serum analysis of cardiac biomarkers like creatinine phosphokinase (CK), creatinine kinase

muscle/brain (CKMB) and cardiac troponin T (Trop T) at three time points: two days prior surgery (pre-surgery), 24 hours after surgery (post-surgery) and 4 weeks after surgery (terminal).

3.3.5.2 Electrocardiogram (ECG)

One week and 4 weeks after surgery, animals were anaesthetized with 1.5% Isoflurane at 100% O_2. Three electrodes were placed on each limb and about three recordings were taken using the BIOPAC Student Lab system once the peaks stabilise. Baseline values were obtained for all the animals before surgery. Elevation or depression in the ST segment indicated successful MI. Quantification of various parameters from the ECG waveforms such as heart rate, RR Amplitude, ST elevation, QT interval, QRS duration, QRS amplitude using the BSL Analysis 4.1 software.

Figure: 5 BIOPAC MP45 machine for ECG recording (Adapted from http://www.oamk.fi/~jjauhiai/opetus/fsk/biopac-ECG%201.pdf accessed on 10/6/2020)

Figure: 6 Positioning of electrodes for ECG recording

3.3.5.3 Echocardiography (ECHO)

To study the structural changes associated with MI induction and subsequent graft placement, M-mode para-sternal short-axis view images were taken using Philips HD11 XE Ultrasound system before surgery, one and four weeks post-surgery. Animals were anaesthetized with an IP injection of Ketamine Hydrochloride (15-25mg/kg). The following measurements were recorded: end-diastolic septum thickness, left ventricular end-diastolic internal diameter (LVIDd), left ventricular end-diastolic posterior wall thickness, end-systolic septum thickness, left ventricular internal dimension at end-systole (LVIDs) and left ventricular posterior wall thickness at end-systole. Changes in left ventricular dimensions were obtained from which ejection fraction (EF) and fractional shortening (FS) were calculated using the following equations:

$$\mathrm{EF} = \frac{\left((\mathrm{LVIDd})^3 - (\mathrm{LVIDs})^3\right)}{(\mathrm{LVIDd})^3} \times 100$$

$$\mathrm{FS} = \frac{(\mathrm{LVIDd}) - (\mathrm{LVIDs})}{(\mathrm{LVIDd})} \times 100$$

Figure: 7 Positioning of the probe for ECHO measurement

Data analysis was carried out by Two-way ANOVA followed by Sidak's multiple comparisons test (p-value <0.05).

3.3.6 Necropsy and gross pathology

All animals were euthanized after four weeks of the induction of MI, the gross lesions were evaluated and fixed in 10% neutral buffered formalin for histomorphological evaluation. Three transverse sections from the lower side of the formalin-fixed hearts were used for histological evaluation (Fig. 8). Gross images were taken and traced the sketch of the sections using Adobe Photoshop software for representation.

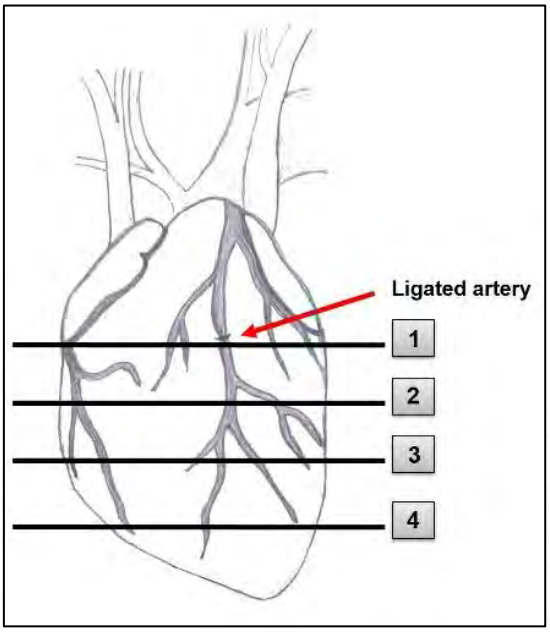

Figure: 8 Sampling plan adopted for histology

3.3.7 Heart weight to body weight ratio

Cardiac hypertrophy can be expressed as the increase in the ratio of heart weight to body weight. So, at the time of necropsy, the body weight and heart weight of all the experimental animals were noted, calculated the ratio of heart weight to body weight (HW/BW).

3.3.8 OES-ICP

C-ECM AuNP contains gold nanoparticles incorporated with ECM. For the detection of gold released *in vivo* from the scaffold to other organs, Optical Emission Spectroscopy with Inductively Coupled Plasma (Perkin Elmer OES-ICP, Model: 5300DV) was performed. Fresh tissue samples (brain, lungs, liver and kidney) weighing 500 mg were digested in an acid mixture and diluted to known volume using de-ionised water and analysed. The concentration of gold in the solution was determined from the calibration plot obtained by analysing the standard solution.

3.3.9 Histology

Three transverse sections from each of the formalin-fixed hearts were used for histological evaluation. Tissue bits were processed using an automated tissue processor Leica TP1020 (Leica Biosystems, Germany) and embedded in paraffin wax. Four micrometer thick tissue sections were prepared using Leica RM2255 microtome

(Leica Biosystems, Germany). These sections were used for various staining procedures for further evaluation.

3.3.8.1 H & E Staining

Same as in section **3.1.4.4.** Morphometric analysis of all the images captured using a BX51 microscope (Olympus Corporation, Japan) was done using Image-Pro version 3DS6.1 software (Media Cybernetics, Silver Spring, MD).

3.3.8.2 Cardiomyocyte diameter and number

An increase in cardiomyocyte diameter and number were also used to define hypertrophy. The diameter of the longitudinally cut cardiomyocytes is the major cell diameter (Dmaj, µm) and the diameter of those cut at cross-sectional planes is defined as the minor cell diameter (Dmin, µm). The diameter of cells in the right ventricle (RV), left ventricular free wall (LVFW) and interventricular septum (IVS) was calculated from the H&E images (30 images from each sample). The number of cardiomyocytes in the interventricular septum was also counted (6 images from each group).

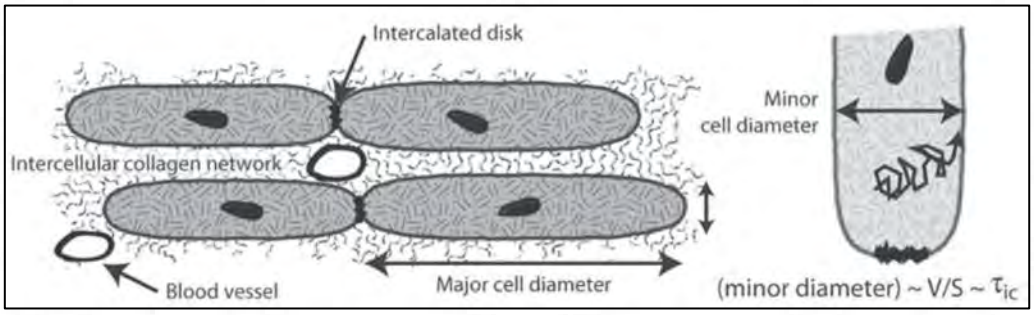

Figure: 9 Diameter of cardiomyocytes, Adapted from (Coelho-Filho *et al*, 2013)

3.3.8.3 Immunohistochemistry

The lymphocytic cells present in the infarct zone were detected using CD4 and CD8 antibodies. Macrophages in the infarct region were detected by immunohistochemistry using CD68 antibody. Neovascularisation at the infarct site was studied using immunostaining with antibodies against CD31 and alpha smooth muscle cell actin. The presence of proliferating cells in the vicinity of the graft was detected by performing immunohistochemistry with an antibody against proliferating cell nuclear

antigen. Cell to cell connections was studied and quantified using Connexin 43 antibody stained tissues. Myofibroblasts in the infarct region were detected by immunohistochemistry using α-smooth muscle cell actin antibody. All these reactions were detected using a Supersensitive polymeric-HRP detection system (BioGenex Laboratories, USA) and counterstained using Haematoxylin. The images were captured by DP71 camera loaded on to a BX51 microscope (Olympus Corporation, Japan) and quantified using Image Pro version 3DS6.1 software (Media Cybernetics, Silver Spring, MD).

Table 1: List of antibodies used for immunohistochemistry

Sl. No:	Target	Host	Dilution	Company	Cat. No:	Retrieval buffer
1.	CD4	Mouse	1:100	Santa Cruz Biotechnology	(MT310):sc 19641	Citrate buffer, pH 6.8
2.	CD8	Mouse	1:400	Abcam	[OX-8] (ab33786)	Citrate buffer, pH 6.8
3.	CD68	Mouse	1:100	Abcam	ab201340	Citrate buffer, pH 6.8
4.	α-Smooth muscle actin	Mouse	1:300	Santa Cruz Biotechnology	(B4):sc 53142	Citrate buffer, pH 6.8
5.	CD31	Rabbit	1:400	Novus Biologicals	NB100-2284	Citrate buffer, pH 6.8
6.	Connexin 43	Mouse	1:200	Abcam	ab11369	Citrate buffer, pH 6.8
7.	PCNA	Mouse	1:400	Santa Cruz Biotechnology	(PC10): sc-56	Citrate buffer, pH 6.8

3.3.8.4 Picro sirius red staining

Picro sirius red is used to stain collagen present in the tissue samples. Sections were deparaffinised to water and incubated in Weigert's haematoxylin solution for 15 minutes. It was washed in tap water for 10 minutes and stained with picro sirius red solution for 90 minutes. After the incubation, the sections were washed with acidified water twice to prevent the loss of stain. The sections were then dehydrated, cleared in xylene and mounted in Leica mounting medium. Using the image analysis software, the infarct area and total area of the heart were measured.

3.3.8.5 Masson's trichrome staining

Sections were also stained for collagen using Masson's trichrome stain to measure the area of tissue damage due to MI. Briefly, the tissue sections were dewaxed in three changes of xylene, dehydrated using serial grades of isopropyl alcohol (70%, 80%, 90% and 100%) and fixed in Bouin's solution for 1hour at 60℃. It was washed in running tap water till the yellow colour was removed. The sections were treated with Weigert's iron haematoxylin solution for 10 minutes and washed with running tap water for 5 minutes followed by treatment with 1% acid alcohol for 1 minute. Bluing was done using ammonia water for 2 minutes and rinsed with distilled water. The sections were stained using acid fuchsin for 5 minutes and rinsed with water. Next, the sections were treated with a 5% phosphomolybdic acid solution for 5 minutes. Then the sections were transferred to an aniline blue solution and incubated for 20 seconds, then rinsed with 1% acetic acid solution for 2 minutes. Finally, the sections were dehydrated, cleared using xylene and mounted.

Further using the trichrome stained sections, area measurement of RV, LVFW, infarct and IVS from each of the three transverse sections were done using the same software tool to predict the extent of hypertrophy with and without the assistance of the graft. Fibrotic areas were also quantified using the image analysis software (30 images per sample) and calculated as percentage fibrosis with the total area of the image.

3.3.8.6 Herovici's staining

To differentiate between young and mature collagen, Herovici's staining was performed. The sections were dewaxed with three changes of xylene and dehydrated using ascending grades of isopropyl alcohol (70%, 80%, 90% and 100%) followed by washing in running tap water for 5 minutes. Then the slides were treated with Weigert's iron Haematoxylin staining solution for 20 minutes, washed in running water for 5 minutes. In the next step, sections were treated with Herovici staining solution for 2 minutes followed by treatment with 1% Acetic acid. Further, the sections were dehydrated, cleared and mounted.

Images were captured using a BX51 microscope (Olympus Corporation, Japan) using Image-Pro version 3DS6.1 software (Media Cybernetics, Silver Spring, MD). Young and mature collagen in the infarct region was differentiated and quantified using the image analysis software. The area occupied by collagen type I and III were calculated as well (30 images per sample).

3.3.10 Statistical analysis

Results were analysed using GraphPad PRISM 6.01 software. One–way ANOVA or two-way ANOVA followed by multiple comparisons with Tukey's test was performed to compare between groups. An α level of $p<0.05$ was considered to indicate a significant difference between the groups.

4. RESULTS

4.1 Evaluation of the properties of C-ECM and its suitable modifications for cardiac tissue engineering

4.1.1 Preparation of C-ECM scaffold

The parent scaffold used for the study was prepared by manually delaminating various tissue layers of porcine gall bladder and recovering the extracellular matrix, as reported earlier from the host laboratory, after controlled crosslinking of biomolecules by *ex-situ* incubation in 10% NBF for 30-36 hours. Pre-freezed hydrated sheets were lyophilised for about 16 hours to form dry sheets (Fig. 10). Discs of 15 mm diameter were cut using a mould for further experiments.

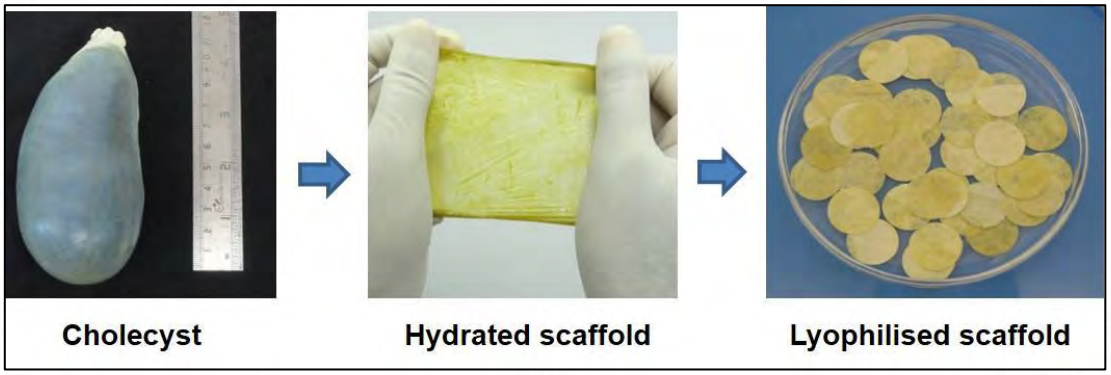

Figure 10: Schematic diagram showing the steps in the preparation of scaffold from porcine cholecyst

4.1.2 Evaluation of the cytocompatibility of the C-ECM scaffold

4.1.2.1 Direct contact test

There was no sign of cell detachment, lysis or vacuolization when the scaffold was in contact with the H9c2 monolayer for 24 hours (Fig. 11). Cellular lysosomes were stained in red colour as only viable cells uptake neutral red dye (Fig. 11 B and C).

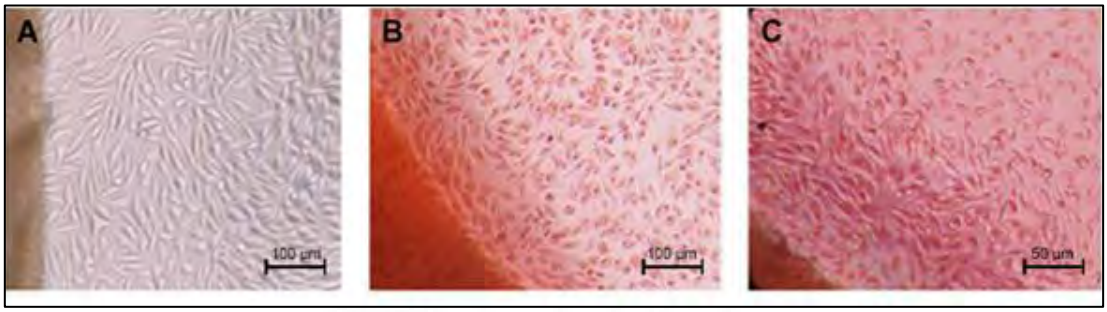

Figure 11: Direct contact test of C-ECM (A) Phase contrast image of C-ECM on H9c2 monolayer, (B & C) viable cells stained with neutral red dye (n=3)

4.1.2.2 Live-dead staining

The viability of H9c2 cells cultured on C-ECM was visualised by staining with FDA and PI. The results indicated that the majority of the cells were viable up to 24 hours (Fig. 12).

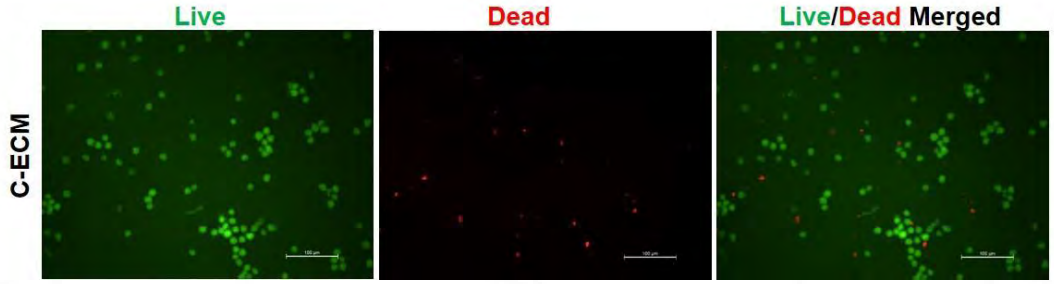

Figure 12: Live-dead staining of C-ECM. Fluorescent microscopic images of H9c2 cells seeded on C-ECM stained with FDA (green) and PI (red) for live and dead cells respectively (n=3). Scale bar indicates 100 µm.

4.1.2.3 MTT assay

The H9c2 cells cultured on C-ECM for 3 days showed a cell viability of 81.2 ± 2.76% (Fig. 13). From the statistical analysis, it was clear that no significant difference was observed between the C-ECM scaffold and the control indicating cytocompatibility of C-ECM.

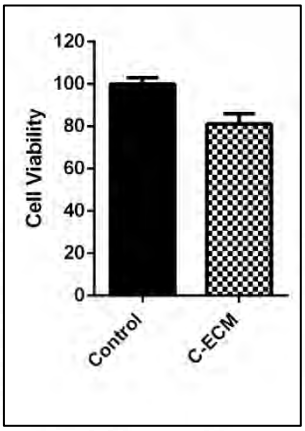

Figure 13: Cell viability of C-ECM. Bar graph representing the percentage viability of cells seeded on C-ECM and tissue culture plastic (control), n=3.

4.1.3 Establishment of myocardial infarction model and implantation of C-ECM as an epicardial graft

4.1.3.1 Clinical monitoring by estimation of cardiac biomarkers

There was an elevation in the level of trop T, CK and CK-MB at 24 hours after ligation of the coronary artery, indicating the induction of myocardial infarction in all the experimental rats (Fig. 14).

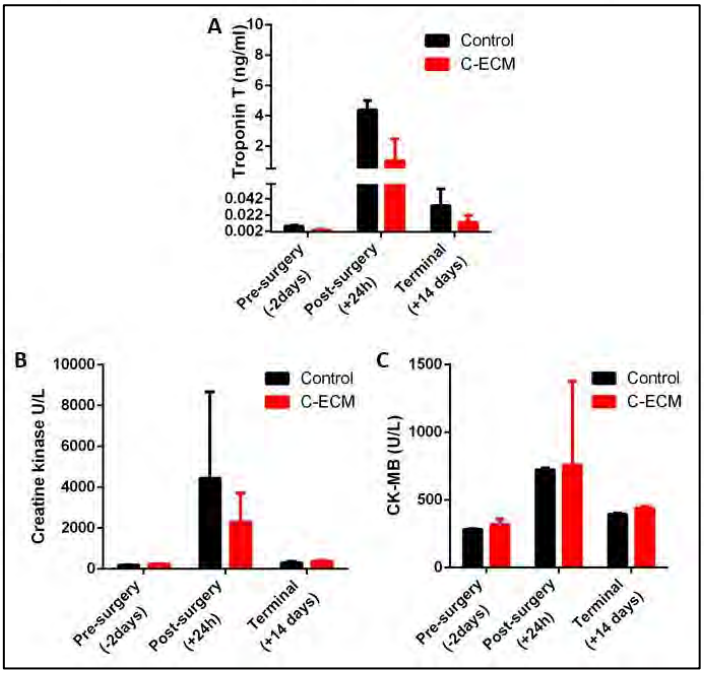

Figure 14: Serum biochemistry (A) Bar graph showing the elevation of trop T (B) CK and (C) CK-MB at 24h after MI induction surgery n=3.

4.1.3.2 Gross and histological evaluation

Gross morphology of the hearts explanted after 2 weeks, showed visible tissue necrosis which indicated successful MI induction in all animals. In addition, there was integration of the C-ECM with the host tissue in the test group suggesting its appropriateness as a cardiac-patch (Fig. 15).

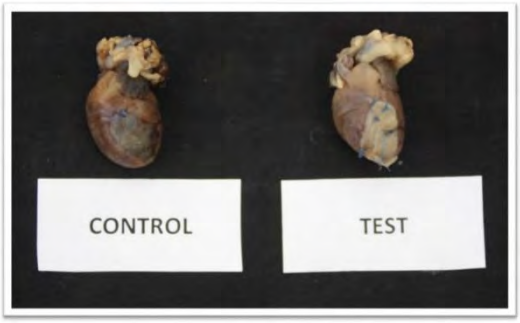

Figure 15: Gross photographs of control and test (C-ECM grafted) hearts after fixation in 10% NBF for 2 days

The healing response in rats, two weeks after MI induction without graft and with C-ECM indicated signs of myocardial necrosis (Fig. 16). Thus, the animal model for MI induction was established and the grafting of C-ECM on to the heart was achieved.

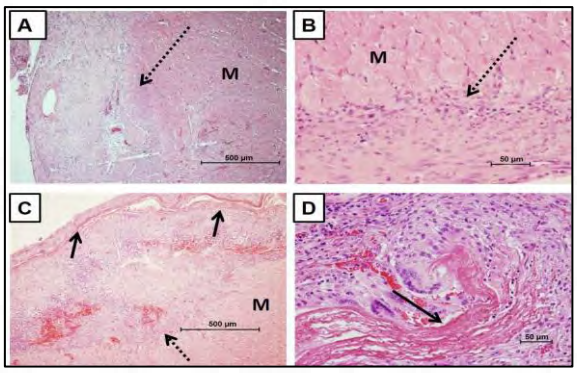

Figure 16: Light micrographs of (A, B) control and (C, D) C-ECM grafted rats depicting tissue necrosis (black dotted arrow) due to surgically induced MI and the integration of graft (black arrow) in the C-ECM group. M denotes muscle tissue. Scale bar indicates 500 and 50 µm.

4.1.4 Modification of C-ECM to enhance conductivity

4.1.4.1 Synthesis of gold nanoparticles (AuNPs)

Gold nanoparticles were synthesized by a conventional citrate reduction method followed by amine functionalisation with cysteine which was visually recognised by a colour change from a cherry red to blue indicating the functionalisation of the bare gold nanoparticles (Fig. 17).

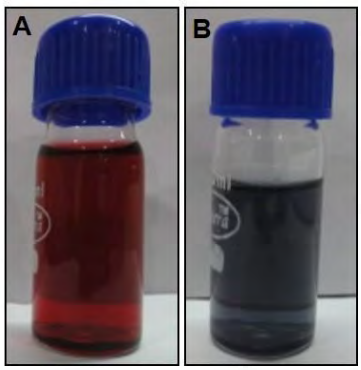

Figure 17: Photographs of gold nanoparticles. (A) Red coloured bare gold nanoparticles and (B) blue coloured amine functionalised gold nanoparticles

4.1.4.2 Characterisation of AuNPs

4.1.4.2.1 UV-Vis spectroscopy

In the UV-Vis spectra, the peak at 523 nm indicated the absorption maxima of bare citrate capped gold nanoparticles (Fig.18). After the amine functionalisation of the bare gold nanoparticles, the functionalised nanoparticles showed a shift in the peak at 686 nm indicating the Au-S bond formation.

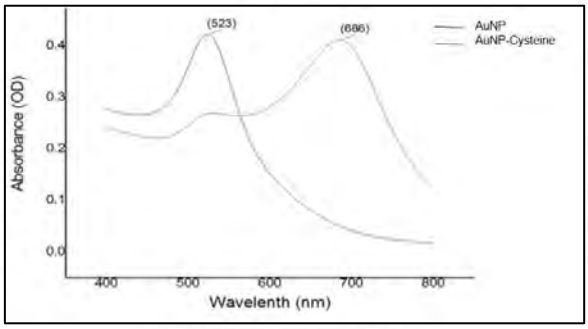

Figure 18: Absorbance spectra of uncapped gold nanoparticle (AuNP) and amine functionalised gold nanoparticle (AuNP-Cysteine) in the visible region

4.1.4.2.2 Transmission electron microscopy

Most of the gold nanoparticles were spherical in shape as observed by TEM, indicating that the gold colloid solution was monodispersed (Fig. 19 A). The size of the gold nanoparticle was measured and it was found to be 20 nm. The electron micrographs of amine functionalised nanoparticles were also spherical in shape with size about 20nm (Fig. 19 B).

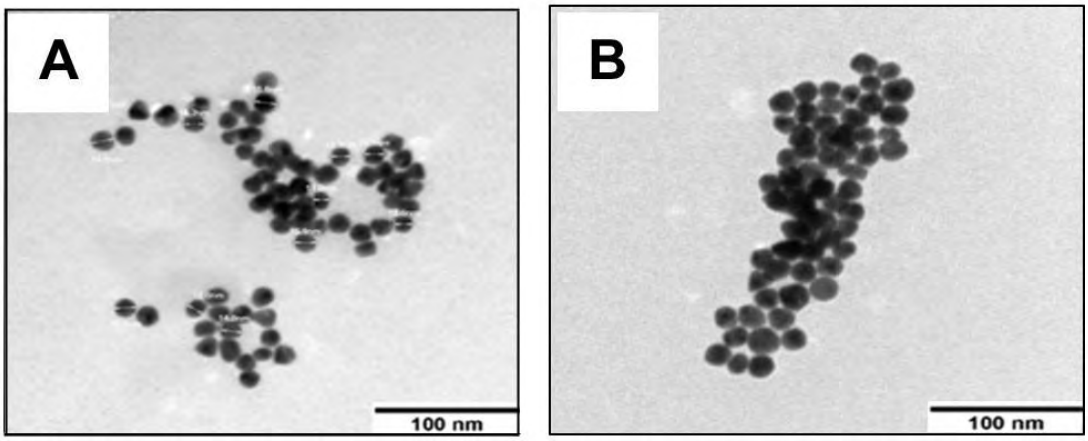

Figure 19: Transmission electron micrographs of gold nanoparticles (A) bare gold nanoparticles (B) and amine functionalised gold nanoparticles. Scale bar indicates 100 nm

4.1.4.2.3 Dynamic light scattering

The average values of zeta potential for bare and amine functionalised AuNPs were -44.7 and -22.1mV respectively indicating optimum stability of the gold nanoparticles before and after amine functionalisation (Fig. 20).

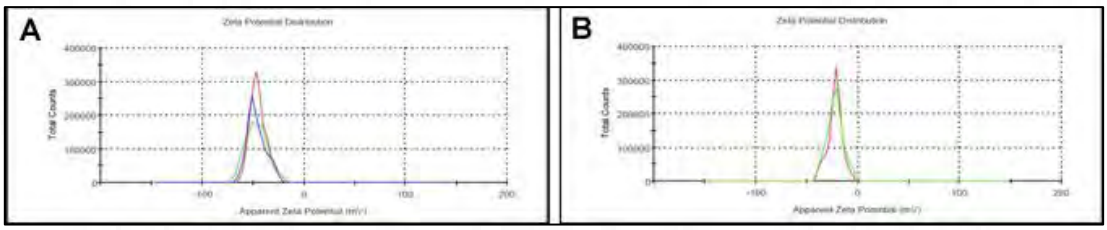

Figure 20: Zeta potential of (A) bare and (B) amine functionalised gold nanoparticles

4.1.4.3 Characterisation of the C-ECM AuNP scaffold

4.1.4.3.1 Conductivity measurement

It was observed that there was a significant increase in the conductivity of the C-ECM AuNP scaffold (0.74±0.03 S/m) compared to C-ECM scaffold (0.53±0.003 S/m) (Fig. 21).

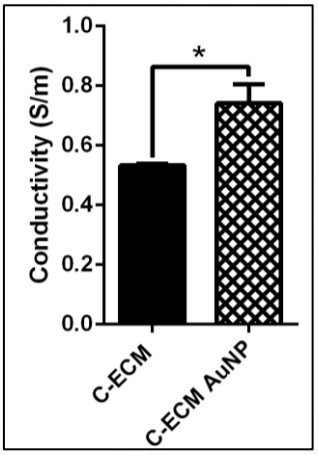

Figure 21: Bar diagram showing the results of conductivity studies conducted on the scaffolds (n=4) p-value <0.05

4.1.4.3.2 Estimation of free amino groups present in the scaffolds

After incorporation of amine functionalised gold nanoparticles to the C-ECM, there was significant increase (1.75 fold) in the number of free amino groups in the modified scaffold (Fig. 22).

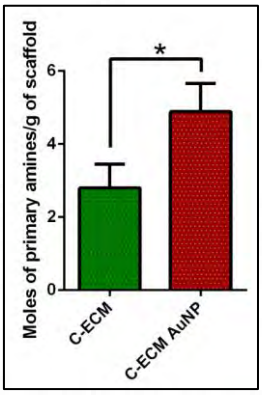

Figure 22: Results of the TNBS assay showing the quantity of primary amines (moles) in the scaffolds before and after the incorporation of gold nanoparticles (n=3) p-value <0.05

4.1.4.3.3 FTIR spectroscopy

In the FTIR spectra of C-ECM and C-ECM AuNP, there was presence of characteristic collagen peaks at 1631 (amide I), 1533 (amide II) and 1236 (amide III) (Fig. 23). There was no difference in the spectra consequent to the conjugation of amine functionalised AuNPs onto C-ECM.

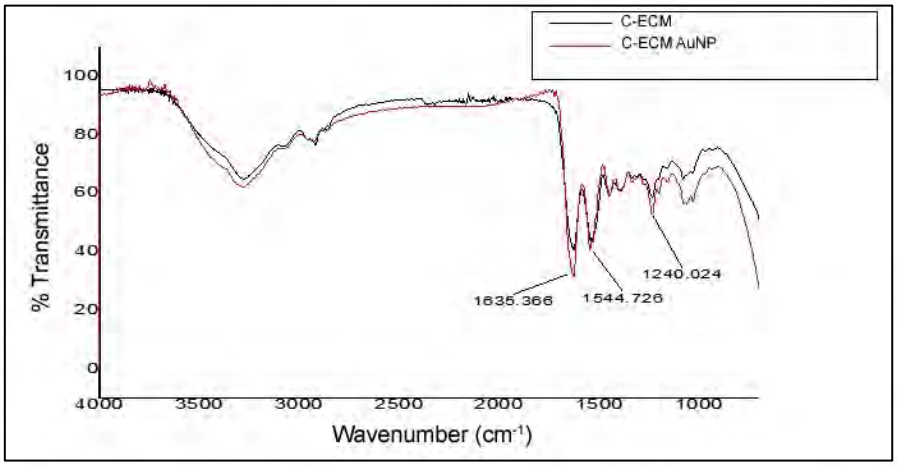

Figure 23: Fourier transform infrared spectra of C-ECM and C-ECM AuNP

4.1.4.3.4 Scanning Electron Microscopy-Energy Dispersive X-Ray Spectroscopy (SEM-EDS)

Compared to the native C-ECM, the micrographs of C-ECM AuNP displayed compact and uniform fibres (Fig. 24).

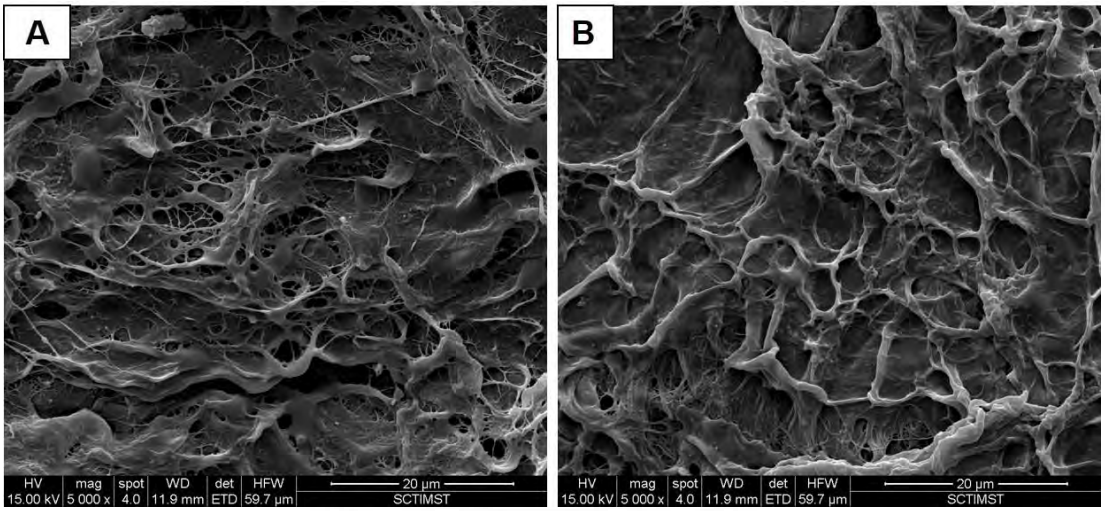

Figure 24: Environmental scanning electron micrographs of (A) C-ECM and (B) C-ECM AuNP

The EDS analysis of the C-ECM AuNP revealed (Fig. 25) peaks of gold along with the peaks of sodium and chlorine.

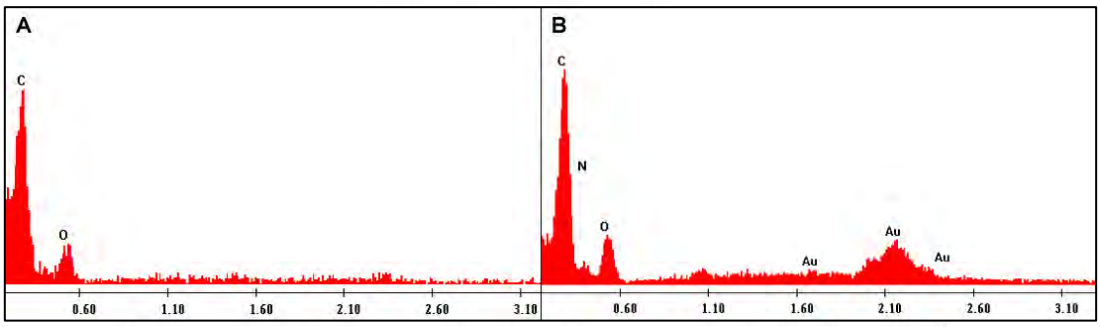

Figure 25: Results of energy dispersive X-ray spectroscopy for elemental analysis of (A) C-ECM and (B) C-ECM AuNP

4.1.4.3.5 Surface profile measurement

The surface profile of the scaffolds before and after incorporation of gold nanoparticles indicated difference in the topography. Surface uniformity was improved in the C-ECM AuNP scaffold compared to the C-ECM (Fig. 26). The quantitative data also showed significant decrease in the surface roughness value of gold nanoparticle incorporated scaffold (Fig. 27).

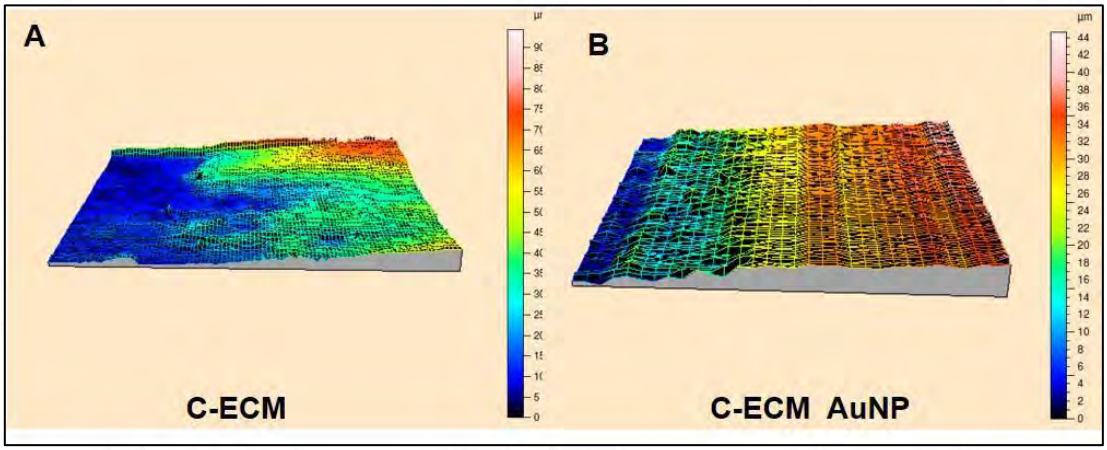

Figure 26: Line profile of (A) C-ECM and (B) C-ECM AuNP C-ECM

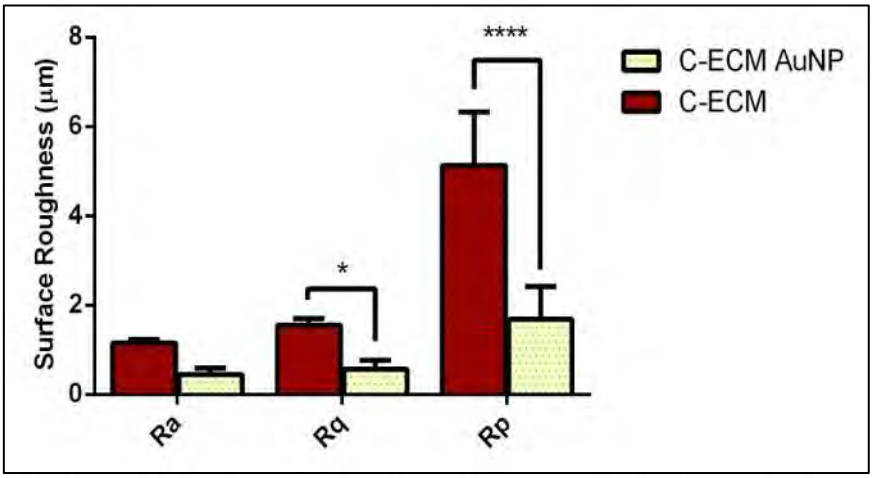

Figure 27: Bar graph indicating the surface roughness of the two scaffolds, p-value <0.05, n=3 (Ra-roughness average, Rq-root mean square roughness, Rp-maximum profile peak height).

4.1.4.3.6 Thermogravimetric analysis (TGA)

The thermograms of C-ECM and C-ECM AuNP revealed considerable weight loss at all temperature-ranges studied. The residual weight recorded for C-ECM AuNP was 25.14% and that of native C-ECM was 24.14% (Fig. 28)

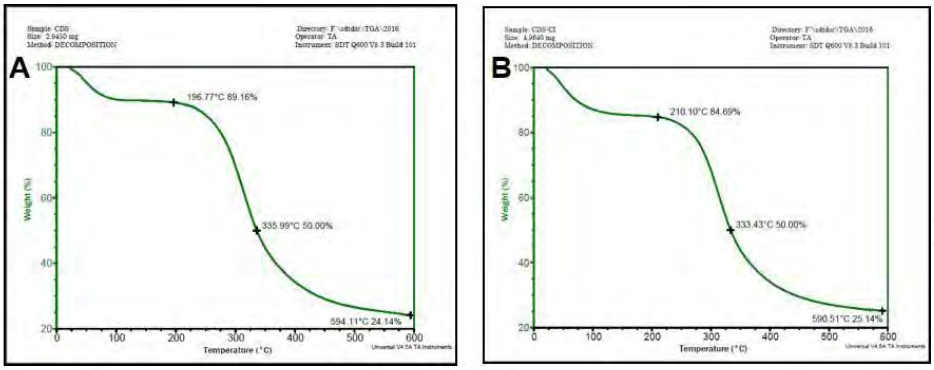

Figure 28: Thermograms of (A) C-ECM and (B) C-ECM AuNP

4.1.4.3.7 Enzymatic degradation assay

The C-ECM and C-ECM AuNP scaffolds showed similar degradation patterns when degraded by collagenase enzyme. There was progressive rate of degradation in both the scaffolds from 24 to 72 hours at 37°C (Fig. 29).

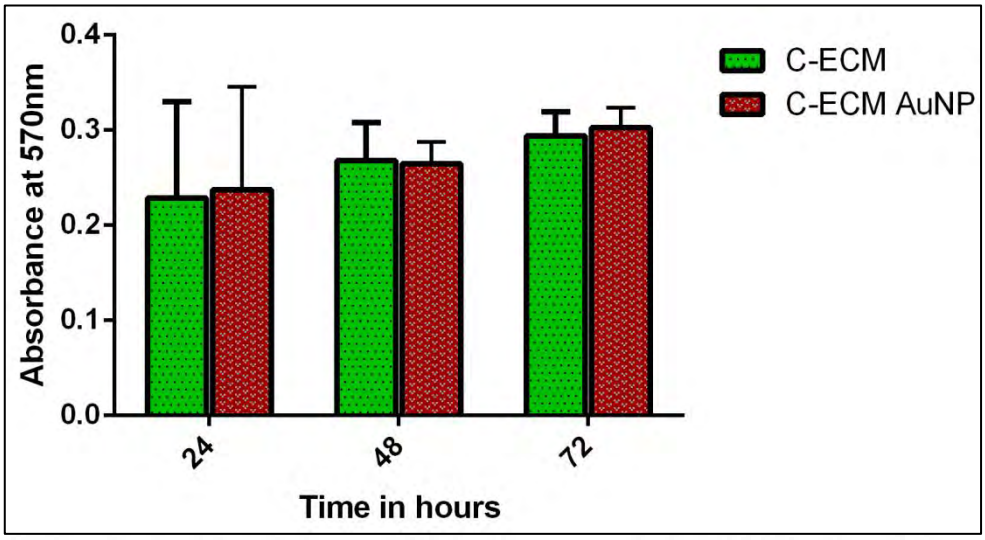

Figure 29: Bar diagram showing the degradation rate of the scaffolds, n=3

4.1.4.4 Evaluation of the cytocompatibility of the C-ECM AuNP scaffold

4.1.4.4.1 Direct contact test

After 24 h of incubation of cells in contact with the C-ECM AuNP, the cells were healthy (Fig. 30) without any signs of cytotoxicity. Neutral red uptake by the cells indicated the viability of the cells in the presence of the scaffold.

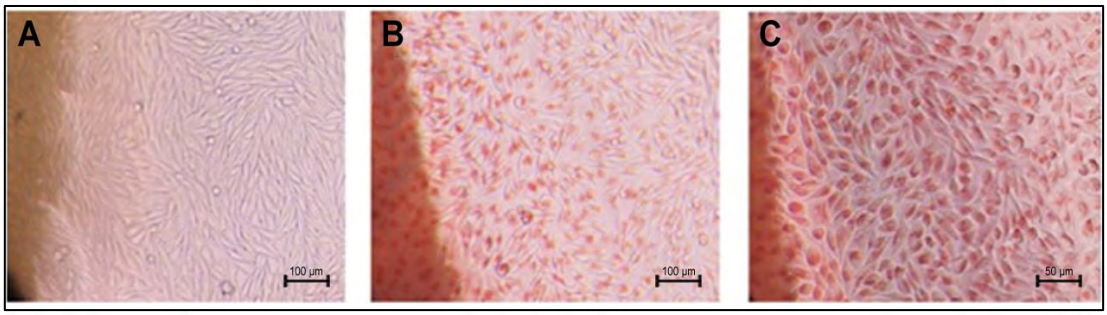

Figure 30: Direct contact test of C-ECM AuNP (A) Phase contrast image of C-ECM AuNP on H9c2 monolayer (B & C) viable cells stained with neutral red dye (n = 3).

4.1.4.4.2 Live-dead staining

The viability of H9c2 cells cultured on the scaffold was visualised by staining with FDA and PI. The results indicated that the majority of the cells were viable up to 24 hours (Fig. 31).

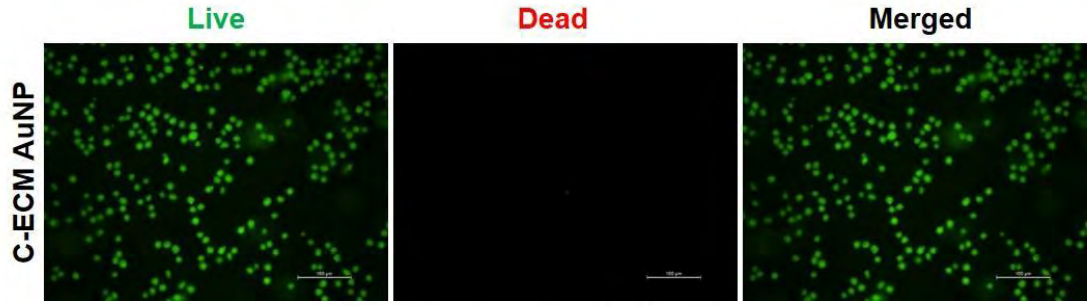

Figure 31: Photomicrographs of the Live-dead test of C-ECM AuNP. Fluorescent microscopic images of H9c2 cells seeded on C-ECM AuNP stained with FDA (green) and PI (red) for live and dead cells respectively (n= 3). Scale bar indicates 100 µm.

4.1.4.4.3 MTT assay

The cells cultured on the C-ECM AuNP showed a cell viability of 87.09 ± 1.09 % (Fig. 32). From the statistical analysis, it was clear that no significant difference was observed between C-ECM AuNP and the control indicating cytocompatibility.

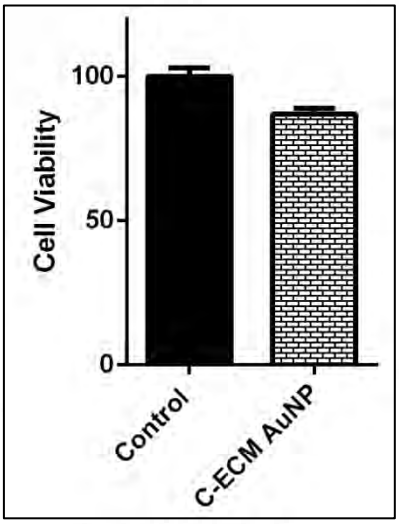

Figure 32: Cell viability of C-ECM AuNP. Bar graph representing the percentage viability of cells seeded on C-ECM AuNP and control (tissue culture plastic) n=3.

4.2 Differentiation of rat cardiomyoblast cell line H9c2 and rat bone marrow mesenchymal stem cells to cardiomyocyte-like cells

4.2.1 Differentiation of rat cardiomyoblast cell line H9c2 to cardiomyocyte-like cells

4.2.1.1 Morphological evaluation/observations

The H9c2 cells cultured in 10% serum condition had the expected spindle to stellate shape but differentiation with retinoic acid in low serum condition caused cell fusion and formed multinucleated cells. which indicated differentiation of cardiomyoblast to cardiomyocyte-like cells (Fig. 33).

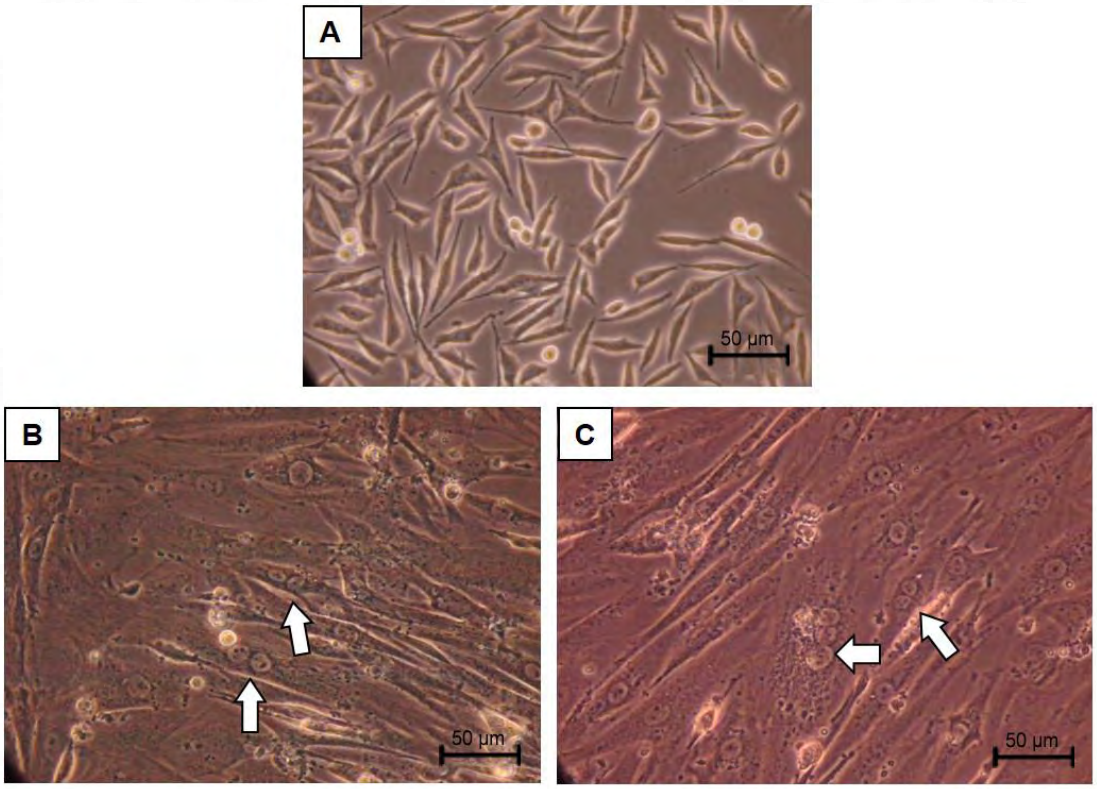

Figure 33: Morphology of H9c2 cells. Phase contrast images of (A) control cells cultured in normal serum condition and (B, C) differentiated cells with multinucleated appearance denoted by white arrows

4.2.1.2 Phalloidin staining

The cytoskeletal structures were observed as green in colour. The nuclei appeared blue in colour due to the binding of Hoechst and demonstrated the presence of multiple nuclei in the differentiated cells (Fig. 34).

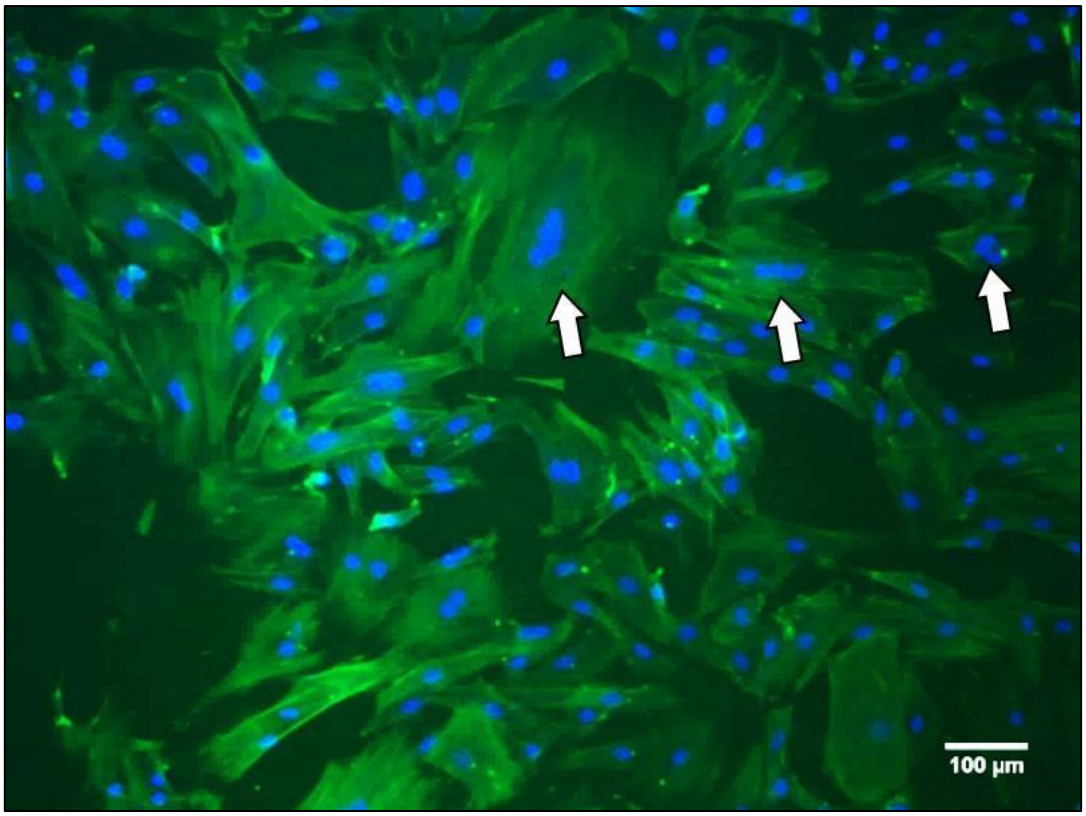

Figure 34: Phalloidin staining of differentiated H9c2 cells. Fluorescent microscopic images of differentiated cells with multinucleated appearance. Scale bar indicates 100 µm

4.2.1.3 Western blotting

After the differentiation of H9c2 cells for 5 days, there was an increase in expression of cardiac proteins such as troponin T, myo D and connexin 43 indicating the differentiation to cardiomyocyte lineage (Fig. 35). β-actin, a housekeeping protein was used as the loading control for normalising the level of protein in the blot.

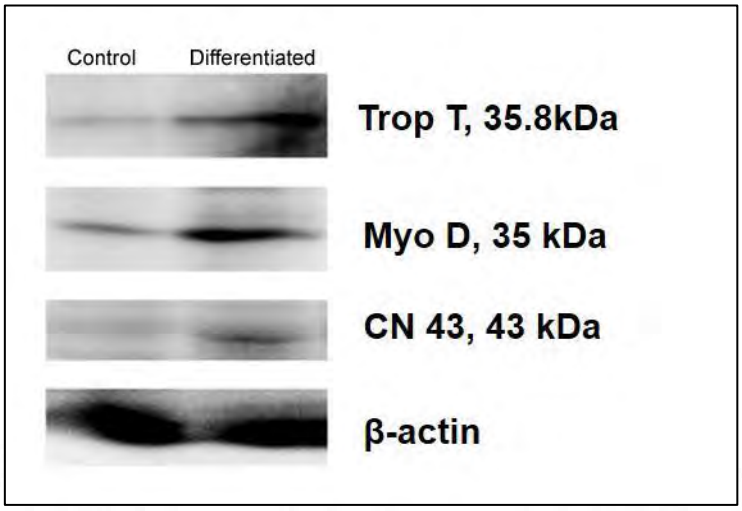

Figure 35: Western blot of differentiated and undifferentiated H9c2 cells (control)

4.2.2 Differentiation of rat bone-marrow mesenchymal stem cells to cardiomyocyte-like cells

4.2.2.1 Isolation of rat bone-marrow derived mesenchymal stem cells

For initial days of seeding, the growth rate of rat bone-marrow derived MSC was considerably slow while rapid multiplication was observed after 7 days. The cells became confluent on day 14th and trypsinised for further experiments (Fig. 36). The calculated doubling time of the isolated cells was 21±5h (Fig. 37).

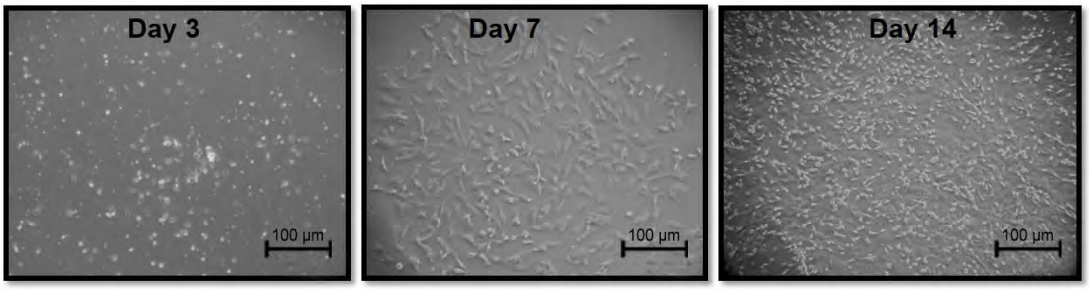

Figure 36: Phase contrast microscopic images showing the growth of the isolated cells at day 3, day 7 and day 14

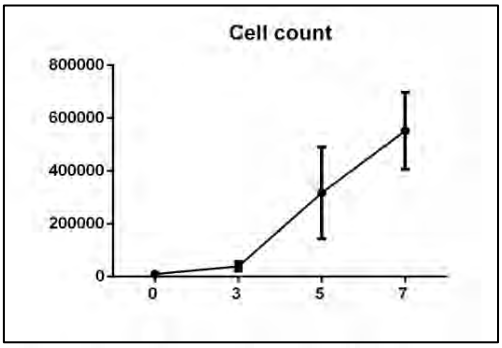

Figure 37: Graph representing the doubling time of isolated rBMSCs

4.2.2.2 Characterisation of rat bone marrow derived mesenchymal stem cells

4.2.2.2.1 Analysis of the expression of cell specific markers by flow cytometry

Flow cytometry results showed that the majority of cells express positive markers such as CD90, CD73 and very few cells expressed CD45, the negative marker (Fig. 38). 99.8% of the isolated mesenchymal stem cells were positive for CD90, and 99.9% positivity for CD73. Only 1.1% cells expressed CD45 positivity.

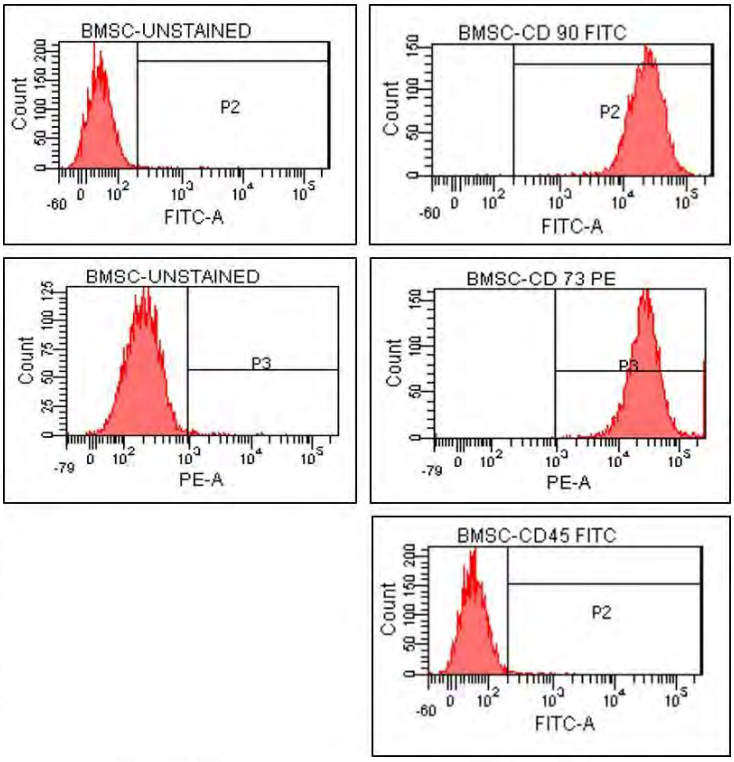

Figure 38: Flow cytometry histograms representing (lane 1) the unstained cells, (lane 2) the positive marker expression for CD90, CD73 and the negative marker expression for CD45.

4.2.2.2.2 Expression of markers by immunostaining

Immunostaining showed the expression of CD90 by rBMSCs isolated and cultured confirming their mesenchymal stem cells characteristics (Fig. 39). There was absence of CD34 expression by the same cells, which is a marker of haematopoietic stem cells.

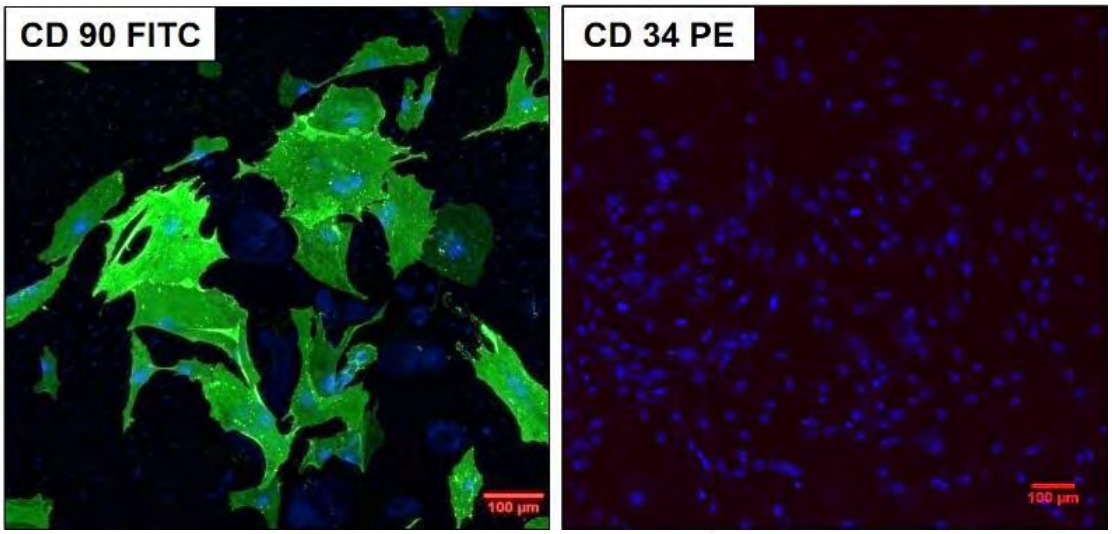

Figure 39: Confocal microscopic images showing the expression of CD90 marker and absence of CD43 marker by the isolated mesenchymal stem cells. Scale bar indicates 100 µm

4.2.2.2.3 Multilineage differentiation of rBMSCs

Lipid droplets secreted by adipocytes were stained with Oil red O stain, glycosaminoglycans produced by chondrocytes were stained by Alcian blue stain and calcium deposits released by osteocytes were stained by Alizarin red dye (Fig. 40). Undifferentiated cells remained unstained after the staining procedure.

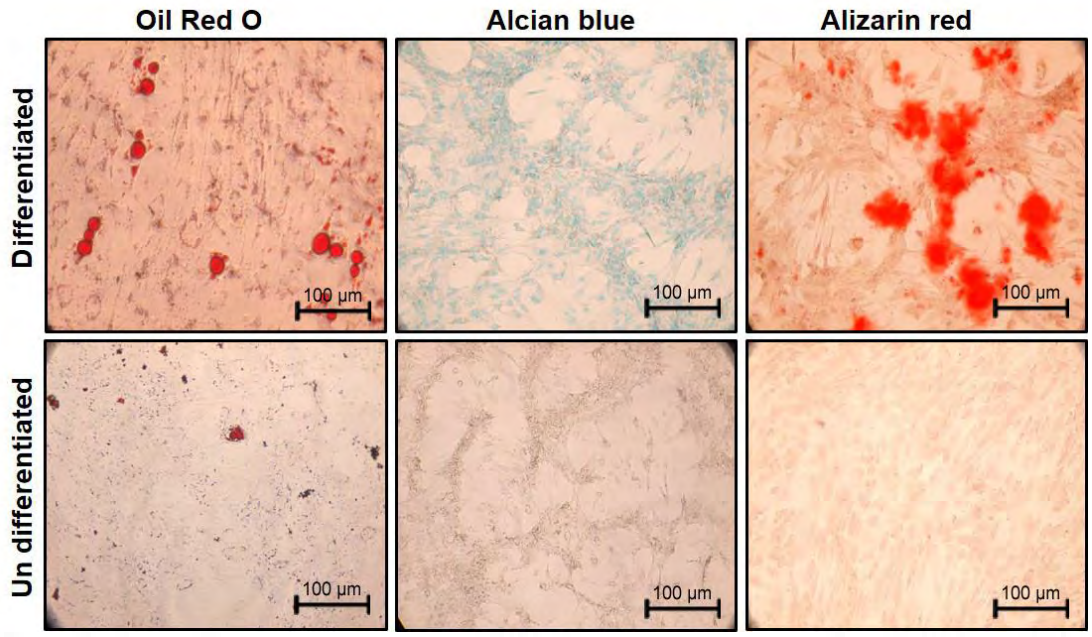

Figure 40: Phase contrast microscopic images of multilineage differentiation showing red coloured lipid droplets stained by Oil red O, blue stained glyocaminoglycans by Alcian blue and red coloured calcium deposits by Alizarin red dye

4.2.2.3 Cytocompatibility evaluation

There were no signs of cell detachment, lysis or vacuolization, when the scaffolds C-ECM and C-ECM AuNP was in contact with the rBMSC monolayer for 24 hours (Fig. 41). The morphology of these cells was similar to the cells in contact with the negative control. Cells in contact with the positive control underwent lysis and death.

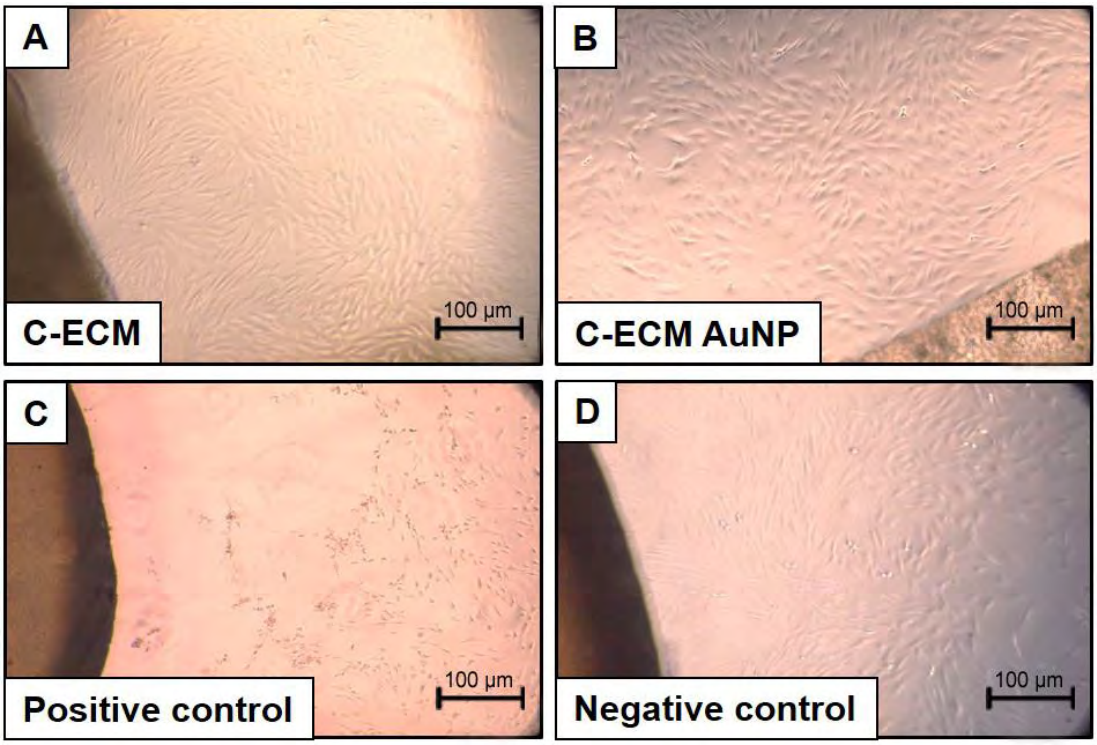

Figure 41: Direct contact test of C-ECM and C-ECM AuNP. Phase contrast image of (A) C-ECM on MSC monolayer, (B) C-ECM AuNP on MSC monolayer and (C, D) positive and negative controls respectively (n=3)

4.2.2.4 Differentiation of rBMSCs to cardiomyocyte-like cells

4.2.2.4.1 Morphological evaluation

Rat bone marrow-derived mesenchymal stem cells cultured in DMEM with 20% serum condition showed spindle morphology but after differentiation with 5-azacytidine, the cellular morphology changed to slender stick-like appearance which indicated differentiation of mesenchymal stem cells to cardiomyocyte-like cells (Fig. 42).

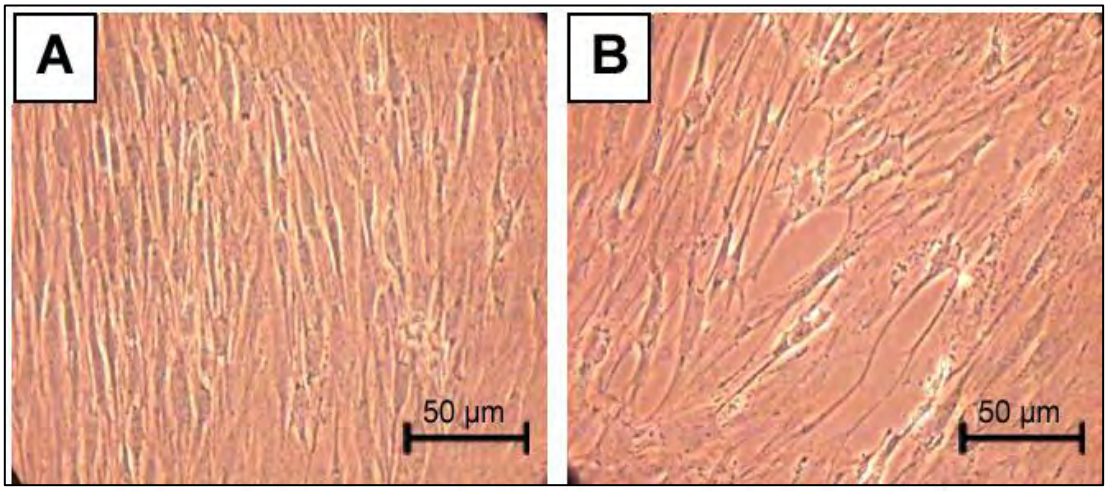

Figure 42: Differentiation of rBMSC using 5-azacytidine. Phase contrast microscopic images showing (A) control rBMSCs and (B) differentiated rBMSCs

4.2.2.4.2 Western blotting

After differentiation of rBMSCs for 7 days, there was an increase in the expression of cardiac proteins such as troponin T, myo D and connexin 43 indicating the differentiation to cardiomyocyte lineage (Fig. 43). β-actin, a housekeeping protein was used as the loading control for normalising the level of protein in the blot.

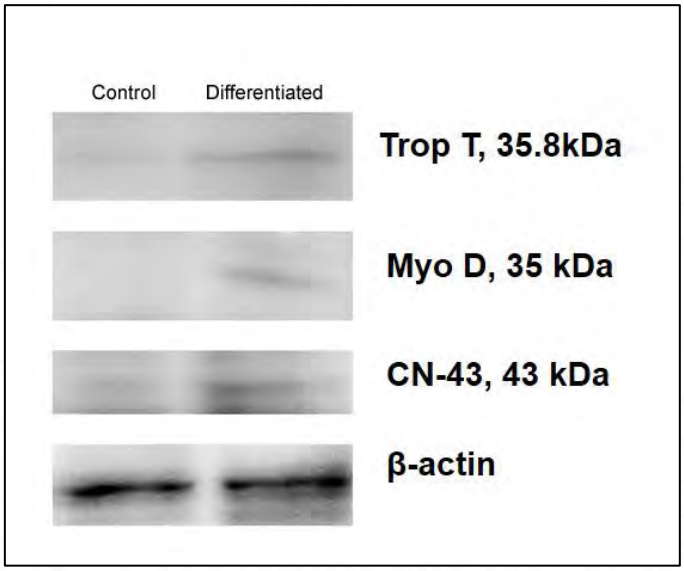

Figure 43: Western blot of differentiated and undifferentiated rBMSCs (control)

4.3 Functional evaluation of cardiac-patches in a rat model of non-fatal MI

In this experiment, the ligation resulted in non-fatal MI of variable degree in all the rats and confirmed by serum biochemistry, electrocardiography and echocardiography.

4.3.1 Clinical monitoring

4.3.1.1 Estimation of cardiac biomarkers

There was elevation in the level of trop T, CK and CK-MB (Fig. 44) at 24 hours after the surgical ligation of the coronary artery in all the experimental rats indicating successful induction of myocardial infarction.

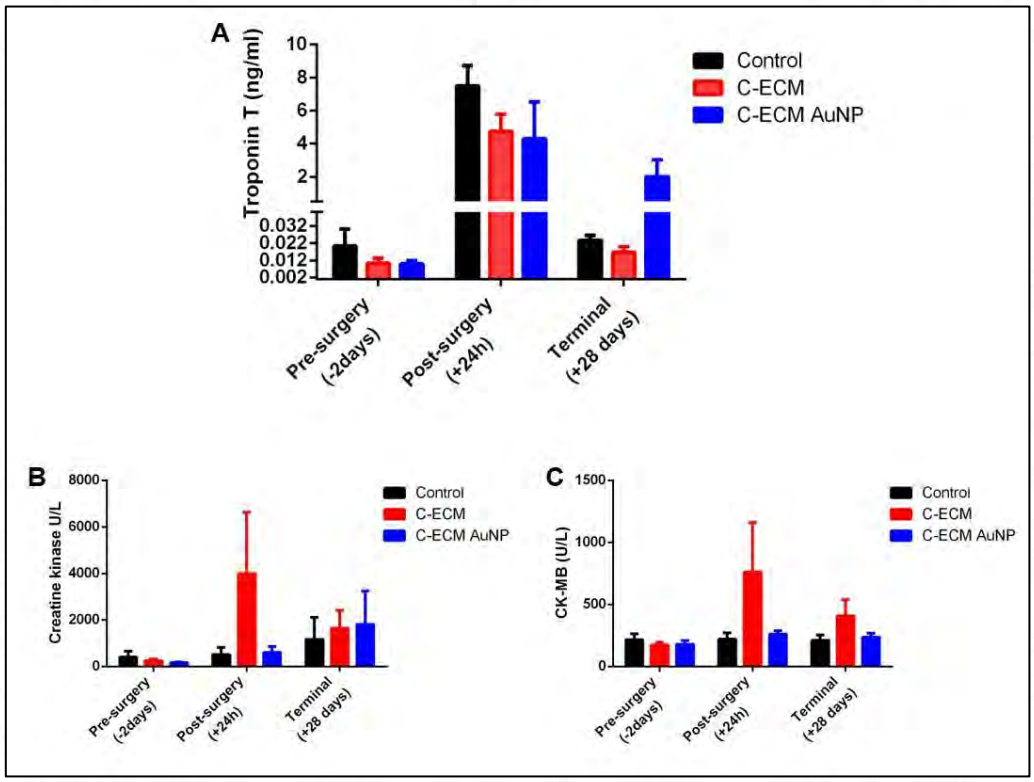

Figure 44: Serum biochemistry (A) Bar graph showing the elevation of troponin T (B) creatine kinase and (C) creatine kinase-MB at 24h after MI induction surgery, n=3

4.3.1.2 Electrocardiogram

In this study, compared to the baseline data, the recorded ECG of all the experimental animals at 1 week and 4 weeks after the surgery had deviations. The depression in ST-segment of the electrocardiograph (Fig. 45) indicated the persistence of MI in all the experimental rats, even a week after the surgery. Widening of the QRS peak was observed in the control group which also indicated the effect of MI. At 4 weeks, recovery was prominent in the C-ECM/C-ECM AuNP grafted animals compared to the control.

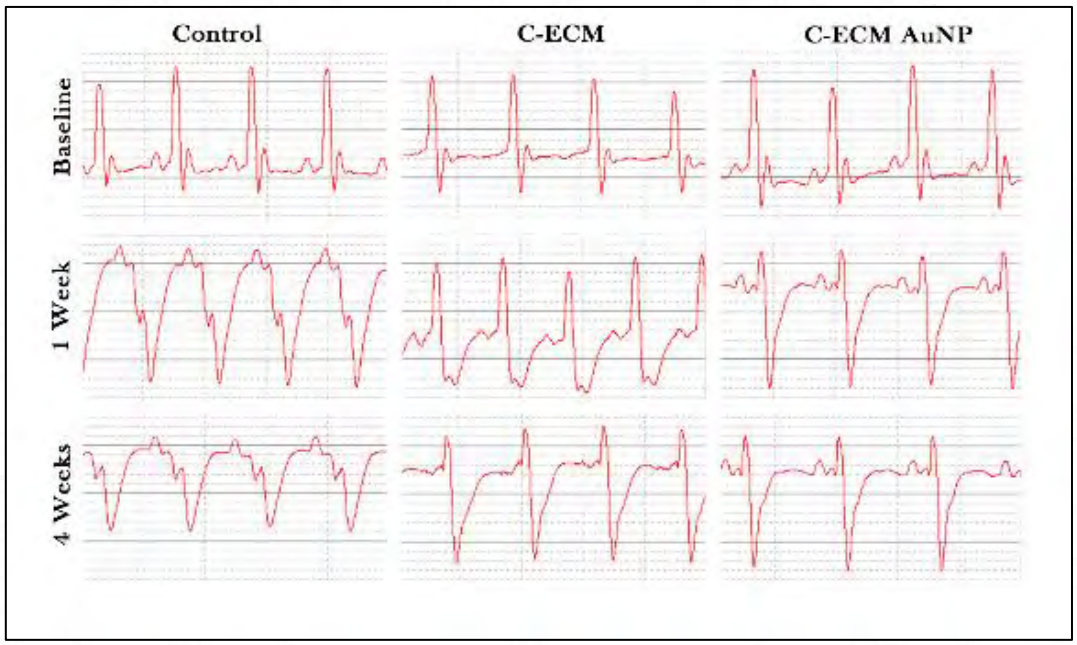

Figure 45: ECG of rat hearts. Functional damage in the heart was evident in representative electrocardiograms recorded from control group and the C-ECM/C-ECM AuNP groups at 1 week and 4 weeks compared to the baseline data, n=3

Quantitative data collected from the ECG recordings clearly indicated the changes in the electrical activity of the heart specifically the left ventricular contractility. Heart rate did not fluctuate much after the MI induction while there were distinct variations in the RR amplitude, ST elevation, QT interval, QRS amplitude and QRS duration at 1 week strongly indicating MI. At 4 weeks, both C-ECM and C-ECM

AuNP showed signs of recovery which was evident from the QRS amplitude, as the values shifted towards the baseline (Fig. 46).

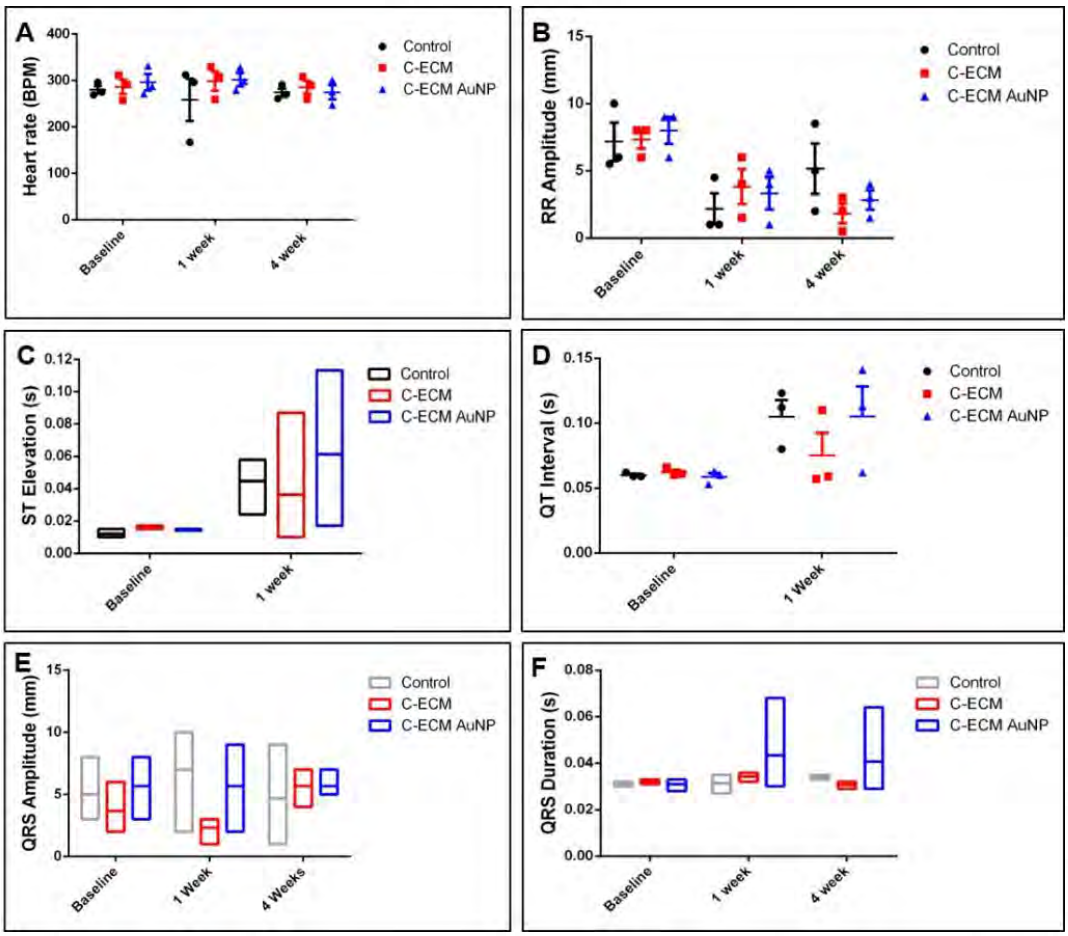

Figure 46: Quantitative data form the ECG recordings (A) heart rate, (B) RR amplitude, (C) ST elevation, (D) QT interval, (E) QRS amplitude and (F) QRS duration, n=3

4.3.1.3 Echocardiography

Similar to the ECG, echocardiograms were recorded from each of the animals at three time points (Fig. 47) and evaluated the structural and functional changes associated with MI induction and graft implantation.

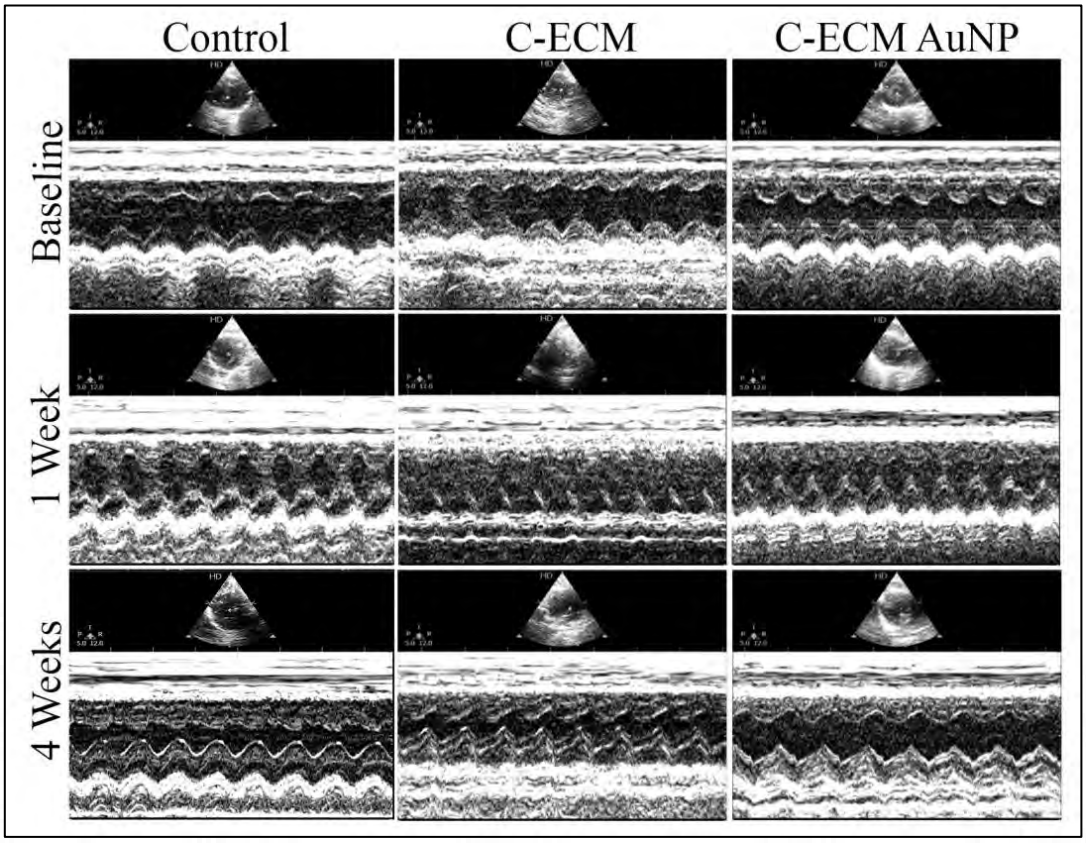

Figure 47: Echocardiogram of rats. The extent of the functional damage demonstrated by deviation in echocardiography, n=3

The end-systolic septum thickness (IVSs), end-diastolic septum thickness (IVSd), fractional shortening and ejection fraction at 1 week and 4 weeks were compared between the groups. There was a significant difference in the IVSs and IVSd between C-ECM and control groups at 4 weeks indicating recovery in the C-ECM group (Fig. 48 A, B). At 4 weeks, the fractional shortening and ejection fraction of the experimental animals were near to the baseline values (Fig. 48 C, D).

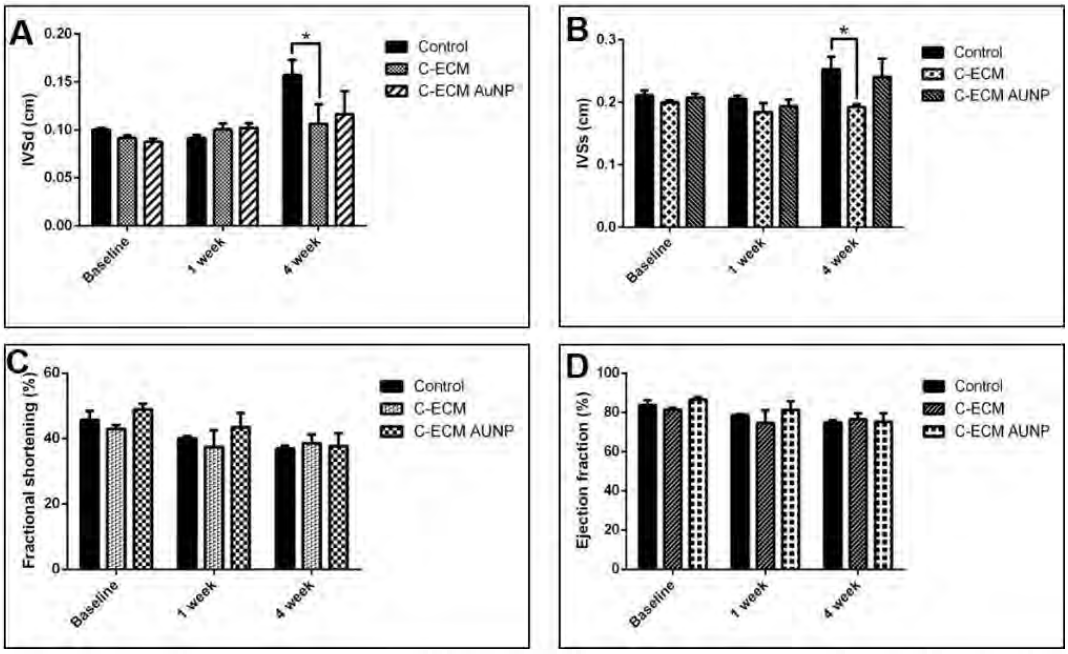

Figure 48: Parameters derived from rat ECHO, p-value < 0.05

4.3.2 Necropsy and gross pathology

The grafts appeared to have integrated with the heart (Fig. 49). However, gross signs of necrosis, mural thinning and the interventricular septal hypertrophy were present in both the groups, as expected for a post-MI healing reaction.

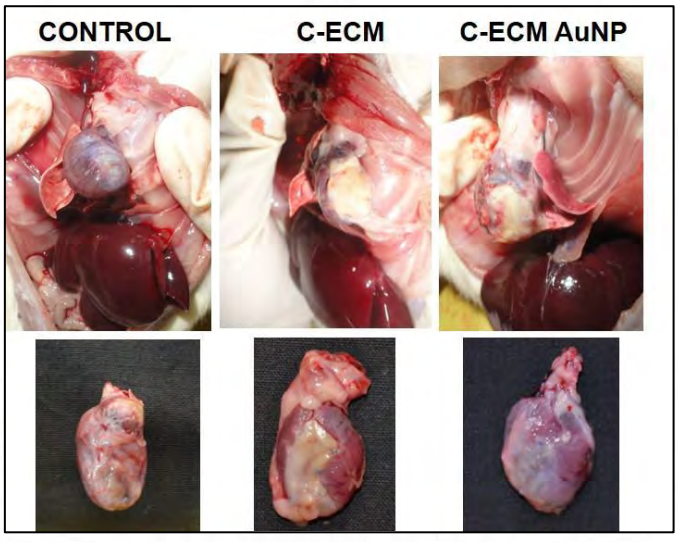

Figure 49: Gross photographs of the hearts explanted from the experimental animals

4.3.3 Heart weight to body weight ratio

All the animals recovered the surgery and their body weight reached the initial value within one to two weeks. C-ECM grafted animals were severely affected due to MI induction surgery and their body weight increased slowly compared to C-ECM AuNP and the control group (Fig. 50).

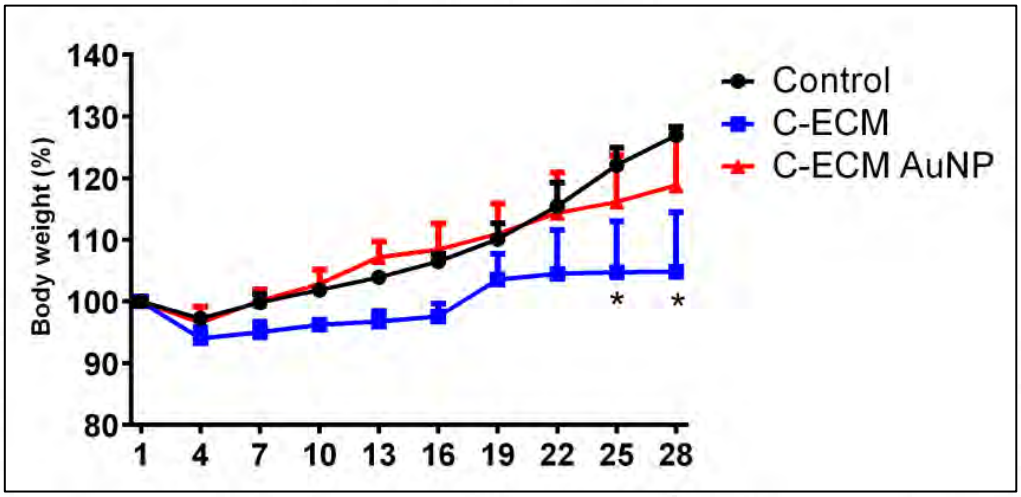

Figure 50: Body weight percentage of animals after surgery till euthanasia, p-value < 0.05

Heart weight to body weight ratio of all the animals were calculated to know the hypertrophic response due to the induced MI. Surprisingly, none of the three groups showed cardiac hypertrophy (Fig. 51). The heart sections showed gross lesions of infarction indicated by the pale necrotic MI region as well as the integration of the scaffold in the grafted animals (Fig. 52).

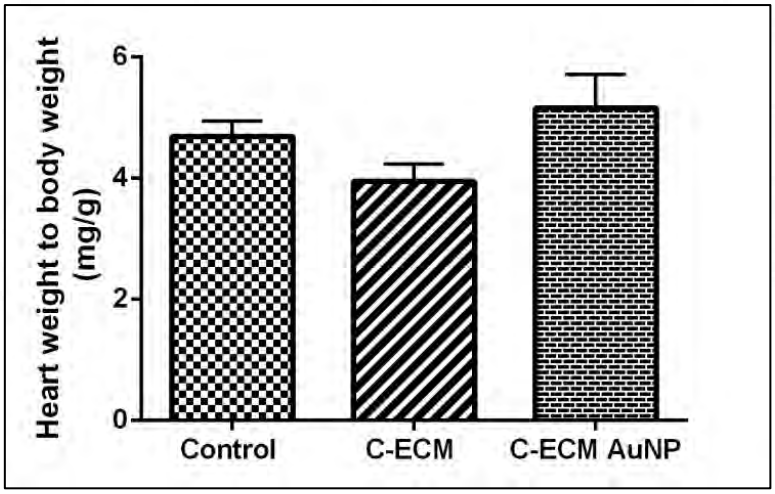

Figure 51: Heart weight to body weight ratio of experimental animals

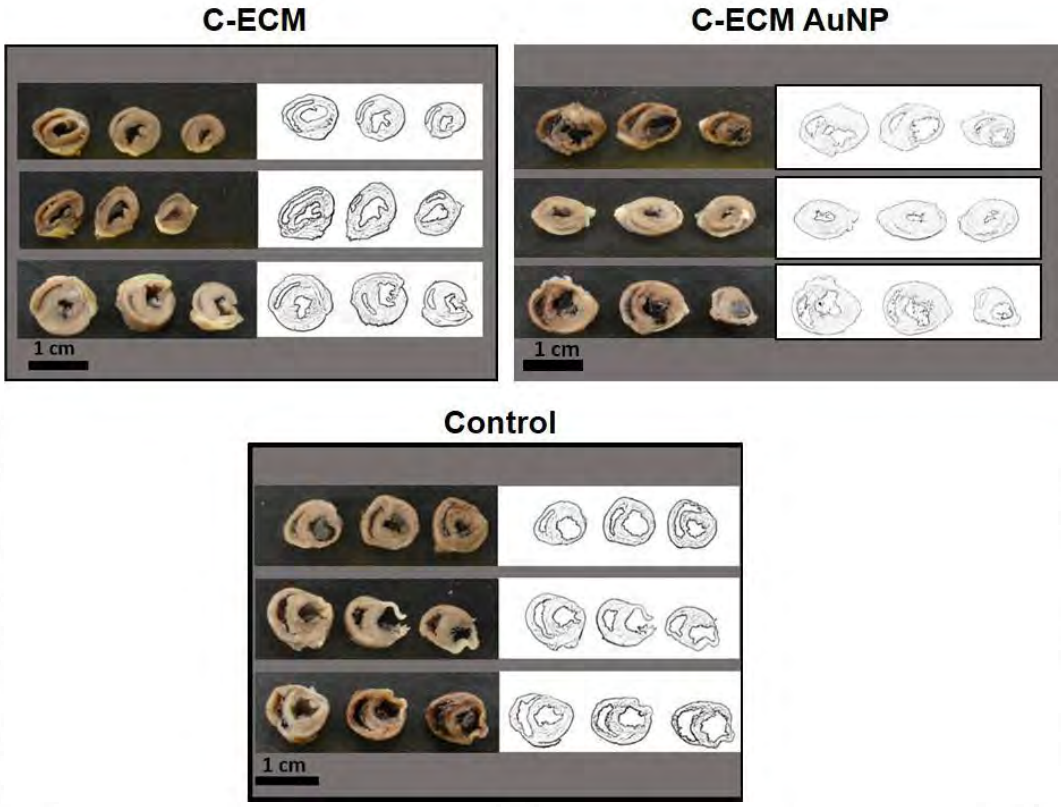

Figure 52: Gross photographs of cross-sections of hearts and their sketches made from the three experimental groups at three planes posterior to the ligature in Sprague Dawley rats. Scale bar indicates 1 cm.

4.3.4 OES-ICP

OES-ICP analysis did not find any detectable amount of gold in the brain, lungs, liver and kidney inferring the elimination of gold from these organs through excretion.

4.3.5 Histology

4.3.5.1 H & E Staining

The haematoxylin and eosin stained sections showed the extent of left ventricular myocardial degeneration/necrosis and replacement fibrosis after MI (Fig. 53). The left ventricular wall thinning due to MI was prevalent in all the three groups. The biomaterials, C-ECM and C-ECM AuNP were found to be partially integrated to the

myocardium. Further, the histomorphological observations provided insights into the extent of MI and the nature of the post-MI healing reaction in all the animals. The organs such as brain, lung, liver, kidney and spleen were sectioned and stained with H&E. There were no obvious signs of necrosis, inflammatory reactions, or loss of cell integrity in the organs between the control and the grafted animals (Fig. 54).

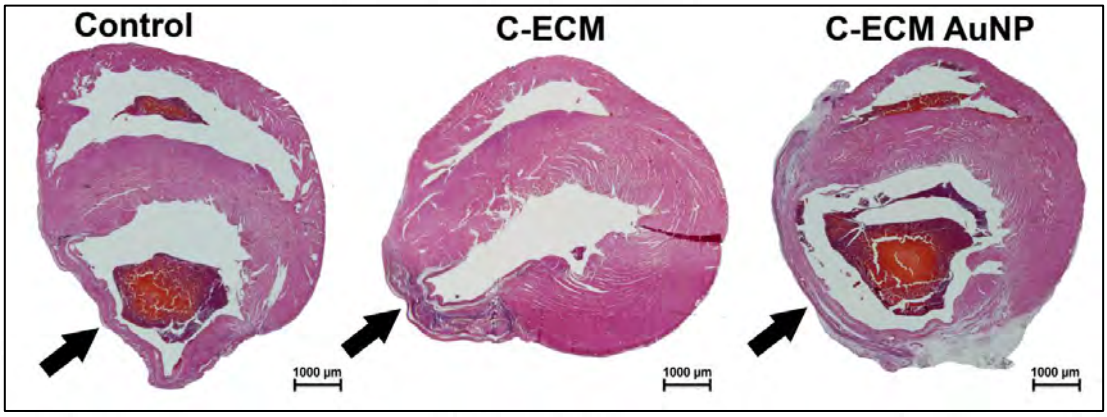

Figure 53: H&E images showing the LV wall thinning due to MI in all the three groups and the integration of graft in C-ECM/C-ECM AuNP groups. Scale bar indicates 1000 µm.

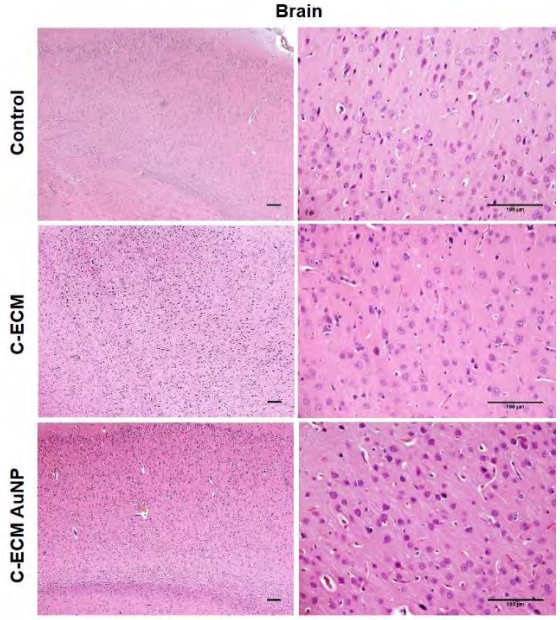

Figure 54 (1 of 5): H&E staining of brain at lower magnification and higher magnifications explanted from experimental animals. Scale bar indicates 100 µm.

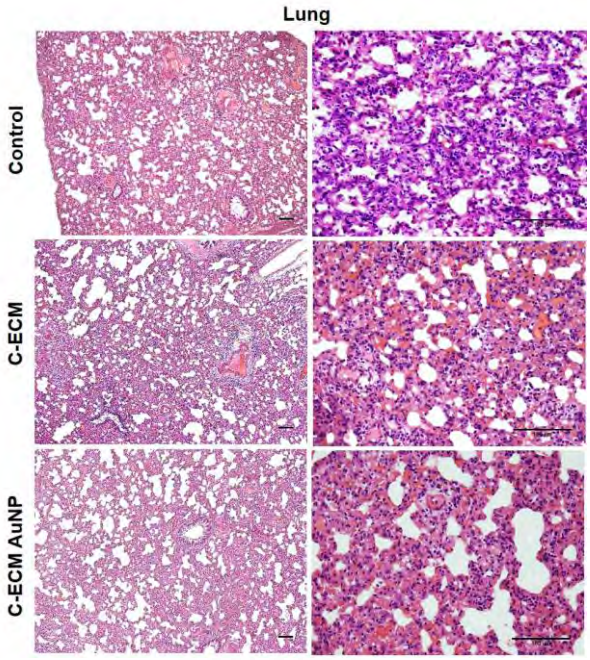

Figure 54 (2 of 5): H&E staining of lung at lower magnification and higher magnifications explanted from experimental animals. Scale bar indicates 100 µm.

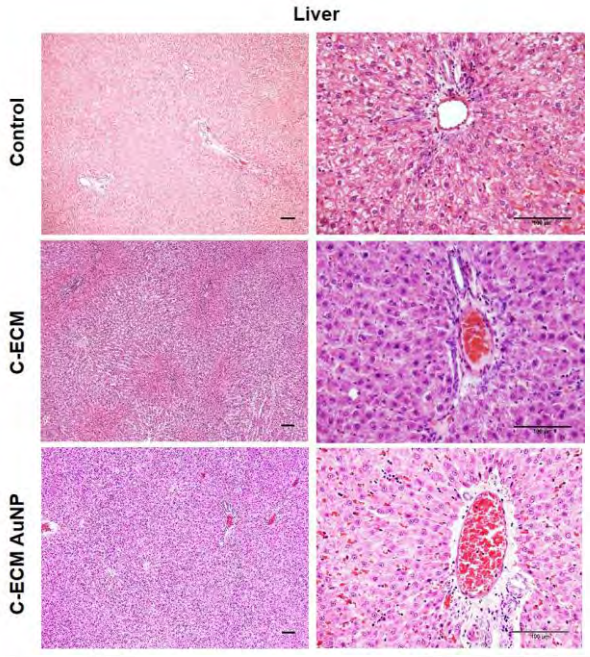

Figure 54 (3 of 5): H&E staining of liver at lower magnification and higher magnifications explanted from experimental animals. Scale bar indicates 100 µm.

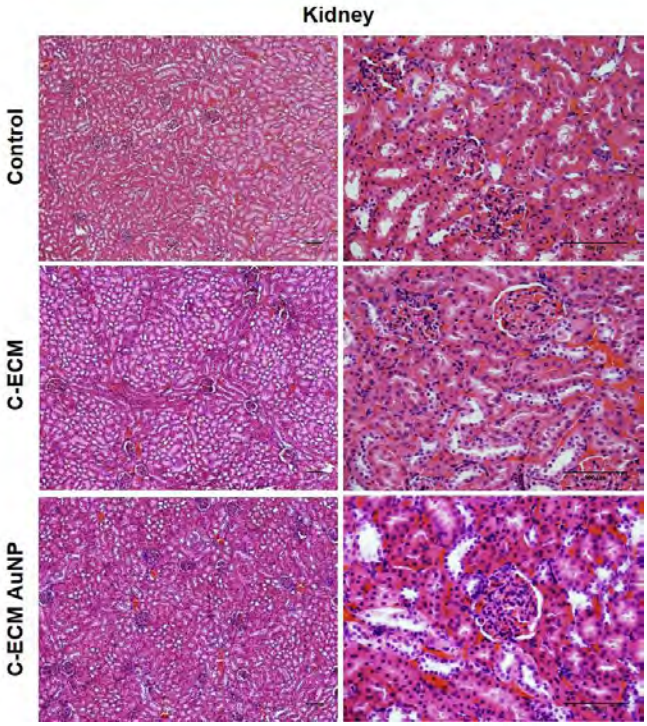

Figure 54 (4 of 5): H&E staining of kidney at lower magnification and higher magnifications explanted from experimental animals. Scale bar indicates 100 µm.

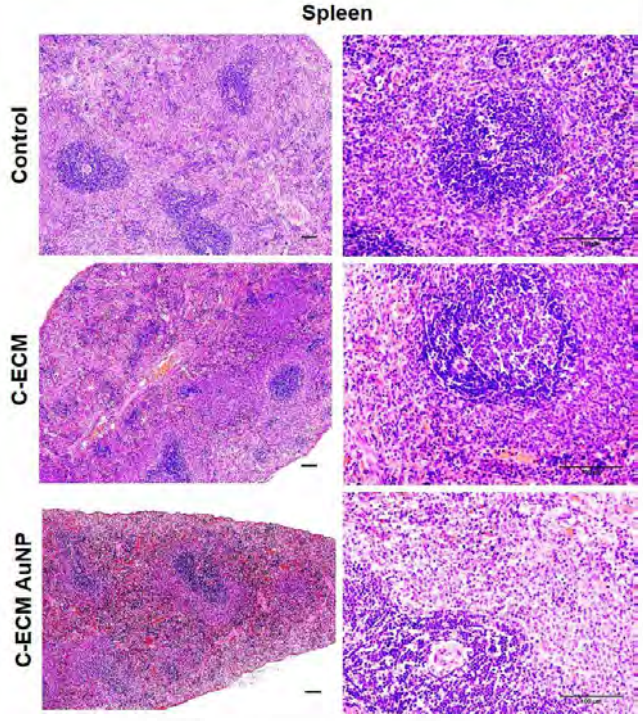

Figure 54 (5 of 5): H&E staining of spleen at lower magnification and higher magnifications explanted from experimental animals. Scale bar indicates 100 µm.

4.3.5.2 Cardiomyocyte diameter and number

Major cell diameter (Dmaj) is the longitudinal diameter and minor cell diameter (Dmin) is the cross sectional diameter (Fig. 55) of cardiomyocytes. The right ventricular cardiomyocyte diameter was measured (Fig. 56) and the values were plotted in bar graphs (Fig. 57). There was no difference in the major cell diameter of the right ventricular cardiomyocytes while significant difference was observed in the minor cell diameter between the biomaterial grafted groups and the control group indicating right ventricular hypertrophy in the control animals.

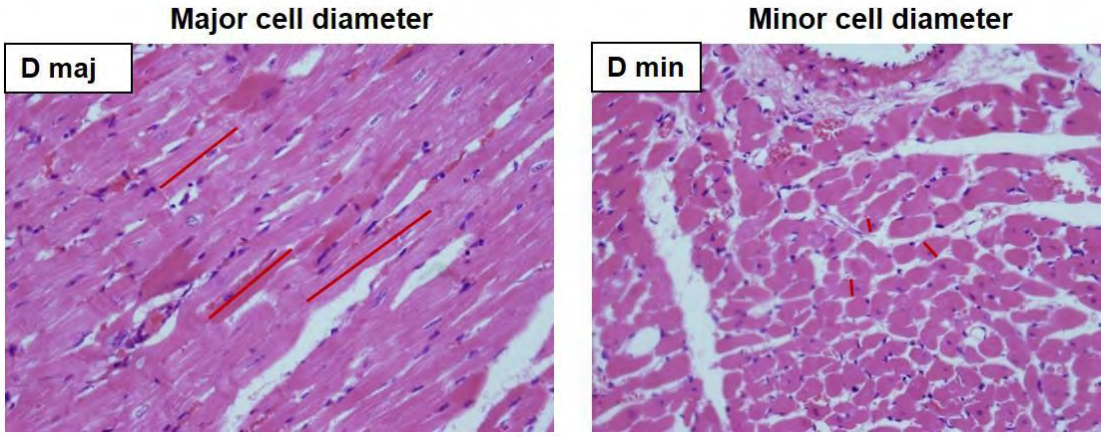

Figure 55: Major and minor cell diameter measurement using image analysis software

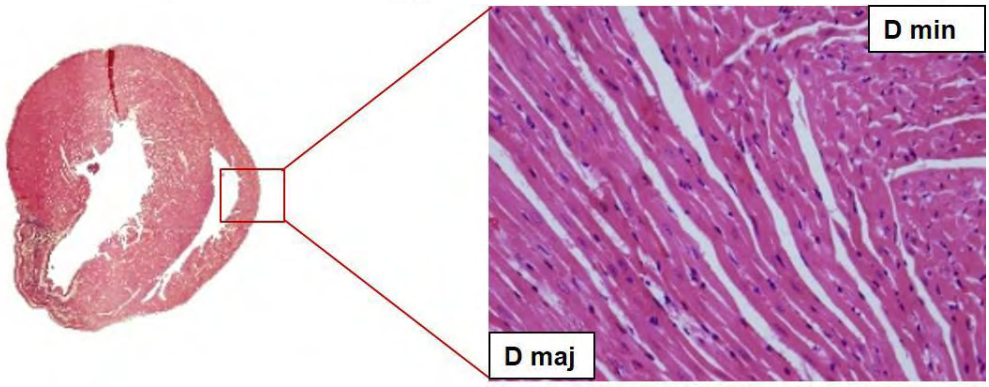

Figure 56: Cardiomyocytes in the right ventricle showing the major and minor cell diameter

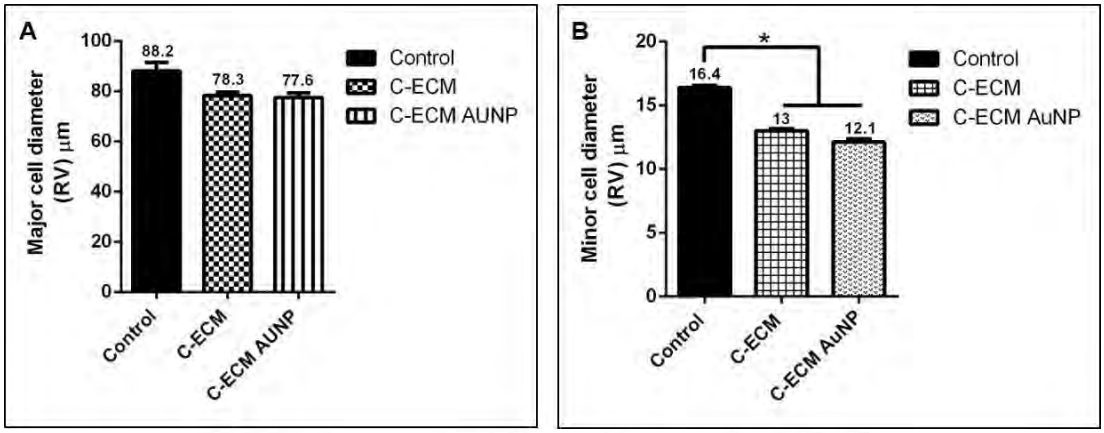

Figure 57: Bar graphs showing (A) the major and (B) the minor cell diameter of cardiomyocytes in the right ventricle, p-value < 0.05

Similarly, the Dmaj and Dmin of the cardiomyocytes in the left ventricular free wall (Fig. 58, 59) and the interventricular septum (Fig. 60) were measured. In the left ventricular free wall, there was a significant difference in the major cell diameter between the grafted animals and the control animals (Fig. 59 A). On the other hand, there was a significant difference in the major and minor cell diameter of cardiomyocytes in the interventricular septum between the grafted animals and the control animals (Fig. 61). Thus, it was observed that in the grafted animals cardiomyocyte hypertrophy was minimal compared to the control.

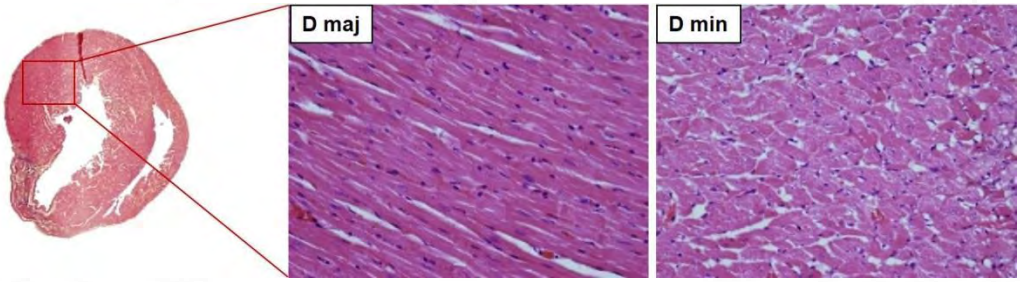

Figure 58: Cardiomyocytes in the left ventricular free wall showing the major and minor cell diameter

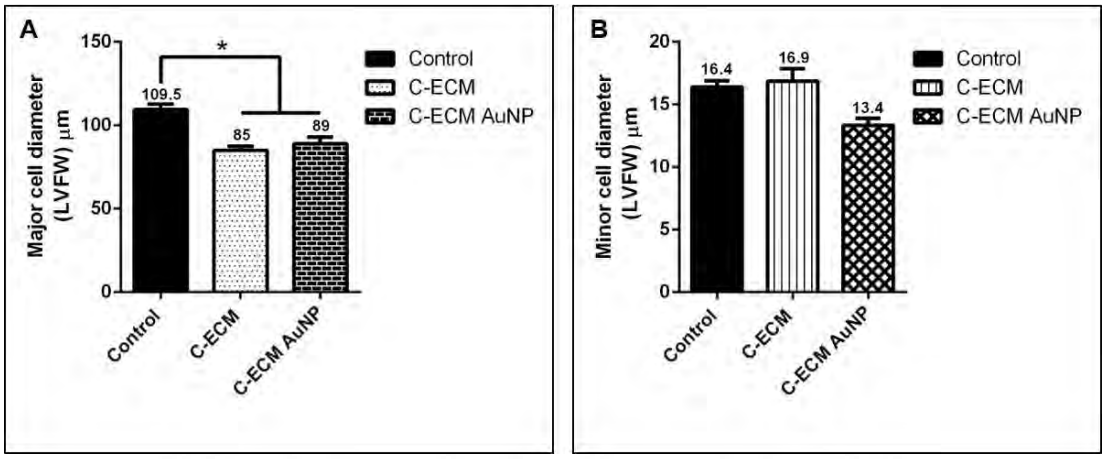

Figure 59: Bar graphs showing (A) the major and (B) the minor cell diameter of cardiomyocytes in the left ventricular free wall, p-value < 0.05

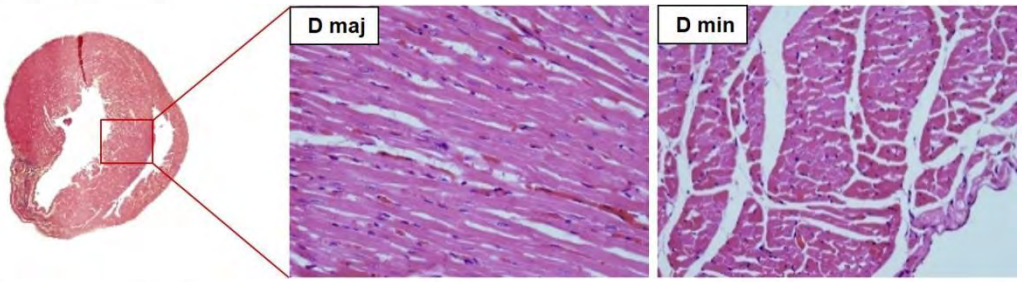

Figure 60: Cardiomyocytes in the interventricular septum showing the major and minor cell diameter

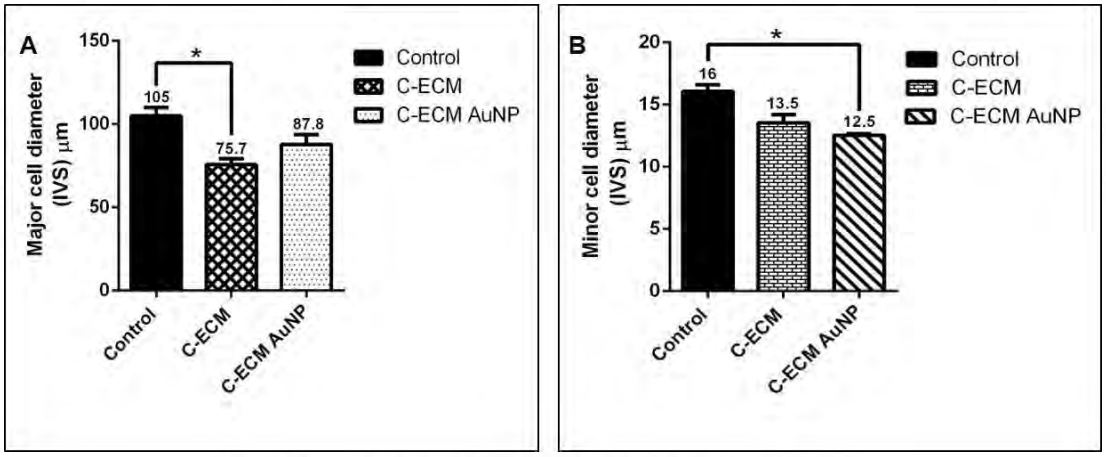

Figure 61: Bar graphs showing (A) the major and (B) the minor cell diameter of cardiomyocytes in the interventricular septum, p-value < 0.05

Furthermore, the observation that the interventricular septal cell number did not reduce in the C-ECM and C-ECM AuNP grafted animals (Fig. 62) confirmed the negligible hypertrophic response in both the grafted animals.

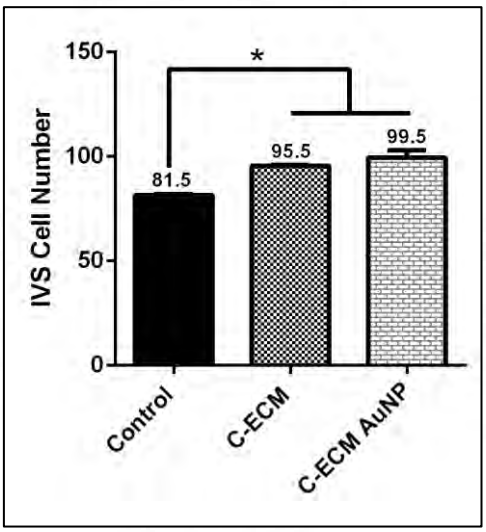

Figure 62: Number of cardiomyocytes in the interventricular septum, p-value < 0.05

4.3.5.3 Immunohistochemistry

Immunohistochemistry for CD4-positive T helper cells, CD8-positive cytotoxic T cells, CD68-positive macrophages, α-smooth muscle actin-positive smooth muscle cells, CD31-positive endothelial cells, proliferating cell nuclear antigen-positive proliferating cells, CN43-positive cells expressing connexin 43 and α-smooth muscle actin-positive myofibroblasts indicated significant infiltration of these cell types into the MI reaction zone. The positive cells stained brown in colour. The quantitative data acquired by performing image analysis are also presented.

At four weeks post-MI, significant chronic inflammation predominated by mononuclear cell infiltration was observed in all tissue sections. These cells had the morphology of lymphocytes and an analysis of CD4 (T helper cells) and CD8 (cytotoxic T cells) lineage of cells was carried out (Fig. 63 and Fig. 64). The number of lymphocytes were higher around the grafted biomaterials. In particular, a higher CD4 to CD8 ratio was also observed in the C-ECM (1.3±0.2) and C-ECM AuNP (1.26±0.5) grafted animals (Fig. 65) indicating a favourable graft acceptance reaction.

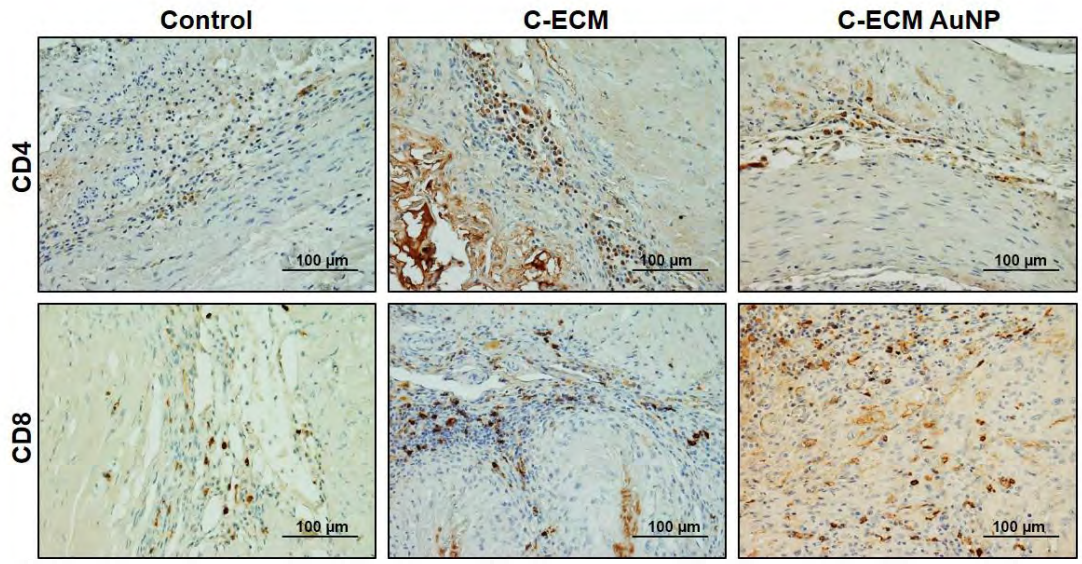

Figure 63: Immunohistochemical demonstration of CD4 and CD8 positive mononuclear cells in the tissue reaction at 4 weeks following MI and implantation of the grafts. Scale bar indicates 100 µm

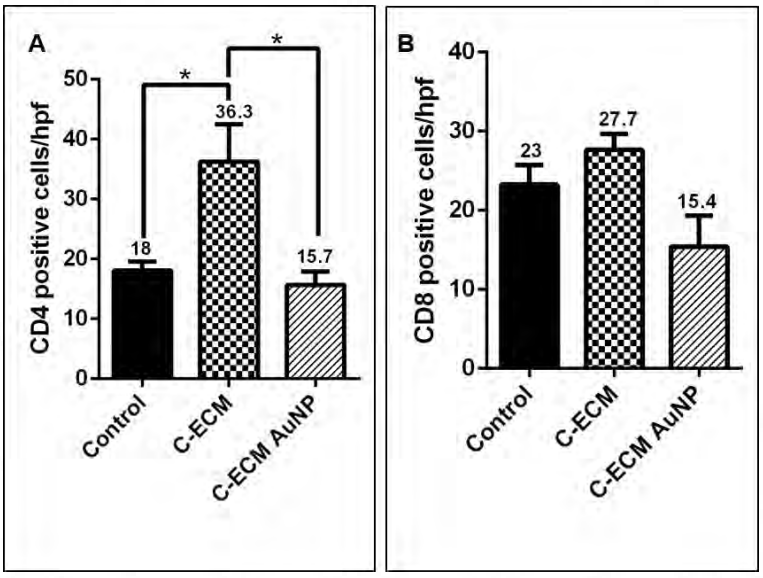

Figure 64: Bar graphs representing the quantitative data collected from CD4 and CD8 immuno-stained sections, p-value <0.05

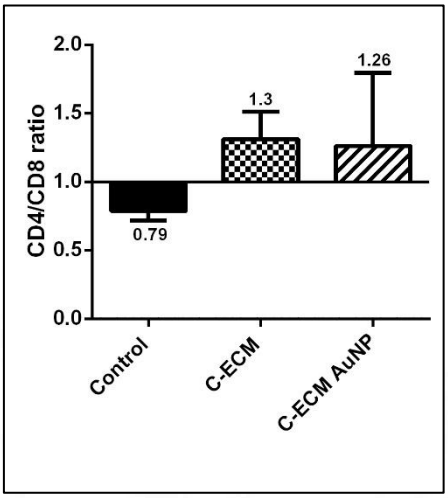

Figure 65: CD4 to CD8 ratio obtained by histomorphometric analysis

The distribution of macrophages was similar in the necrotic tissue of all the three groups of animals. But the biomaterial appeared to have induced a differential inflammatory reaction with additional moderate infiltration of mononuclear cells (Fig. 66).

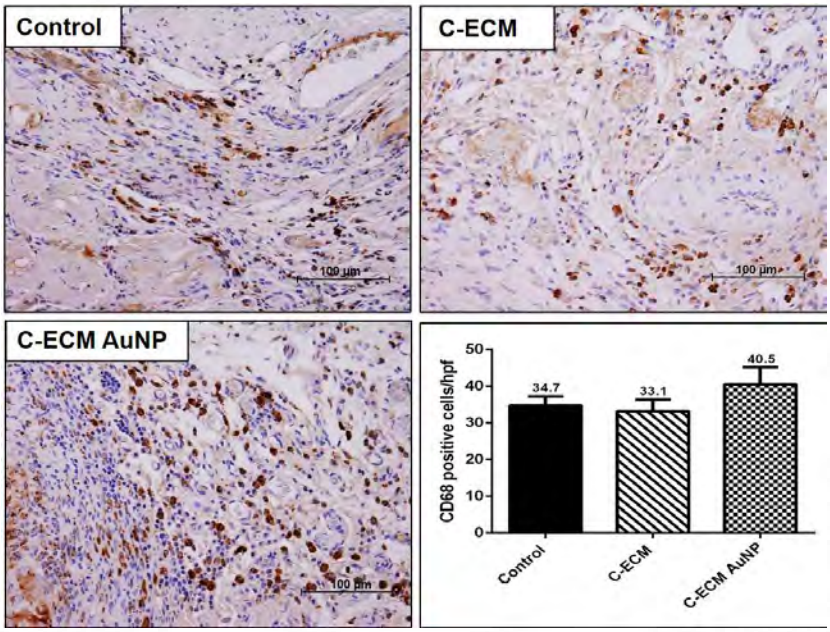

Figure 66: Immunohistochemical demonstration of CD68 positive macrophages in the tissue reaction at 4 weeks following MI and implantation of the grafts. Scale bar indicates 100 µm. The quantitative data collected is represented in the form of bar graph.

Immunohistochemistry for CD31 (a vascular endothelial cell marker) and alpha-smooth muscle actin (smooth muscle cell marker) revealed the presence of budding capillaries and several medium sized blood vessels (Fig. 67 and Fig. 68). In comparison to the control group, significant increase in the number of CD31 and ASMA positive blood vessels in the C-ECM and C-ECM AuNP biomaterial grafted groups were observed.

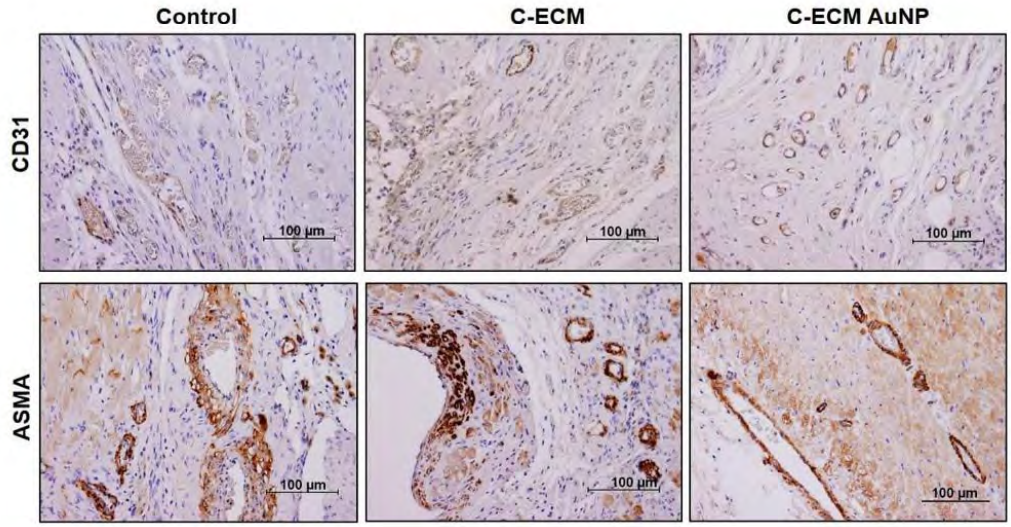

Figure 67: Immunohistochemical demonstration of CD31 positive endothelial cells for capillaries and alpha-smooth muscle actin positive smooth muscle cells of mature blood vessels in the tissue reaction at 4 weeks following MI and implantation of the grafts. Scale bar indicates 100 µm

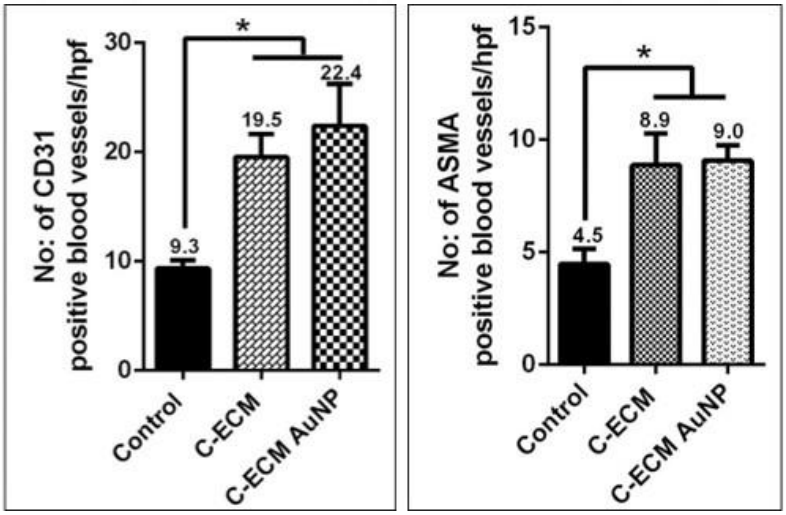

Figure 68: Bar diagram representing the quantitative data collected from CD31 and ASMA immuno-stained sections, p-value <0.05

Interestingly in both the biomaterial grafted animals, there was excessive infiltration of proliferating cells around the graft material as evidenced by the immunohistochemistry using PCNA antibody (Fig. 69). The abundance of PCNA positive cells were more proximal to the graft and less distal to the graft (Fig. 70). On the contrary, there were only a few proliferating cells in the myocardium of control animals.

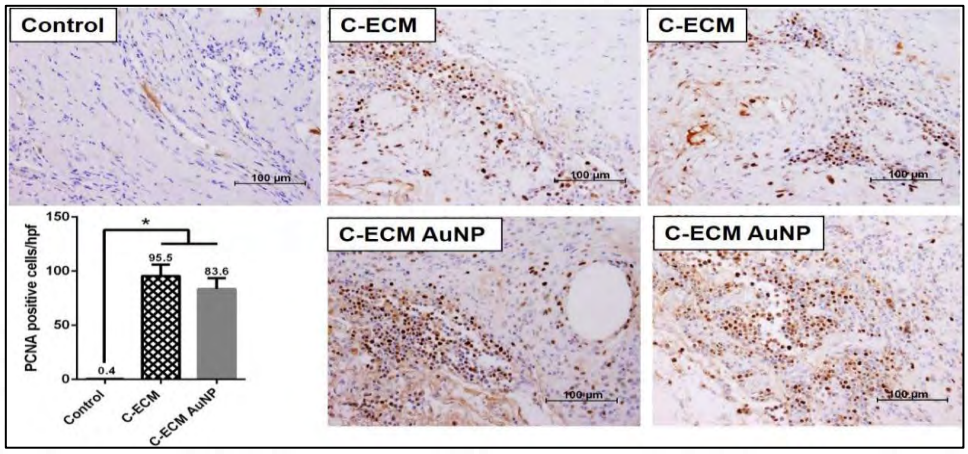

Figure 69: Immunohistochemical demonstration of proliferating cell nuclear antigen positive cells in the tissue reaction at 4 weeks following MI and implantation of the grafts. Scale bar indicates 100 µm. The quantitative data collected is represented in the form of bar graph, p-value <0.05

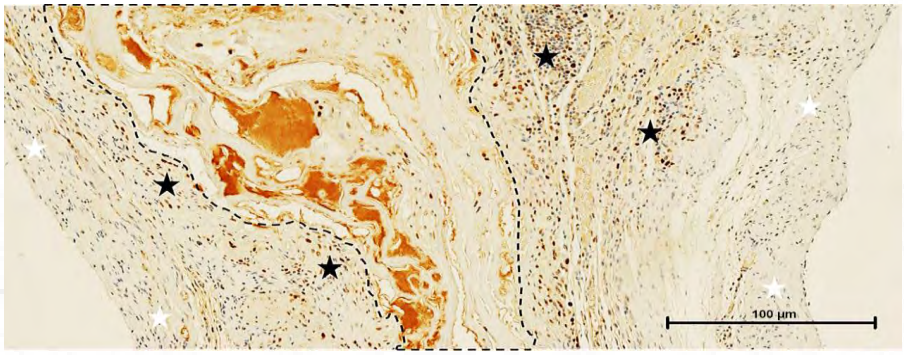

Figure 70: Light micrograph demonstrating the abundance of PCNA positive cells having brown nuclei proximal (black asterisk) and scarce positive cells distal (white asterisk) to the biomaterial (dotted line) detected by immunohistochemistry (8 images have been stitched to elucidate the distribution of proliferating cells). Scale bar indicates 100µm.

Cardiomyocyte function in the nearby infarct area was assessed by immunohistochemistry for connexin 43, a gap junction protein located predominantly in the intercalated disk region between cells. Increased number of positive cells were observed in the grafted groups compared to the control indicating the retention of cell to cell connection in the myocardium (Fig. 71).

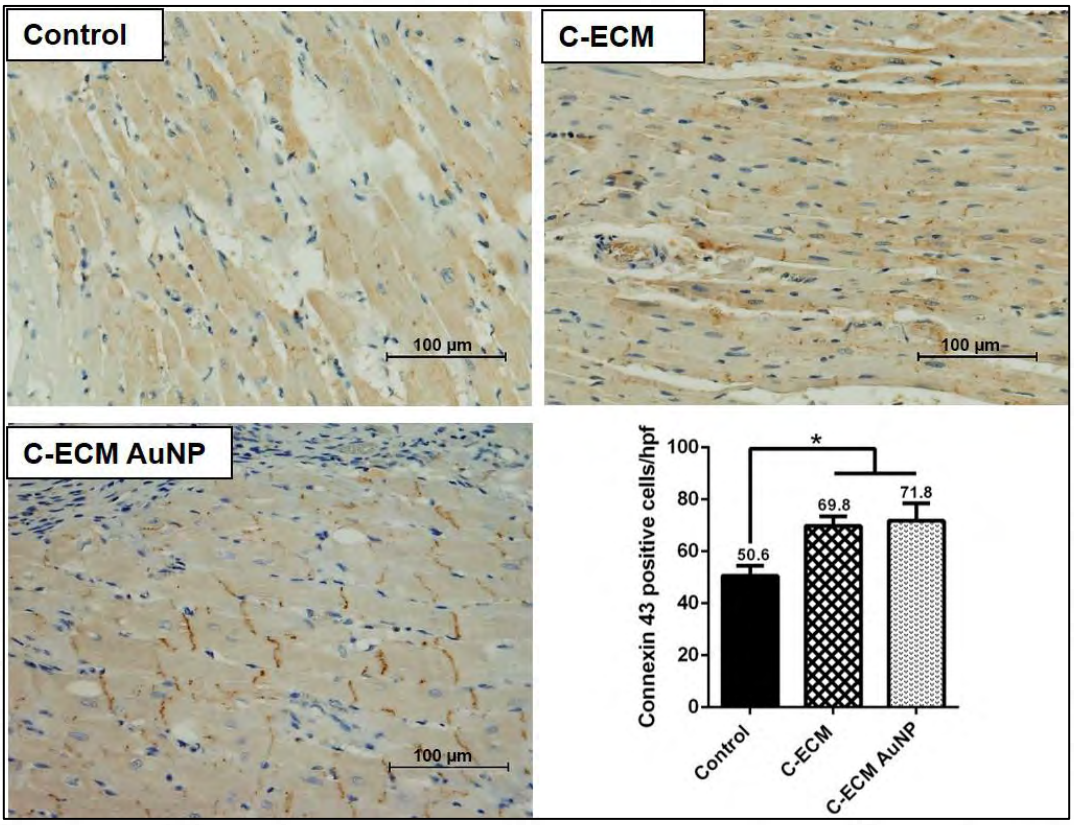

Figure 71: Immunohistochemical demonstration of connexin 43 positive cells in the tissue reaction at 4 weeks following MI and implantation of the grafts. Scale bar indicates 100 µm. The quantitative data collected is represented in the form of bar graph, p-value <0.05

The nature of post-MI replacement fibrosis was investigated by studying the distribution of myofibroblasts, a cell type known to orchestrate fibrosis in most tissues including the heart (Fig. 72). Remarkably, there was no difference in the number of myofibroblasts in the experimental groups despite the presence of grafts.

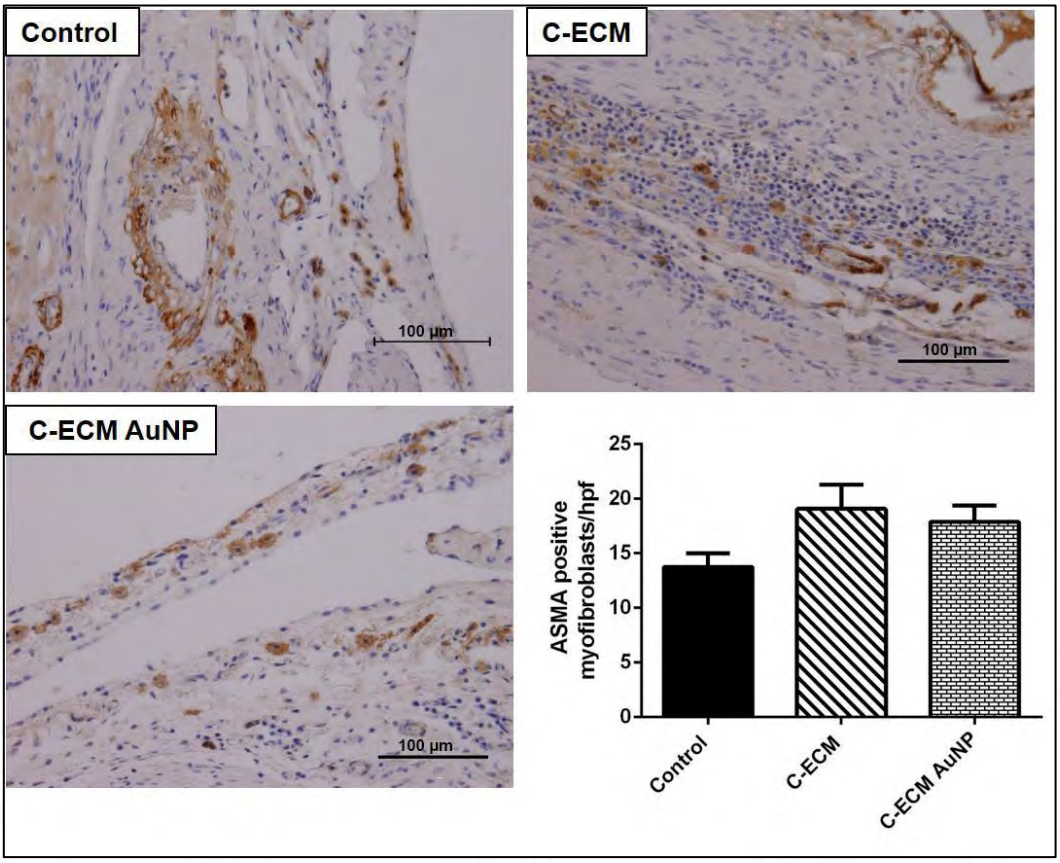

Figure 72: Immunohistochemical demonstration of alpha-smooth muscle actin positive myofibroblasts in the tissue reaction at 4 weeks following MI and implantation of the grafts. Scale bar indicates 100 µm. The quantitative data collected is represented in the bar graph.

4.3.5.4 Picro sirius red staining

The presence of collagen in the necrotic tissue was determined using picro sirius red staining which gives red colour to collagen and yellow colour to muscle tissue. The grafts viz. C-ECM and C-ECM AuNP being rich in collagen, stained red in colour. The necrotic region in the left ventricular region was well distinguished by this staining as evident from the compact collagen fibres (Fig. 73).

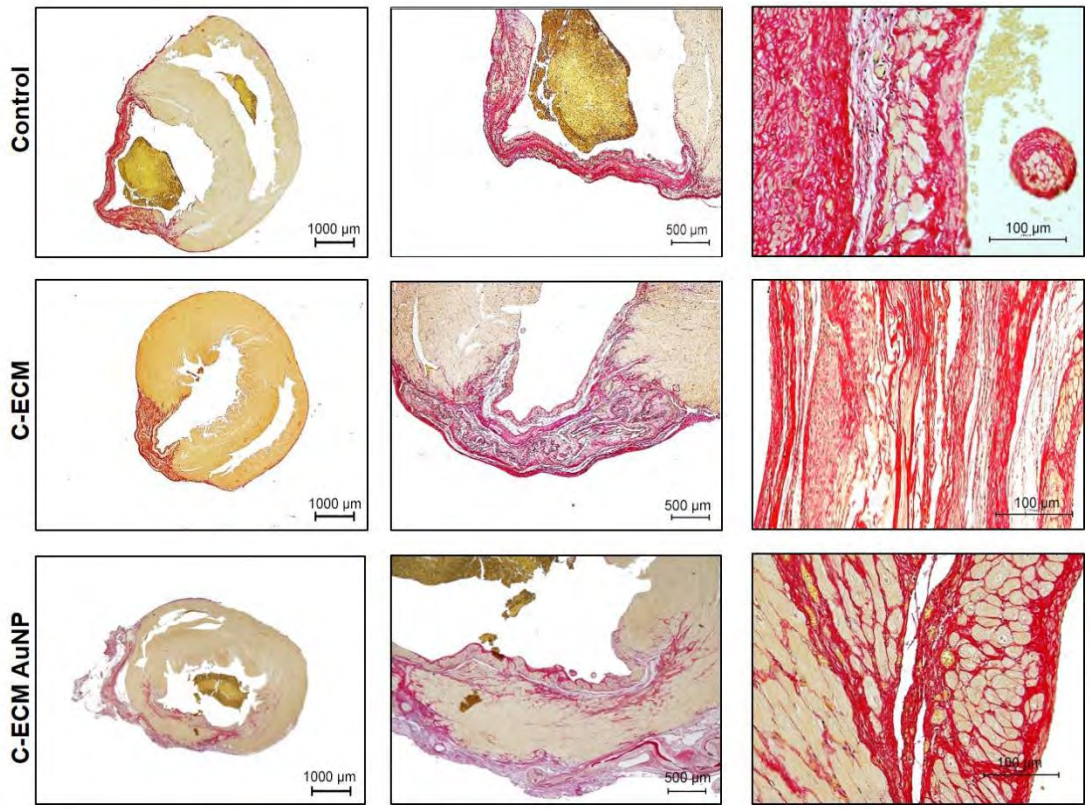

Figure 73: Light micrographs of picro sirius red stained tissue sections showing the collagenous necrotic myocardium due to induced MI at 4 weeks in all the three groups. Scale bar indicates 1000, 500 and 100 µm.

4.3.5.5 Masson's trichrome staining

The lower magnification of the Masson's trichrome stained section was used for area morphometry (Fig. 74). Using the image analysis software, the area of right ventricle, left ventricular free wall, infarct and interventricular septum were measured (Fig. 75). Right ventricular hypertrophy was minimal in the grafted animals compared to the control.

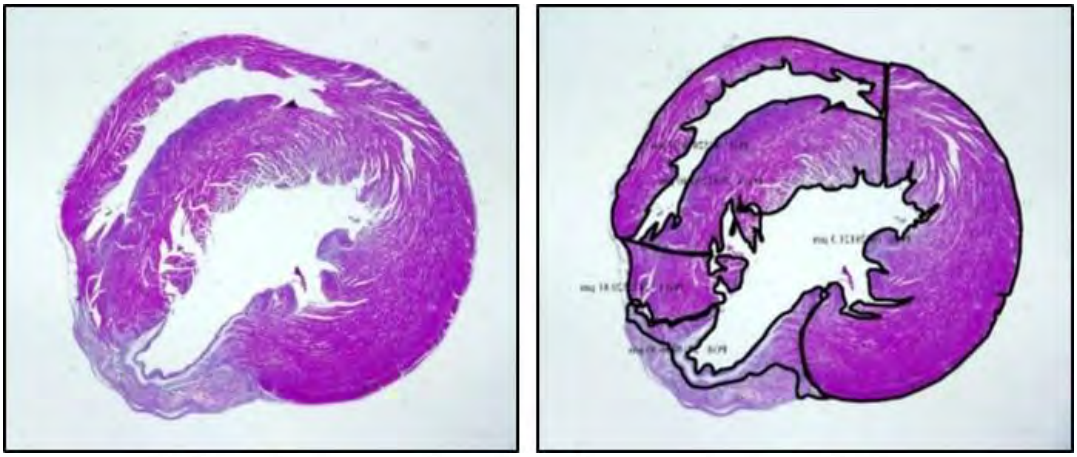

Figure 74: Light micrographs of Masson's trichrome stained sections used for area measurement

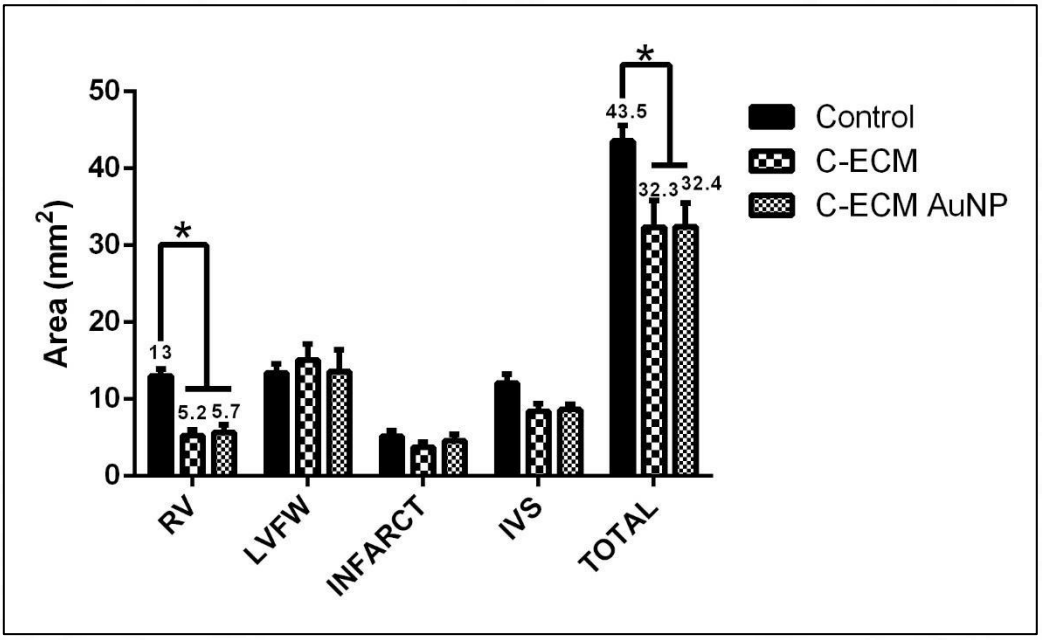

Figure 75: Histomorphometric data showing the area, p-value <0.05

In addition, the left ventricular thinning due to MI was appreciated in all the three groups (Fig. 76). The collagen rich necrotic tissue was stained blue in colour. Both the grafts C-ECM and C-ECM AuNP stained blue in colour and found integrated to the infarct region (Fig. 77).

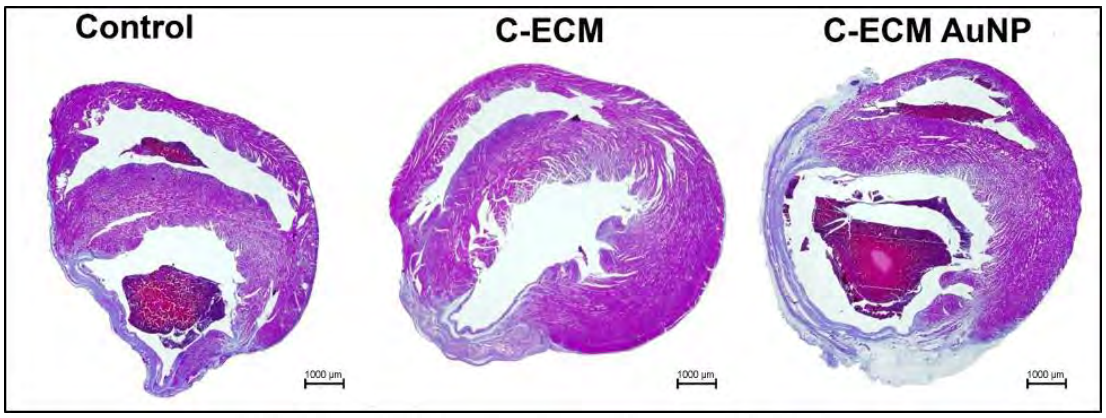

Figure 76: Light micrographs of the Masson's trichrome stained hearts at lower magnification x1.25. Scale bar indicates 1000 µm.

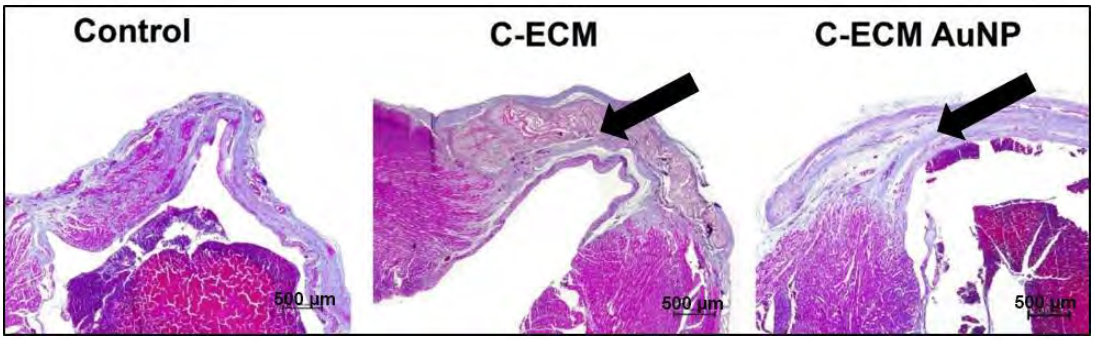

Figure 77: Light micrographs of the Masson's trichrome stained hearts at lower magnification x4 indicating collagen in scar tissue and the grafts (denoted by arrow). Scale bar indicates 500 µm.

In the higher magnification images of the Masson's trichrome stained sections, it was appreciated that the nature of collagen deposition (Fig. 78) was different in the presence of grafts in comparison to the control group. Using histomorphometry, the area occupied by total collagen was quantified and was found to be significantly reduced in the C-ECM and C-ECM AuNP grafted groups compared to the control group (Fig. 79).

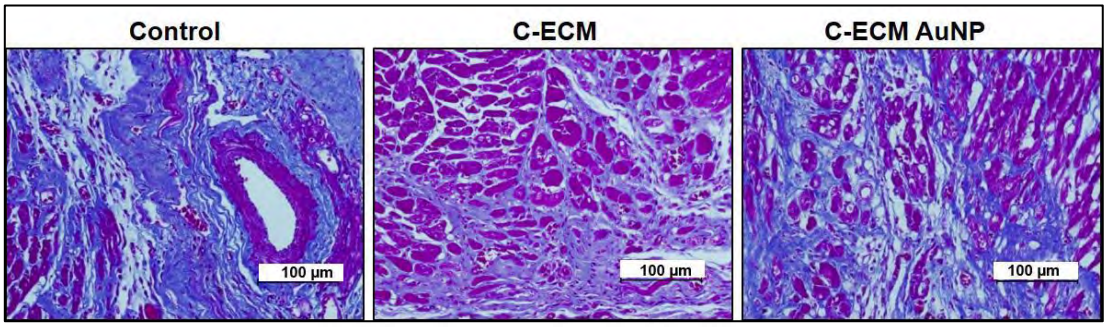

Figure 78: Light micrographs of the Masson's trichrome stained hearts at higher magnification x40 indicating the difference in the type of cardiac fibrosis between grafted groups and the control group. Scale bar indicates 100 µm.

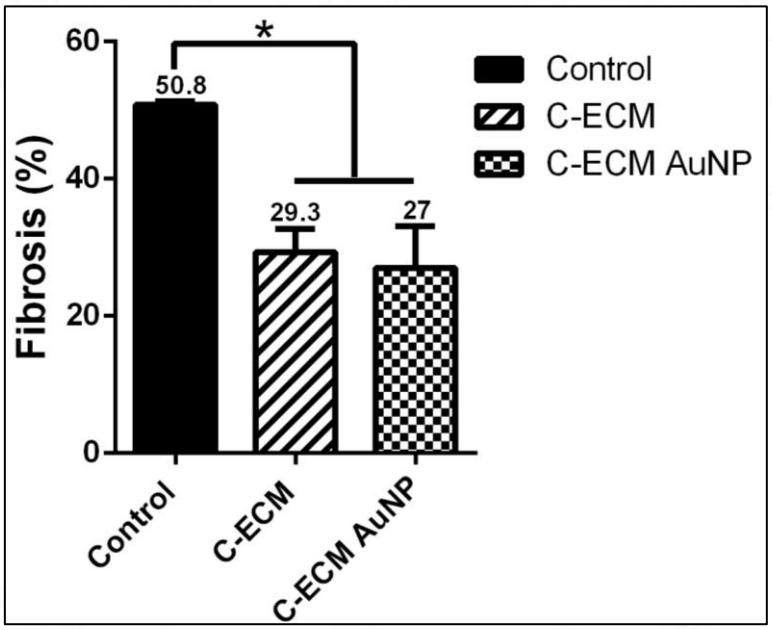

Figure 79: Bar graph representing the percentage of fibrosis obtained by histomorphometry, p-value <0.05

4.3.5.6 Herovici's staining

In this study, Herovici's polychromatic staining reaction was used to elucidate the differential nature of the fibrotic tissue reaction in the affected myocardium (Fig. 80). Through this staining technique, type 1 and type III collagen can be distinguished as pink and blue colour respectively (Fig. 81).

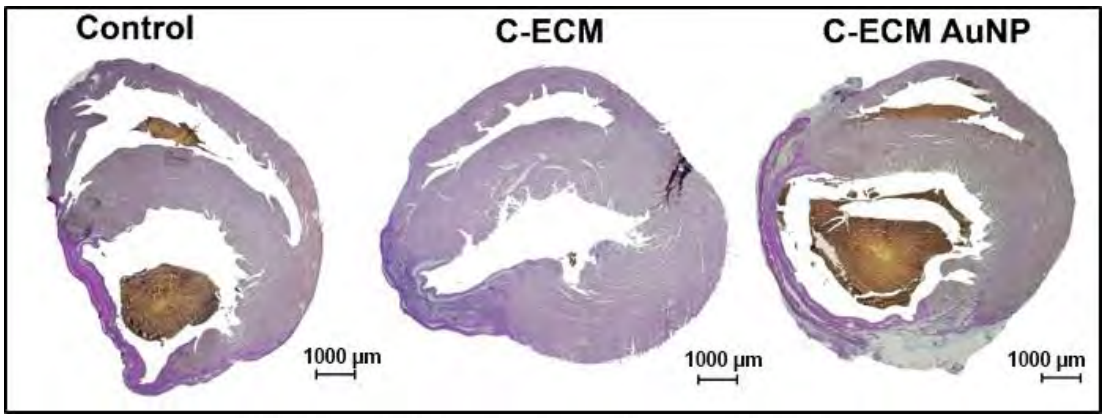

Figure 80: Light micrographs of the Herovici's stained hearts at lower magnification x1.25. Scale bar indicates 1000 µm.

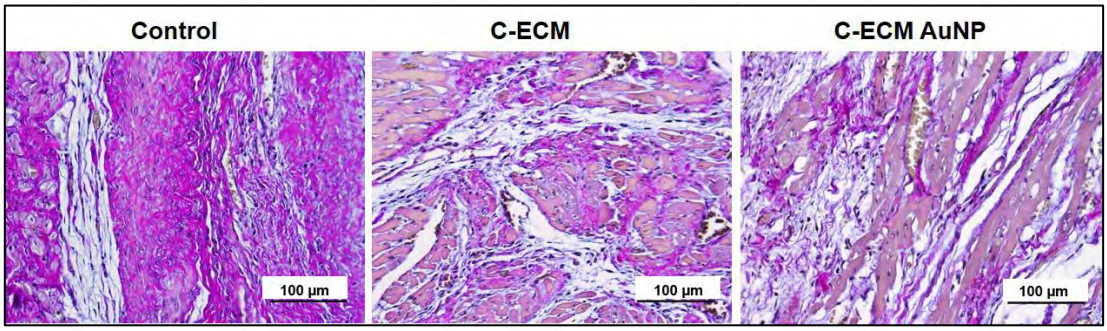

Figure 81: Light micrographs of the Herovici's stained hearts at higher magnification x40 indicating the differential deposition of collagen between grafted groups and the control group. Scale bar indicates 100 µm.

The post-MI remodelling reaction in the C-ECM and C-ECM AuNP groups was largely contributed by type III collagen rather than type I collagen (Fig.82 A and B). In the present instance, type I/type III collagen ratio in the control group was 2.4±0.5. Following the C-ECM-graft assisted healing, the ratio was 1.8±0.4 and that of C-ECM AuNP was 1.2±0.2. The ratio of type I to type III collagen was lowered in the grafted animals due to the decreased deposition of type I collagen (Fig. 82 C). It is certain that the presence of the biomaterial had prevented or delayed the formation of type I collagen.

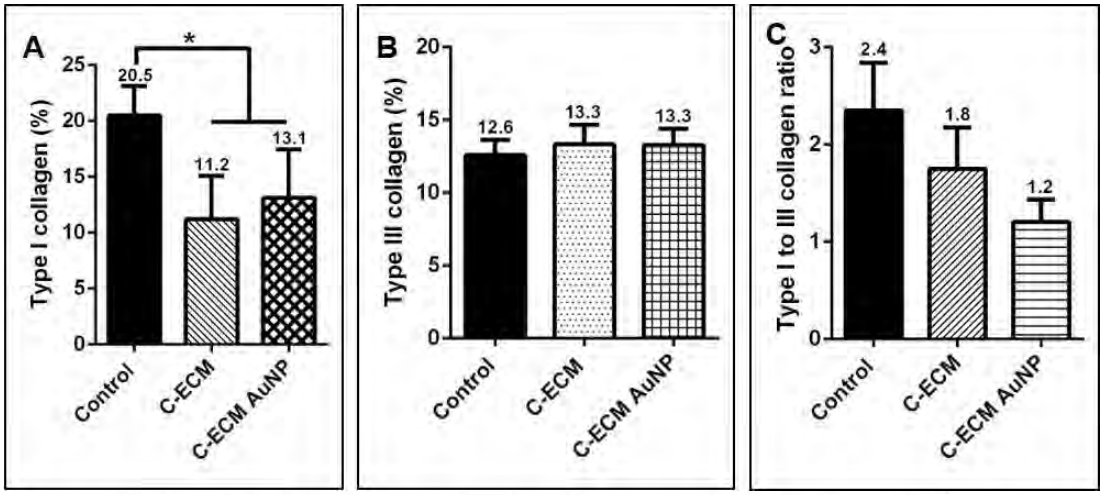

Figure 82: Bar graphs representing the histomorphometric data obtained from Herovici's stained sections (A) percentage of type I collagen, (B) percentage of type III collagen and (C) type I collagen to type III collagen ratio, p-value <0.05

5. DISCUSSION

Originally described as a xenogeneic scaffold with mesh-like architecture, C-ECM has been used as a biomaterial for graft assisted healing of wound in many tissues: small intestine (Burugapalli *et al*, 2008), skin (Revi *et al*, 2013; Karthika *et al*, 2018), subcutaneous tissue (Muhamed *et al*, 2015b), cornea (Anoop *et al*, 2017) and skeletal muscle (Balakrishnan-nair *et al*, 2018). However, the potential use of C-ECM for cardiac tissue engineering applications has not been explored. This study examined if C-ECM is suitable for cardiac application as a cardiac-patch. Specifically, a gold nanoparticle conjugation was proposed for modifying the electrical conductivity of the scaffold, a prerequisite for maintaining electrical conduction between the patch and the host myocardium.

5.1 Preliminary studies

Initial studies on porcine C-ECM prepared by a non-detergent/non-enzymatic method (Anilkumar *et al*, 2014; Mony & Anilkumar, 2020) were carried out to evaluate its suitability in cardiac tissue engineering. Biocompatibility is a key concept in biomaterial science that defines the ability of a material to perform its desired function (Ghasemi-Mobarakeh *et al*, 2019). Cytocompatibility evaluation is a major biocompatibility test (Keong & Halim, 2009). Earlier, cytocompatibility of C-ECM with other cell types like L929, mouse fibroblasts (Anilkumar *et al*, 2014; Raj *et al*, 2018) and C2C12, mouse skeletal myoblasts (Raj *et al*, 2020) was evaluated for tissue engineering. Generally, primary cardiomyocytes are the cells of choice for studying compatibility with any scaffold intended for cardiac application. Due to the difficulty in acquisition and maintenance in culture for a long time prevented researchers from using them because of the well-differentiated status and inability to return to S phase of the cell cycle. Therefore, traditionally immortalised cardiomyoblast cell lines like H9c2 derived from rat ventricular tissue are used for such studies (Garbern *et al*, 2013). Here, in this study the cytocompatibility of the C-ECM with H9c2 cells was evaluated by three tests namely direct contact test, live dead assay and MTT assay (Prasad *et al*, 2015). The direct contact test was performed to determine the cytotoxicity of C-ECM to H9c2. The result of the direct contact test (Fig. 11) showed that the material is non-

cytotoxic, the cells were viable and remained healthy in the vicinity of the scaffold. Further, the suitability of the C-ECM for cardiac tissue engineering was demonstrated by live-dead staining. In the live dead assay (Fig. 12), consistently there were higher numbers of live cells than dead cells when the cells were cultured on the C-ECM for 24 hours. Additionally, in order to demonstrate the ability of C-ECM to provide a suitable microenvironment for the survival of H9c2 cells, MTT assay was performed. More than 80% of H9c2 cells cultured on the C-ECM scaffold were viable (Fig. 13). Thus, the scaffold was found to provide a non-cytotoxic microenvironment suitable for the viability of cardiomyoblast cell line H9c2.

Since the *in vitro* evaluations confirmed the non-cytotoxic behaviour of C-ECM, *in vivo* response of the material was evaluated in a rat model of myocardial infarction. Even though various animal models have been used for the induction of MI, the rat model of MI is preferred because of the convenience in handling, housing and maintenance (Venkata *et al*, 2009). Here, MI was induced in Sprague Dawley rats by surgical ligation method (Kainuma *et al*, 2017) and C-ECM was implanted as an epicardial graft (n=3). The surgical ligation method is one of the most commonly used methods for MI induction but the mortality rate is very high (De Andrade *et al*, 2015). So in this study, the surgical procedure needed standardisation to minimise the mortality rate during the surgery. MI in these animals was confirmed by the estimation of serum biomarkers (Thygesen *et al*, 2018). There was an elevation in serum cardiac biomarkers such as troponin T, creatine kinase and creatine kinase-MB (Fig. 14) at 24 hours after the surgical ligation of the coronary artery indicating that the animals suffered from MI. After 2 weeks of surgery, the animals were euthanized and the hearts were explanted. The necrosis due to MI (Fig. 15) was appreciated macroscopically and microscopically. The effect of MI at the tissue level was studied by histology (Michaud *et al*, 2020). Histomorphologically, the healing response in rats implanted with or without C-ECM indicated signs of myocardial necrosis (Fig. 16). Thus, the animal model for MI induction and the procedure of grafting C-ECM on to the MI region was established.

5.2 Evaluation of the properties of C-ECM and its suitable modifications for cardiac tissue engineering

There are several approaches for achieving optimum electrical conductivity (Ye & Qiu, 2017; Solazzo *et al*, 2019; Saberi *et al*) of scaffolds intended for cardiac tissue engineering. Here, the C-ECM was conjugated with gold nanoparticles considering that gold nanoparticles can improve matrix conductivity and helps to establish electrical connectivity (Hasan *et al*, 2018). Besides, gold nanoparticle incorporated scaffolds were known to promote electrical signal conduction in cardiomyocytes (Shevach *et al*, 2014; Saravanan *et al*, 2018).

In the present instance, gold nanoparticles of about 20 nm size were synthesised by a citrate reduction method in which trisodium citrate was used as the stabilising and capping agent (Dobrowolska *et al*, 2015). The method was chosen because of its known simplicity and reliability for yielding nanoparticles of the desired size. The resulting citrate-capped gold nanoparticles were examined visually by the instantaneous colour change of the solution from pale yellow to cherry red colour, indicating the reduction of gold ions ($Au^{3+)}$ to gold atoms (Au^{+}). Various combinations of tetrachloroauric acid and trisodium citrate yielded gold nanoparticles of different size ranges. Thus, a combination of 0.5 mM tetrachloroauric acid and 1% trisodium citrate was selected to synthesise gold nanoparticles of 20 nm size. Gold nanoparticles prepared by this method had a negative surface charge capable of binding to functional molecules such as thiol, amine, cyanide and diphenyl phosphine (Majzik *et al*, 2010). In this study, cysteine was used for amine functionalisation as they have a relatively high affinity for gold nanoparticles through the formation of Au-S bonds. Here, functionalisation is expected to take place by the displacement of citrate anions and aggregation of particles through hydrogen bonding and electrostatic interactions (Acres *et al*, 2014). Amine functionalisation with cysteine was then visually recognised (Fig. 17) by a colour change from red to blue. The bare and amine functionalised gold nanoparticles were further characterised by UV-Vis spectroscopy, transmission electron microscopy and dynamic light scattering. In the UV-Vis spectra, the peak at 523 nm (Fig.18) indicated the absorption maxima of bare citrate-capped gold nanoparticles. The peak shift at 686 nm represented the amine functionalised

nanoparticles. The broad peak at the longer wavelength in the visible region was due to the coupling of surface plasmon resonance of two adjacent nanoparticles indicating the anisotropic optical properties of the aggregated gold nanoparticles (Hormozi-Nezhad *et al*, 2012). Transmission electron microscopic observations (Fig. 19) facilitated the determination of the size, shape and morphology of the gold nanoparticles before and after amine functionalisation (Rice *et al*, 2013). The results indicated that spherical gold nanoparticles (20 nm size) were maintained even after the amine functionalisation without any change in size. Later, the stability of the prepared gold nanoparticles was analysed by dynamic light scattering (Fig. 20). Negative zeta potential was obtained for both bare and amine functionalised nanoparticles, indicating optimum stability of the synthesised nanoparticles.

The synthesised gold nanoparticles were incorporated in the C-ECM by EDC-NHS chemistry (Mondalek *et al*, 2008; Miyagi *et al*, 2011). The most important biomaterial property expected to be introduced in C-ECM by the gold nanoparticle conjugation was electrical conductivity. The conductivity (Fig. 21) of the C-ECM AuNP scaffold improved significantly compared to the C-ECM scaffold. The obtained values were within the range of the electrical conductivity of the native myocardium, normally between 1.6×10^{-1} S/m (longitudinally) and 0.05×10^{-1} S/m (transversally) (Walker *et al*, 2019). Conductive scaffolds such as chitosan/carbon scaffolds (Martins *et al*, 2014) and gold nanoparticle-chitosan thermo-responsive hydrogels (Baei *et al*, 2016) have also been used for cardiac tissue engineering which facilitated the enhanced transmission of electrical signals between cardiac cells. Here, a conductive scaffold was fabricated from C-ECM by incorporating gold nanoparticles which was used for further studies.

The C-ECM AuNP was then characterised for the biomaterial properties like the presence of free amino groups, presence of functional groups by Fourier transform infrared spectroscopy, surface morphology by scanning electron microscopy, presence of elemental gold by energy-dispersive X-ray spectroscopy, surface topography by profilometry, thermal stability by thermogravimetric analysis and degradation property by enzymatic degradation assay. The important biomaterial properties of the C-ECM AuNP are discussed below.

The number of free amino groups in the scaffold before and after the incorporation of amine functionalised gold nanoparticles was estimated by TNBS assay (Davidenko *et al*, 2015). It was observed that the number of free amines significantly increased (Fig. 22) in the C-ECM AuNP indicating the binding of gold nanoparticles to C-ECM.

The detection of the functional groups present in C-ECM AuNP was performed by FTIR spectroscopy (Fig. 23). Extracellular matrices from mammalian organs/tissues are rich in collagen, therefore characteristic collagen peaks were expected (Movasaghi *et al*, 2008). In the C-ECM AuNP, the characteristic collagen peaks for amide I, amide II and amide III were observed suggesting that the modified scaffold had no change in the basic composition of C-ECM.

Scanning electron microscopy (Fig. 24) revealed the compact mesh-like architecture of the C-ECM AuNP which is more or less similar to that of C-ECM (Burugapalli *et al*, 2007). The increase in the compactness was probably due to the chemical cross-linking of the gold nanoparticles to the C-ECM scaffold. Moreover, the original architecture of collagen fibres was retained even after the incorporation of the gold nanoparticles to the C-ECM.

The energy-dispersive X-ray spectroscopy is associated with a scanning electron microscope which can detect the presence of elements in a specimen (Scimeca *et al*, 2018). The presence of elemental gold (Fig. 25) in the C-ECM AuNP scaffold indicated successful conjugation of gold nanoparticles onto the C-ECM.

Extracellular matrix-based scaffolds suffer from the lack of uniformity in surface topography resulting in poor integration to the host tissue (Mondalek *et al*, 2008). Here, the incorporation of gold nanoparticles onto the surface of C-ECM resulted in a smooth surface profile (Fig. 26) compared to the bare scaffold. This observation further supported the notion that C-ECM AuNP is a better scaffold than bare C-ECM for cardiac tissue engineering.

Thermal stability is an inherent property of any material intended for cardiac tissue engineering (Prasath Mani *et al*, 2019). It is known that while crosslinking increases the thermal stability of materials (Meyer, 2019). Here, the thermal stability

of the scaffolds was assessed using thermogravimetric analysis. The increase in the residual weight (Fig. 28) recorded for C-ECM AuNP compared to pristine C-ECM was due to the additional crosslinking with gold nanoparticles.

Enzymatic degradation of the scaffold was estimated by Ninhydrin assay. The presence of soluble amines in the solution indicated a higher absorbance value, which indicated faster degradation in the presence of collagenase enzyme (Grover *et al*, 2014). Here, both the C-ECM and C-ECM AuNP scaffolds showed a similar degradation rate (Fig. 29) from 24 to 72 hours.

After the physicochemical characterisation of the modified scaffold, the potential cytotoxic effect of C-ECM AuNP to cardiomyocyte cell line H9c2 was determined by direct contact test (Fig. 30), live dead staining (Fig. 31) and MTT assay (Fig. 32). From the results obtained, it was inferred that the C-ECM AuNP scaffold was non-cytotoxic and the scaffold was deemed to be a suitable niche H9c2 cells.

Thus, the overall results of the physico-chemical and biological evaluations conducted on the biomaterial properties of C-ECM AuNP largely indicated that it is indeed a candidate material for cardiac tissue engineering applications.

5.3 Differentiation of rat cardiomyoblast cell line H9c2 and rat bone marrow mesenchymal stem cells to cardiomyocyte-like cells

5.3.1 Differentiation of rat cardiomyoblast cell line H9c2 to cardiomyocyte-like cells

This part of the study was conducted to explore the *in vitro* differentiation efficiency of rat cardiomyoblast cell line H9c2 to cardiomyocyte-like cells. Generally, H9c2 cells are widely used for the differentiation to skeletal and cardiac muscle cells (Branco *et al*, 2015). Recently, a combination of H9c2 co-cultured with fibroblasts in appropriate substrates was used for cardiogenic differentiation (Navaee *et al*, 2020). Traditionally H9c2 cells differentiated with retinoic acid exhibited partially poly nucleated and elongated appearance (Kankeu *et al*, 2018). In this study, all-trans retinoic acid was used for the differentiation of H9c2 cells to cardiomyocyte-like cells under low serum conditions. It was observed that the morphology of the cells (Fig. 33)

altered from spindle to stellate structure with multiple nuclei. The multinucleated appearance (Fig. 34) of the differentiated cells was demonstrated by phalloidin staining. The FITC conjugated phalloidin binds to the F-actin, which is a cytoskeletal protein and was observed as green in colour. Multinucleation of H9c2 cells is considered as a morphological indication of its differentiation to cardiac lineage rather than to a rhabdomyocyte lineage (Branco *et al*, 2015). Previous reports have shown that H9c2 cells differentiated in the presence of low serum concentration and daily supplementation with retinoic acid exhibited features specific for cardiac differentiation. These included the increased expression of cardiac-specific proteins such as myosin light chain-2v and cardiac troponin-T together with a shift in metabolic preference from glycolytic to oxidative metabolism (Patten *et al*, 2017). Here, the differentiated cells showed (Fig. 35) increased expression of troponin-T, myo-D and connexin 43 indicative of cardiomyocyte-lineage specific proteins.

5.3.2 Differentiation of rat bone marrow mesenchymal stem cells to cardiomyocyte-like cells

The classical tissue engineering approach uses a combination of scaffolds, cells and growth factors (Caddeo *et al*, 2017). For cardiac tissue engineering, many cell types have been used as candidates such as bone marrow derived stem cells, embryonic stem cells, smooth muscle cells, adipose tissue derived stem cells, cardiac stem cells and induced pluripotent stem cells (Rodrigues *et al*, 2018). Bone marrow-derived mesenchymal stem cell transplantation is a promising clinical strategy for cardiovascular therapy (Bagno *et al*, 2018). In this study, rat bone marrow mesenchymal stem cells were selected for the differentiation to cardiomyocyte-like cells due to ease of availability, proliferative capacity and immune-modulatory properties (Guo *et al*, 2018). This section focus on the isolation, characterisation and differentiation of rat bone marrow-derived mesenchymal stem cells to cardiomyocyte-like cells. Mesenchymal stem cells (MSCs) are isolated from adult tissues and are multipotent (Ullah *et al*, 2015). They can differentiate to chondrocytes, adipocytes and osteocytes when a specific differentiation medium is supplied. Earlier evidence suggests that MSCs can express phenotypes of endothelial, neural, smooth muscle, skeletal myoblasts, and cardiomyocyte cells (Pittenger & Martin, 2004). In cell

therapy, MSCs prevent ventricular remodelling and improved recovery when delivered to the injured heart (Thakker & Yang, 2014).

For these experiments, MSCs were isolated from the femur of young Sprague Dawley rats (Huang *et al*, 2015). Once the cells reached the stage of confluency, they were trypsinised and used for the characterisation studies (Fig. 36). The doubling time of the isolated mesenchymal stem cells was 21±5h, indicated a good proliferation capacity. It is known that highly proliferating cells have shorter doubling time (Zhan *et al*, 2019).

The essential criteria for defining MSCs according to the International Society for Cellular Therapy (Dominici *et al*, 2006) was followed to characterise the differentiation potential of the isolated cells. More than 90% of cells expressed the positive markers such as CD90, CD73 and only less than 2% expressed the negative marker CD34 on flow cytometry analysis (Fig. 38). Immunostaining with CD90-FITC conjugated antibody revealed the surface expression (Fig. 39) of the marker by the isolated MSCs. Multilineage differentiation is considered as a convincing property of mesenchymal stem cells (Han *et al*, 2017). Therefore, differentiation of the isolated MSCs to other lineages is often studied by adding specific differentiation factors to the medium to direct their differentiation to adipocytes, chondrocytes and osteocytes. In this study, the isolated MSCs differentiated to adipocytes, chondrocytes and osteocytes indicating the multilineage differentiation potential (Fig. 40).

After the characterisation of the rat bone marrow-derived mesenchymal stem cells, the cytotoxic effect of the scaffolds C-ECM and C-ECM AuNP with the isolated rat bone marrow mesenchymal stem cells was determined by direct contact test (Fig. 41) confirming the scaffolds as non-cytotoxic to the stem cell.

Differentiation of MSCs to cardiomyocyte-like cells has been reported by many research groups (Pittenger & Martin, 2004; Guo *et al*, 2018). In this study, 5-azacytidine was used for the differentiation of mesenchymal stem cells to cardiomyocyte-like cells. 5-Azacytidine is a hypomethylating agent commonly used for the treatment of the myelodysplastic syndrome, which functions as a DNA methyltransferase inhibitor causing hypomethylation of DNA. Low doses of 5-

azacytidine have been used for inducing differentiation of stem cells while higher doses are cytotoxic (Supokawej *et al*, 2013). With the influence of 5-azacytidine, the spindle morphology of the MSCs changed to a slender stick-like morphology indicating differentiation towards a cardiac lineage (Fig. 42). In addition to this, the differentiated cells showed (Fig. 43) increased expression of cardiac proteins such as troponin-T, myo-D and connexin-43. These are further supported by the fact that MSCs derived from human bone marrow as well as human umbilical cord differentiated into cardiomyocytes with the expression of desmin, β-myosin heavy chain, cardiac troponin T, A-type natriuretic peptide, and Nkx2.5 (Xu *et al*, 2004; Qian *et al*, 2012).

5.4 Functional evaluation of the C-ECM and CECM AuNP as cardiac-patches in a rat model of non-fatal myocardial infarction

An appropriate animal model was established and the method of grafting the scaffold was standardised as described in section 5.1. The surgical induction of MI in the experimental animals was demonstrated by serum biochemistry, electrocardiography, echocardiography and histopathology. The serum biochemical estimation of cardiac biomarkers (Fig. 44) such as troponin T, creatine kinase and creatine kinase-MB at 24 hours confirmed that the experimental animals suffered from MI. Troponins, creatine kinases, lactate dehydrogenase increases in blood during myocardial infarction and detection of cardiac troponins is the gold standard for the early diagnosis (Mythili & Malathi, 2015). After MI induction and the epicardial patch grafting, the animals were observed for 4 weeks.

One of the most widely used techniques in cardiovascular research is ECG, which reflects the electrical activity of the heart and provide information about the functional and structural characteristics of the myocardium (Konopelski & Ufnal, 2016). During pathological conditions, variations in the ECG helps in diagnosing and monitoring the progression of the disease. Now, ECG is also used as a research tool for studying the effect of drugs or other cardiac interventions (Sattar & Chhabra, 2020). Evaluation of the elevation or depression of ST-segment is an essential

parameter considered for the diagnosis of myocardial infarction. Also, the QRS complexes reflect ventricular rhythms as well as disturbances of intraventricular conduction resulting from heart failure and myocardial ischemia (Konopelski & Ufnal, 2016). In this study, ECG was used to monitor the changes in the electrical activity of the heart after MI induction as well as the recovery after scaffold grafting. A baseline recording was taken from all the animals to compare it with the subsequent ECG recording after the surgical procedure. One week post-MI, the effect of MI was evident in all the three groups. The depression in ST-segment in the grafted groups and the widening of the QRS peak in the control group (Fig. 45) indicated that the animals suffered from non-fatal MI. But at 4 weeks, recovery was prominent in the C-ECM/C-ECM AuNP grafted animals and the ECG peaks appeared similar to the baseline data. The C-ECM AuNP being a conductive scaffold, animals grafted with them had near-normal ECG pattern at 4 weeks compared to the bare C-ECM grafted animals. This observation indicated that the probable effect of a conductive biomaterial in modulating the left ventricular contractility. Quantification of the various ECG parameters (Fig. 46) indicated the persistence of MI in all the animals at one week while the recovery was prominent in the grafted animals at 4 weeks.

Echocardiography is another non-invasive technique (Sadeghizadeh *et al*, 2017) used for monitoring cardiac anatomy and function. On evaluating various parameters derived from the echocardiogram, it was concluded that there was no significant difference in any of the parameters between the three groups at one week indicating the uniformity in MI induction. On the 4^{th} week post-MI, there was a significant change in the IVSs and IVSd (Fig. 48 A, B) between C-ECM and control group indicating recovery in the C-ECM group. The interventricular septal dimensions of the C-ECM grafted animals were near to the baseline but it was higher for the control group indicating septal hypertrophy in control animals. During MI, it has been observed that the regions adjacent to the non-infarcted region undergo hypertrophy at the later phase to compensate for the damage (French & Kramer, 2007). In this study, such a response was not observed in the grafted animals but was prominent in the control animals indicating minimal hypertrophy and decompensation in the grafted animals.

Four weeks post-MI all the animals were euthanized and the tissues were collected for gross and histopathological evaluations. Gross necropsy examination of the hearts (Fig. 49) indicated the integration and *in vivo* compatibility of the C-ECM and C-ECM AuNP. It was noted that the bodyweight of all the animals (Fig. 50) decreased after the surgery and increased gradually to attain the initial body weight. The reduction in body weight soon after the procedure may be due to the general effect of the surgery but the animals survived the MI induction procedure demonstrated by the steady increase in body weight. However, the C-ECM grafted animals were more severely affected and attained the initial body much later than the other groups. Earlier similar studies have also used the heart weight to body weight ratio of animals as an index of myocardial hypertrophy (Voucharas *et al*, 2011). Here, the ratio was within the normal range indicative of minimal hypertrophic response (Fig. 51) inconsistence with the previous findings.

Tri-phenyl tetrazolium chloride staining is a commonly used method to differentiate the infarct area from the normal area and also for the assessment of the extent of the infarct (Redfors *et al*, 2012). Here in this study, at necropsy, the MI was appreciated grossly as a pale non-vascular area and the result was confirmed by a veterinary pathologist. Significant myocardial necrosis (Fig. 52) was observed in all the animals confirming the uniformity of MI induction.

The OES-ICP is an emerging powerful technique for the detection of elements and isotopes distributed in a material (Reddy *et al*, 2018). The C-ECM AuNP incorporated with gold nanoparticles was grafted in animals, therefore the biodistribution of gold to other organs was studied by OES-ICP analysis. The tissue samples such as the brain, lungs, liver and kidney were collected from the animal during the necropsy procedure and were analysed for the presence of gold using this method. It was observed that there was no detectable amount in gold suggesting the clearing of gold from the animals at 4 weeks.

The host biomaterial interaction and the effect of MI at the tissue level was investigated by histological methods. According to Pasotti *et al*, 2006, MI can be diagnosed histomorphologically by the presence of coagulative necrosis of the

myocardium. Haematoxylin and eosin stained heart sections (Fig. 53) revealed the left ventricular myocardial degeneration/necrosis in all the animals. However, there were no evident signs of necrosis (Fig. 54), inflammatory reactions, or loss of cell integrity in other organs such as the brain, lung, liver, kidney and spleen between the control and the grafted animals indicating the safety of the biomaterial.

Cardiomyocyte hypertrophy is an early stress response happening in the heart leading to the expansion of the cardiac extracellular matrix, deposition of connective tissue and finally resulting in heart failure (Coelho-Filho *et al*, 2013). In this study, the cardiomyocyte hypertrophy at the cellular level was quantified with the help of an image analysis software. It was observed that in the presence of C-ECM/C-ECM AuNP, the cardiomyocyte hypertrophic response (Fig. 55-61) was minimal in the animals compared to the control animals.

Cell death is a characteristic feature of various cardiac diseases leading to hypertrophy of the surviving cells (Chiong *et al*, 2011). This is associated with increased cell volume, enhanced protein synthesis, and heightened organization of the sarcomere of surviving cells (Frey *et al*, 2004). In the present study, it was observed that in the grafted animals the number of interventricular septal cells (Fig. 62) was preserved while there was a reduction in the control animals. The observation indicated the continued progression of compensatory hypertrophic response in the non-grafted controls. It is known that post-MI hypertrophy may lead to decompensation (Toepfer *et al*, 2016). The minimal hypertrophic response in the biomaterial grafted animals possibly indicated the protective effect of the grafts.

To study the cellular response associated with MI and the cellular and molecular changes associated with the graft implantation, immunohistochemistry for various cellular proteins was carried out. Initially, the distribution of lymphocytes in the infarct zone was investigated. Lymphocytes, especially T cells are the key players in the tissue repair process, including that following myocardial infarction (Rieckmann *et al*, 2019). Several studies have shown that T lymphocytes are involved in cardiac remodelling after MI (Laroumanie *et al*, 2014). T cells promote early cardiac healing by regulating macrophage polarisation, fibroblast activity and extracellular purinergic signalling but chronic T cell activation in the myocardium leads to the development of adverse remodelling reactions resulting in heart failure (Rieckmann *et al*, 2019).

Having a role in adaptive immunity, CD4 positive T cells are limited to major histocompatibility complex class (MHC) II and act as helper cells for various immune responses, while CD8 positive T cells recognize antigens using MHC class I and perform cytotoxic function (Bueno & Pestana, 2002). During C-ECM-assisted healing in the heart, both the CD4 and the CD8 cell numbers increased indicating the influence of the graft in modulating the immune cells. However, out of these cells, the CD4 positive cells (Fig. 63) predominated indicating pro-graft acceptance reaction. The number of CD4 and CD8 positive cells was almost equal in the C-ECM AuNP group which also indicated a beneficial reaction. However, the number of pro-inflammatory CD8 positive cells predominated in the control group, definitely, an indication of progression to heart failure.

The proportion of CD4 to CD8 indicates the health of the immune system. A ratio between 1.5 to 2.5 is considered normal (McBride & Striker, 2017). After the MI induction, a lower number of CD4 cells and an inversion of the ratio were observed in acute myocardial infarction (Fig 65) suggesting a continued pro-inflammatory reaction. On the other hand, the grafts appeared to have induced a pro-regenerative reaction with a dominant proportion of CD4 positive T cells.

Another cell type investigated was macrophages which are key mediators of innate immune response participating in the recognition and elimination of pathogens by phagocytosis (O'Rourke *et al*, 2019). One to three days after MI, macrophages show a pro-inflammatory M1 phenotype and later at about 4 weeks, an anti-inflammatory M2 phenotype is expressed with distinct and opposite functions (Ma *et al*, 2018). In this study, the macrophages were demonstrated by immunohistochemistry and observed no significant difference between the three groups (Fig. 66) suggesting a similarity in the extent of inflammatory reaction between the groups. A detailed study on the distribution of M1 and M2 macrophage might have elucidated the extent of pro-inflammatory and pro-regenerative responses in different experimental groups as observed with the distribution of CD4 and CD8 lymphocytes.

Angiogenesis post-MI can reduce cell damage by stimulating blood supply (Kobayashi *et al*, 2017). The increase in the number (Fig. 67 and 68) of CD31 positive endothelial cells and alpha smooth muscle actin positive smooth muscle cells in the tissue reaction at 4 weeks indicated enhanced angiogenesis in the grafted animals. The

C-ECM/C-ECM AuNP displayed a pro-angiogenic effect through which the ischemic myocardium was salvaged with the formation of new blood vessels. Even though an assessment of oxygenation and blood supply was not possible in these tissue sections by these techniques, the morphometric data suggested differential reperfusion between the three groups. The grafts promoted the recruitment of cells that participated in angiogenesis at the MI site. CD31 positive capillaries is a definite indication of sprouting blood vessels which may mature into functional blood vessels in later phase of healing reaction. This is an indication that both the ECM scaffolds promote reperfusion in the myocardium which can restore blood flow and limit the infarct size (Mongiat *et al*, 2016).

Generally, following an injury tissue remodelling is essentially contributed by the regenerative response of the parenchyma and the reparative process by connective tissue (Iismaa *et al*, 2018). Myocardial parenchyma may not mount a significant regenerative response because of its terminally differentiated G_0 status (Siddiqi & Sussman, 2014). In consistence with these knowledge, cell proliferation was absent in the infarcted myocardium in all the groups. Contrastingly, many cells (Fig. 69 and Fig 70) infiltrating around the C-ECM/C-ECM AuNP had proliferative potential. These were definitely non-native cells and may include progenitor cells participating in the tissue remodelling of the necrotic tissue. Recruitment of non-native endogenous cells, triggered by biological cues hidden in the extracellular matrix, to the defect site is considered as one of the major mechanisms by which ECM-based biomaterials induce healing in the infarct site (Mewhort *et al*, 2016; Frangogiannis, 2017). However, here, it remains unclear from the investigations performed so far concerning the identity of cells infiltrating the infarcted myocardium and the molecular signals elaborated by these cells.

Cardiomyocyte function in the nearby infarct area was assessed by immunohistochemistry for connexin 43, a gap junction protein located predominantly in the intercalated disk region between cells (Schulz *et al*, 2015) revealed higher number of positive cells (Fig. 71) indicating the retention of the cell to cell connection in the myocardium in the grafted groups compared to the control group.

Cardiac injury of any type results in fibrotic scarring because of the limited regenerative potential of the surviving cardiomyocytes, for repopulating the lost

myocardial parenchyma (Prabhu & Frangogiannis, 2016). Taking this into consideration, the nature of post-MI replacement fibrosis was investigated by studying the distribution of myofibroblasts, a cell type known to orchestrate fibrosis in most tissues including the heart (van Putten *et al*, 2016). There was no difference in the distribution of myofibroblast (Fig. 72), implying the similarity in the potential for post-MI-fibrogenesis in all the three groups.

However, the nature of the collagen deposition was significantly different in the treated groups compared to the control animals. Specially, the assessment of collagen deposition in the tissue sections was evaluated by three types of histochemistry reactions *viz*. picro sirius red (Vogel *et al*, 2015), Masson's trichrome (Schipke *et al*, 2017) and Herovici's (Turner *et al*, 2013) stains. In the sections stained with picro sirius red (Fig. 73), the infarct area was differentiated as red coloured collagenous region in all the experimental animals.

Histomorphometric analysis of the low magnification Masson's trichrome stained sections (Fig. 75) showed preservation of the area of the right ventricle, left ventricular free wall, infarct and interventricular septum in the grafted animals whereas, the right ventricular area increased in the control. This data had a correlation with the cardiomyocyte diameter measurement to confirm the minimal hypertrophic response in the C-ECM/C-ECM AuNP grafted animals. Similar to picro sirius red staining, the area occupied by collagen (Fig.76) in the infarcted myocardium was elucidated by Masson's trichrome stained section as blue in colour. The grafts also stained blue in colour as the porcine cholecystic extracellular matrix is rich in collagen (Burugapalli *et al*, 2007). Surprisingly, the nature of the perceived fibrotic reaction in the C-ECM/C-ECM AuNP grafted animals was remarkably different from the non-grafted animals which were established from the high magnification trichrome images. The fibrosis in the grafted animals was more of an interstitial type while in the control group, it was a replacement type of fibrosis. Interstitial fibrosis is characterised by increased ECM deposition without any significant loss of cardiomyocytes whereas in replacement fibrosis excess collagen deposition together with the damage of cardiac cells occurs. Here, dead cells are replaced and a predominantly collagen type I-containing scar is formed (Hinderer & Schenke-Layland, 2019).

The extent of collagen deposition (Fig. 77-79) was significantly low in the grafted animals irrespective of the presence of gold nanoparticles. The main cells which participate in the synthesis of collagen are myofibroblasts and they can secrete at least two subtypes of collagen, type I and type III (van Putten *et al*, 2016). The type I collagen is essentially composed of highly cross-linked fibrillar collagen relatively insensitive for enzymatic degradation compared to reticular type III collagen amenable for degradation as in tissues with considerable elasticity (Rusu *et al*, 2019). Both these collagen types will be present in any tissue but the relative proportion defines elasticity. Terminally matured inelastic scar has an abundance of type I collagen in proportion to type III collagen.

In the present study, the results of the Herovici's staining reaction (Fig. 80-82) further elucidated the differential nature of the fibrotic tissue reaction in the affected myocardium. The post-MI-remodelling reaction in the C-ECM/C-ECM AuNP groups was largely contributed by type III collagen rather than type I mature collagen responsible for fibrotic scarring. Given the fact that no known synthetic or natural biomaterial is known to reverse cardiac fibrosis, the observation that the C-ECM/C-ECM AuNP mitigated deposition of type I collagen is significant. In cardiac tissue, the ratio of type I to type III collagen is 8:1 which gets altered with progressive fibrotic reaction either due to tissue injury or old age (Horn & Trafford, 2016). In the graft-assisted groups, the decreased type I/III collagen ratio was contributed by the reduction in type I collagen content. This cannot be considered as clear evidence of fibrosis reversal, but certainly an indication of reduced or delayed deposition of type I collagen. Previously, it was reported that increased expression of type III collagen improved heart function by altering the balance of collagen distribution and ratio in LV remodelling (Uchinaka *et al*, 2018). Certainly, the presence of porcine cholecystic extracellular matrix with or without gold nanoparticles had prevented or delayed the formation of type I collagen. The use of a larger number of animals and euthanizing them at more frequent intervals would have clarified these deductions, especially the dynamics in the extend of collagen deposition.

Graft assisted healing of injured myocardium in regenerative medicine is not novel (Venugopal *et al*, 2012), and both synthetic as well as non-synthetic grafts are

available for this purpose (Cui *et al*, 2016). Acellular xenogeneic extracellular matrix biomaterials have been used as constructive scaffolds for tissue regeneration including porcine small intestinal submucosa and urinary bladder derived ECM (Mewhort *et al*, 2014; Robinson *et al*, 2005). Such natural scaffolds are apparently superior to synthetic scaffolds which elicits unfavourable tissue reaction with foreign-body giant cells, necrosis, and calcification. Bovine pericardium based ECM scaffolds such as Peri-Guard®, PhotoFix™ and CardioCel® have been used in cardiac repair but all of them displayed poor integration to the native tissue often complicated with calcification (Pattar *et al*, 2019). Cormatrix® ECM,™ a porcine small intestinal ECM has recently gained popularity in the cardiovascular field due to its unique surface architecture and ability to initiate, control cell proliferation and differentiation (Mosala Nezhad *et al*, 2016). In addition, basic fibroblast growth factor enhanced Cormatrix improved cardiac performance after sub-acute myocardial infarction (Mewhort *et al*, 2014). Epicardial infarct repair with Cormatrix boosted the myocardial repair process and vasculogenesis in an ischemia-reperfusion pig model (Mewhort *et al*, 2016).

In short, in the present study a relative abundance of degradable reticular type III over type I collagen, a congenial environment for cell proliferation, enhanced angiogenesis and favourable graft acceptance reaction was observed, when the C-ECM/C-ECM AuNP was used for graft-assisted healing, despite uniformity in the extent of MI between the groups. The data largely points to the modulatory effect of the biomaterial on the pathogenesis of post-MI fibrotic reaction. Further investigations are certainly essential for unravelling the cellular/molecular mechanisms responsible for the delayed scarring and the pathobiology of the cardiac remodelling process. As clinicians strive for strategies to mitigate cardiac fibrosis, the C-ECM/C-ECM AuNP as an epicardial graft offers a credible option. If not a reversal, the induction of delayed fibrosis offers a wider window period to clinicians for identifying and deploying different therapeutic strategies for managing post-MI scarring.

6. SUMMARY & CONCLUSION

6.1 Summary

- Porcine cholecystic extracellular matrix scaffold prepared by a non-detergent/non-enzymatic process was proved as an excellent scaffold for the growth of H9c2 cardiomyoblast cells.
- An animal model for myocardial infarction was established for inducing non-fatal myocardial infarction by surgical ligation of the left anterior descending coronary artery in Sprague Dawley strain of rats.
- The induction of myocardial infarction in experimental rats was confirmed through the estimation of serum cardiac biomarkers such as troponin T, creatine kinase and creatine kinase-MB and clinically monitoring with electrocardiography and echocardiography.
- The nature of *in vivo* healing response induced by the porcine cholecystic extracellular matrix scaffold was evaluated by histomorphology.
- Conjugation of functionalised gold nanoparticles to porcine cholecystic extracellular matrix scaffold was possible and the modified scaffold was a potential conductive biomaterial for cardiac tissue engineering.
- Biological properties of the gold nanoparticle incorporated porcine cholecystic extracellular matrix scaffold was also evaluated by growing H9c2 cells and found to be a suitable substrate for their growth.
- H9c2 cells were cultured and differentiated to cardiomyocyte-like cells using all-trans retinoic acid in serum reduced condition and evaluating the expression of cardiac proteins like troponin T, myo D and connexin 43 by the differentiated cells.
- Rat bone marrow-derived mesenchymal stem cells were isolated from Sprague Dawley rats and characterised.
- Cytocompatibility of rat bone marrow-derived mesenchymal stem cells on porcine cholecystic extracellular matrix scaffold as well as on the nanoparticle incorporated porcine cholecystic extracellular matrix scaffold was evaluated.

- The rat bone marrow-derived mesenchymal stem cells were made to differentiate in to cardiomyocyte-like cells using 5-Azacytidine.
- Myocardial infarction was induced in Sprague Dawley rats and serum biochemistry showed an elevation in cardiac biomarkers. Two epicardial grafts: C-ECM and C-ECM AuNP were used for the *in vivo* study.
- Electrocardiogram and echocardiogram data suggested the preservation of cardiac function in the grafted rats at 4 weeks.
- Both the grafts partially integrated to the host tissue as evident in gross and histology images. Myocardial necrosis due to the induced infarction was evaluated by histomorphology and histomorphometry.
- Biodistribution of gold nanoparticles was studied using optical emission spectroscopy- inductively coupled plasma and it was observed to be below the detectable limit in the brain, lungs, kidney and liver indicated clearance from the system.
- Cardiac hypertrophy was minimal in both the porcine cholecystic extracellular matrix scaffold group as well as in the nanoparticle incorporated porcine cholecystic extracellular matrix scaffold group.
- A favourable graft acceptance reaction was observed as evidenced by increased CD4 (helper T lymphocytes) to CD8 (cytotoxic T lymphocytes) ratio in the grafted groups. There was no significant difference in the number of macrophages and myofibroblasts between the grafted and control animals.
- Angiogenesis was enhanced in the presence of grafts as demonstrated by CD31 positive (sprouting) and alpha smooth muscle actin (functional) blood vessels in the infarcted myocardium.
- Cell proliferation was observed in abundance near the vicinity of the grafts indicating the recruitment for extra-myocardial cells for the graft-assisted healing. Thus, the porcine cholecystic extracellular matrix scaffold can act as a niche for proliferating cells.
- Higher number of connexin 43 cells was observed in the presence of both the grafts which demonstrated functional cardiomyocytes in the myocardium.

- A significant reduction in collagen deposition was observed in the presence of the grafts indicated delayed remodelling reaction.
- The post-infarction-remodelling reaction in the grafted animals was largely contributed by type III reticular collagen instead of type I mature collagen. Thus, porcine cholecystic extracellular matrix delayed the myocardial scarring process by mitigating collagen deposition specifically type I collagen.
- Although, the gold nanoparticle incorporated porcine cholecystic extracellular matrix scaffold had higher conductivity compared to the bare scaffold, there was no significant difference between the two groups in the various evaluations carried out in the study. Both the scaffolds, C-ECM and C-ECM AuNP can be used as candidate epicardial-patches for further investigations.

6.2 Clinical significance

- Porcine cholecystic extracellular matrix scaffold delays fibrotic scarring during healing of non-fatal myocardial infarction.
- Porcine cholecystic extracellular matrix scaffold increases cardiomyocyte survival
- The graft-assisted healing with porcine cholecystic extracellular matrix scaffold widens the window period between infarction and scarring.

6.3 Conclusion

- Porcine cholecystic extracellular matrix scaffold prepared by a non-enzymatic/detergent method is a suitable biomaterial for cardiac tissue engineering.
- Incorporation of gold nanoparticle enhances electrical conductivity of cholecystic extracellular matrix, as required for cardiac tissue engineering applications.
- Porcine cholecystic extracellular matrix, as a tissue graft for repairing myocardial infarction, significantly alters the nature of endogenous repair by modulating reduction in fibrotic scarring.
- As an epicardial graft, porcine cholecystic extracellular matrix scaffold probably can be used as an adjunct to any current treatment strategies.

- The porcine cholecystic extracellular matrix is a potential biomaterial for fabricating cardiac patches.

6.4 Limitations and future perspectives

- The present study involved only a short duration animal study of 4 weeks (equivalent to 2 years in human) and histological evaluation of the epicardial graft-assisted healing was performed at only one-time point. Although the current results are encouraging, long term studies and histological evaluation at various time points are warranted to delineate the mechanism of the healing reaction.
- The same study has to be conducted in large animals for validation of the results.
- The comparison of C-ECM and C-ECM AuNP scaffold grafted animals shall be performed to study the electrical potential between patch and the myocardium using patch clamp technique.
- The study compared only the grafted animals and non-grafted animals. Comparison studies of grafted animals with the clinically used cardiac-patch such as Cormatrix® ECM™ need to be carried out.
- More investigations are to be performed for fabricating a cardiac-patch product prototype acceptable for clinical trials.
- This study does not involve any *in vivo* implantation of cell loaded scaffolds which may form a tissue construct for cardiac repair.
- Here, in this study sheet form of porcine cholecystic extracellular matrix scaffold was used for the *in vivo* application. Efforts need to be carried out to prepare injectable hydrogel from the native scaffold which can be easily delivered to the damaged site.

BIBLIOGRAPHY

Acres RG, Feyer V, Tsud N, Carlino E & Prince KC (2014) Mechanisms of Aggregation of Cysteine Functionalized Gold Nanoparticles. *J. Phys. Chem. C* **118:** 10481–10487

Alba AC, Bain E, Ng N, Stein M, O'brien K, Foroutan F, Ross H & Alba C (2016) Complications after Heart Transplantation: Hope for the Best, but Prepare for the Worst. Int J Transplant Res Med **2**:022

De Andrade JNBM, Tang J, Hensley MT, Vandergriff A, Cores J, Henry E, Allen TA, Caranasos TG, Wang Z, Zhang T, Zhang J & Cheng K (2015) Rapid and efficient production of coronary artery ligation and myocardial infarction in mice using surgical clips. *PLoS One* **10:** 143221

Anilkumar T V., Vineetha VP, Revi D, Muhamed J & Rajan A (2014) Biomaterial properties of cholecyst-derived scaffold recovered by a non-detergent/enzymatic method. *J. Biomed. Mater. Res. - Part B Appl. Biomater.* **102:** 1506–1516

Anoop S., Pallavi K.S., Eassow S., Venugopal S.K., Joyous T.V., Devanand C.B. Anilkumar T.V. (2017) Cholecyst derived collagen as an extracellular matrix scaffold graft for the corneal injuries in dogs- a report of three cases. *Ind. J.Vet. Surg.* **38**: 55-56

Arnal-Pastor M, Chachques JC, Monleón Pradas M & Valles-Lluch A (2013) Biomaterials for Cardiac Tissue Engineering. *Intechopen***:** 275–323

Baei P, Jalili-Firoozinezhad S, Rajabi-Zeleti S, Tafazzoli-Shadpour M, Baharvand H & Aghdami N (2016) Electrically conductive gold nanoparticle-chitosan thermosensitive hydrogels for cardiac tissue engineering. *Mater. Sci. Eng. C* **63:** 131–141

Bagno L, Hatzistergos KE, Balkan W & Hare JM (2018) Mesenchymal Stem Cell-Based Therapy for Cardiovascular Disease: Progress and Challenges. *Mol. Ther.* **26:** 1610–1623

Balakrishnan-nair DK, Nair ND, Venugopal SK, Das VN, George S, Abraham MJ, Eassow S, Alison MR, Sainulabdeen A & Anilkumar TV (2018) An Immunopathological Evaluation of the Porcine Cholecyst Matrix as a Muscle Repair Graft in a Male Rat Abdominal Wall Defect Model. *Toxicol. Pathol.* **46:** 169–183

Barsotti MC, Felice F, Balbarini A & Di Stefano R (2011) Fibrin as a scaffold for cardiac tissue engineering. *Biotechnol. Appl. Biochem.* **58:** 301–310

Bat E, Zhang Z, Feijen J, Grijpma DW & Poot AA (2014) Biodegradable elastomers for biomedical applications and regenerative medicine. *Regen. Med.* **9:** 385–398

Behfar A, Crespo-Diaz R, Terzic A & Gersh BJ (2014) Cell therapy for cardiac repair-lessons from clinical trials. *Nat. Rev. Cardiol.* **11:** 232–246

Betts J, Desaix P, Johnson E, Johnson J, Korol O, Kruse D & et al. (2017) 19.5 Development of the Heart – Anatomy and Physiology. *Anat. Physiol.***:** 129 Available at: https://opentextbc.ca/anatomyandphysiology/chapter/19-5-development-of-the-heart/ [Accessed April 20, 2020]

Bonafè F, Govoni M, Giordano E, Caldarera CM, Guarnieri C & Muscari C (2014) Hyaluronan and cardiac regeneration. *J. Biomed. Sci.* **21:**100

Branco AF, Pereira SP, Gonzalez S, Gusev O, Rizvanov AA & Oliveira PJ (2015) Gene Expression Profiling of H9c2 Myoblast Differentiation towards a Cardiac-Like Phenotype. *PLoS One* **10:** e0129303

Bueno V & Pestana JOM (2002) The role of CD8 + T cells during allograft rejection**.** Braz J Med Biol Res**.** 35**:** 1247-1258

Burugapalli K, Chan JCY, Kelly JL & Pandit A (2008) Buttressing staples with cholecyst-derived extracellular matrix (CEM) reinforces staple lines in an ex vivo peristaltic inflation model. *Obes. Surg.* **18:** 1418–1423

Burugapalli K, Thapasimuttu A, Chan JCY, Yao L, Brody S, Kelly JL & Pandit A

(2007) Scaffold with a natural mesh-like architecture: Isolation, structural, and in vitro characterization. *Biomacromolecules* **8:** 928–936

By Mayo Clinic Staff (2018) Heart disease - Symptoms and causes - Mayo Clinic. © *1998-2019 Mayo Found. Med. Educ. Res. (MFMER). All rights Reserv.* Available at: https://www.mayoclinic.org/diseases-conditions/heart-disease/symptoms-causes/syc-20353118 [Accessed January 2, 2020]

Caddeo S, Boffito M & Sartori S (2017) Tissue engineering approaches in the design of healthy and pathological in vitro tissue models. *Front. Bioeng. Biotechnol.* **5:** 40

Camci-Unal G, Annabi N, Dokmeci MR, Liao R & Khademhosseini A (2014) Hydrogels for cardiac tissue engineering. *NPG Asia Mater.* **6:** e99-12

Chan EWC, Bennet D, Baek P, Barker D, Kim S & Travas-Sejdic J (2018) Electrospun Polythiophene Phenylenes for Tissue Engineering. *Biomacromolecules* **19:** 1456–1468

Chaudhuri R, Ramachandran M, Moharil P, Harumalani M & Jaiswal AK (2017) Biomaterials and cells for cardiac tissue engineering: Current choices. *Mater. Sci. Eng. C* **79:** 950–957

Chen CH, Sereti KI, Wu BM & Ardehali R (2015) Translational aspects of cardiac cell therapy. *J. Cell. Mol. Med.* **19:** 1757–1772

Chiong M, Wang Z V., Pedrozo Z, Cao DJ, Troncoso R, Ibacache M, Criollo A, Nemchenko A, Hill JA & Lavandero S (2011) Cardiomyocyte death: Mechanisms and translational implications. *Cell Death Dis.* **2:** e244–e244

Coelho-Filho OR, Shah R V., Mitchell R, Neilan TG, Moreno H, Simonson B, Kwong R, Rosenzweig A, Das S & Jerosch-Herold M (2013) Quantification of cardiomyocyte hypertrophy by cardiac magnetic resonance: Implications for early cardiac remodeling. *Circulation* **128:** 1225–1233

Cui Z, Yang B & Li RK (2016) Application of Biomaterials in Cardiac Repair and

Regeneration. *Engineering* **2:** 141–148

Davidenko N, Schuster CF, Bax D V., Raynal N, Farndale RW, Best SM & Cameron RE (2015) Control of crosslinking for tailoring collagen-based scaffolds stability and mechanics. *Acta Biomater.* **25:** 131–142

Dengler J & Radisic M (2007) Tissue engineering approaches for the development of a contractile cardiac patch. *Future Cardiol.* **3:** 425–434

Dhingra S, Weisel RD & Li RK (2014) Synthesis of aliphatic polyester hydrogel for cardiac tissue engineering. *Methods Mol. Biol.* **1181:** 51–59

Dobrowolska P, Krajewska A, Gajda-Raczka M, Bartosewicz B, Nyga P & Jankiewicz BJ (2015) Application of turkevich method for gold nanoparticles synthesis to fabrication of SiO2@Au and TiO2@Au core-shell nanostructures. *Materials (Basel).* **8:** 2849–2862

Dominici M, Le Blanc K, Mueller I, Slaper-Cortenbach I, Marini FC, Krause DS, Deans RJ, Keating A, Prockop DJ & Horwitz EM (2006) Minimal criteria for defining multipotent mesenchymal stromal cells. The International Society for Cellular Therapy position statement. *Cytotherapy* **8:** 315–317

Drury R (1983) Theory and Practice of Histological Techniques Elsevier Health Sciences

Echave MC, Burgo LS, Pedraz JL & Orive G (2017) Gelatin as Biomaterial for Tissue Engineering. *Curr. Pharm. Des.* **23:** 3567-3584.

Forough R, Scarcello C & Perkins M (2011) Cardiac biomarkers: a focus on cardiac regeneration. *J. Tehran Heart Cent.* **6:** 179–86

Frangogiannis NG (2017) The extracellular matrix in myocardial injury, repair, and remodeling. *J. Clin. Invest.* **127:** 1600–1612

French BA & Kramer CM (2007) Mechanisms of postinfarct left ventricular remodeling

Frey N, Katus HA, Olson EN & Hill JA (2004) Hypertrophy of the Heart: A New Therapeutic Target? *Circulation* **109:** 1580–1589

Gálvez-Montón C, Prat-Vidal C, Roura S, Soler-Botija C & Bayes-Genis A (2013) Cardiac Tissue Engineering and the Bioartificial Heart. *Rev. Española Cardiol. English Ed.* **66:** 391–399

Garbern JC, Mummery CL & Lee RT (2013) Model systems for cardiovascular regenerative biology. *Cold Spring Harb. Perspect. Med.* **3:** a014019

Ghasemi-Mobarakeh L, Kolahreez D, Ramakrishna S & Williams D (2019) Key terminology in biomaterials and biocompatibility. *Curr. Opin. Biomed. Eng.* **10:** 45–50

Gilbert TW, Sellaro TL & Badylak SF (2006) Decellularization of tissues and organs. *Biomaterials* **27:** 3675–3683

Gilpin A & Yang Y (2017) Decellularization Strategies for Regenerative Medicine: From Processing Techniques to Applications. *Biomed Res. Int.* **2017:** 9831534

Grover GN, Rao N & Christman KL (2014) Myocardial matrix-polyethylene glycol hybrid hydrogels for tissue engineering. *Nanotechnology* **25:** 014011

Guo X, Bai Y, Zhang L, Zhang B, Zagidullin N, Carvalho K, Du Z & Cai B (2018) Cardiomyocyte differentiation of mesenchymal stem cells from bone marrow: New regulators and its implications. *Stem Cell Res. Ther.* **9:** 0773-9

Han I, Kwon BS, Park HK & Kim KS (2017) Differentiation potential of mesenchymal stem cells is related to their intrinsic mechanical properties. *Int. Neurourol. J.* **21:** S24–S31

Hasan A, Morshed M, Memic A, Hassan S, Webster TJ & Marei HES (2018) Nanoparticles in tissue engineering: Applications, challenges and prospects. *Int. J. Nanomedicine* **13:** 5637–5655

Hashimoto H, Olson EN & Bassel-Duby R (2018) Therapeutic approaches for cardiac regeneration and repair. *Nat. Rev. Cardiol.* **15:** 585–600

Hastings CL, Roche ET, Ruiz-Hernandez E, Schenke-Layland K, Walsh CJ & Duffy GP (2015) Drug and cell delivery for cardiac regeneration. *Adv. Drug Deliv. Rev.* **84:** 85–106

He L & Zhou B (2017) Cardiomyocyte proliferation: remove brakes and push accelerators. *Nat. Publ. Gr.* **27:** 959–960

Hinderer S & Schenke-Layland K (2019) Cardiac fibrosis – A short review of causes and therapeutic strategies. *Adv. Drug Deliv. Rev.***146**: 77-82

Hirt MN, Hansen A & Eschenhagen T (2014) Cardiac tissue engineering : State of the art. *Circ. Res.* **114:** 354-367

Hormozi-Nezhad MR, Seyedhosseini E & Robatjazi H (2012) Spectrophotometric determination of glutathione and cysteine based on aggregation of colloidal gold nanoparticles. *Sci. Iran.* **19:** 958–963

Horn MA & Trafford AW (2016) Aging and the cardiac collagen matrix: Novel mediators of fibrotic remodelling. *J. Mol. Cell. Cardiol.* **93:** 175–185

Huang S, Xu L, Sun Y, Wu T, Wang K & Li G (2015) An improved protocol for isolation and culture of mesenchymal stem cells from mouse bone marrow. *J. Orthop. Transl.* **3:** 26–33

Hussey GS, Dziki JL & Badylak SF (2018) Extracellular matrix-based materials for regenerative medicine. *Nat. Rev. Mater.* **3:** 159–173

Huyer LD, Montgomery M, Zhao Y, Xiao Y, Conant G, Korolj A & Radisic M (2015) Biomaterial based cardiac tissue engineering and its applications. *Biomed. Mater.* **10:** 1748-6041

Iismaa SE, Kaidonis X, Nicks AM, Bogush N, Kikuchi K, Naqvi N, Harvey RP, Husain A & Graham RM (2018) Comparative regenerative mechanisms across different mammalian tissues. *npj Regen. Med.* **3:** 6

St. John Sutton MG & Sharpe N (2000) Left ventricular remodeling after myocardial infarction: Pathophysiology and therapy. *Circulation* **101:** 2981–2988

Kai D, Prabhakaran MP, Jin G & Ramakrishna S (2011) Polypyrrole-contained electrospun conductive nanofibrous membranes for cardiac tissue engineering. *J. Biomed. Mater. Res. - Part A* **99 A:** 376–385

Kainuma S, Miyagawa S, Fukushima S, Tsuchimochi H, Sonobe T, Fujii Y, Pearson JT, Saito A, Harada A, Toda K, Shirai M & Sawa Y (2017) Influence of coronary architecture on the variability in myocardial infarction induced by coronary ligation in rats. *PLoS One* **12:** e0183323

Kajbafzadeh A-M, Sabetkish S, Heidari R & Ebadi M (2014) Tissue-engineered cholecyst-derived extracellular matrix: a biomaterial for in vivo autologous bladder muscular wall regeneration. *Pediatr. Surg. Int.* **30:** 371–380

Kankeu C, Clarke K, Van Haver D, Kris Gevaert bcd, Francis Impens bc, Anna Dittrich bcd, Llewelyn Roderick H, Passante E & Huber HJ (2018) Quantitative proteomics and systems analysis of cultured H9C2 cardiomyoblasts during differentiation over time supports a 'function follows form' model of differentiation †. **14:** 181

Kapnisi M, Mansfield C, Marijon C, Guex AG, Perbellini F, Bardi I, Humphrey EJ, Puetzer JL, Mawad D, Koutsogeorgis DC, Stuckey DJ, Terracciano CM, Harding SE & Stevens MM (2018) Auxetic Cardiac Patches with Tunable Mechanical and Conductive Properties toward Treating Myocardial Infarction. *Adv. Funct. Mater.***28**: 1800618

Karthika S, Anoop S, Devanand CB, Narayanan MK, Unni M, Eassow S & Anilkumar T (2018) A porcine-cholecyst-derived scaffold for treating full thickness lacerated skin wounds in dogs. *Vet. Res. Commun.* **42:** 233–242

Kc P, Hong Y & Zhang G (2019) Cardiac tissue-derived extracellular matrix scaffolds for myocardial repair: advantages and challenges. *Regen. Biomater.* **6:** 185–199

Keong LC & Halim AS (2009) In Vitro models in biocompatibility assessment for biomedical-grade chitosan derivatives in wound management. *Int. J. Mol. Sci.* **10:** 1300–1313

Kikuchi K & Poss KD (2012) Cardiac Regenerative Capacity and Mechanisms. *Annu. Rev. Cell Dev. Biol.* **28:** 719–741

Kitsara M, Agbulut O, Kontziampasis D, Chen Y & Menasché P (2017) Fibers for hearts: A critical review on electrospinning for cardiac tissue engineering. *Acta Biomater.***48***:* 20-40

Kobayashi K, Maeda K, Takefuji M, Kikuchi R, Morishita Y, Hirashima M & Murohara T (2017) Dynamics of angiogenesis in ischemic areas of the infarcted heart. *Sci. Rep.* **7:** 1–13

Konopelski P & Ufnal M (2016) Electrocardiography in rats: A comparison to human. *Physiol. Res.* **65:** 717–725

Langer R & Vacanti JP (1993) Tissue engineering. *Science (80-.).* **260:** 920–926

Laroumanie F, Douin-Echinard V, Pozzo J, Lairez O, Tortosa F, Vinel C, Delage C, Calise D, Dutaur M, Parini A & Pizzinat N (2014) CD4+ T cells promote the transition from hypertrophy to heart failure during chronic pressure overload. *Circulation* **129:** 2111–24

Leong YY, Ng WH, Ellison-Hughes GM & Tan JJ (2017) Cardiac Stem Cells for Myocardial Regeneration: They Are Not Alone. *Front. Cardiovasc. Med.* **4:** 47

Leor J, Amsalem Y & Cohen S (2005) Cells, scaffolds, and molecules for myocardial tissue engineering. *Pharmacol. Ther.* **105:** 151–163

Li Z & Guan J (2011) Hydrogels for cardiac tissue engineering. *Polymers (Basel).* **3:** 740–761

Liberski A, Latif N, Raynaud C, Bollensdorff C & Yacoub M (2016) Alginate for cardiac regeneration: From seaweed to clinical trials. *Glob. Cardiol. Sci. Pract.* **1**:e201604

Liu MB (2014) Cardiovascular diseases. *Chin. Med. J. (Engl).* **127:** 6–7 Available at: http://www.who.int/news-room/fact-sheets/detail/cardiovascular-diseases-(cvds) [Accessed September 4, 2018]

Ma SP & Vunjak-Novakovic G (2016) Tissue-engineering for the study of cardiac biomechanics. *J. Biomech. Eng.* **138:** 0210101

Ma Y, Mouton AJ & Lindsey ML (2018) Cardiac macrophage biology in the steady-state heart, the aging heart, and following myocardial infarction. *Transl. Res.* **191:** 15–28

Majzik A, Fülöp L, Csapó E, Bogár F, Martinek T, Penke B, Bíró G & Dékány I (2010) Functionalization of gold nanoparticles with amino acid, β-amyloid peptides and fragment. *Colloids Surfaces B Biointerfaces* **81:** 235–241

Martins AM, Eng G, Caridade SG, Mano JF, Reis RL & Vunjak-Novakovic G (2014) Electrically conductive chitosan/carbon scaffolds for cardiac tissue engineering. *Biomacromolecules* **15:** 635–643

Mathew P & Bordoni B (2019) Embryology, Heart StatPearls Publishing

Maulik N & Thirunavukkarasu M (2008) Growth factor/s and cell therapy in myocardial regeneration. *J. Mol. Cell. Cardiol.* **44:** 219–227

McBride JA & Striker R (2017) Imbalance in the game of T cells: What can the CD4/CD8 T-cell ratio tell us about HIV and health? *PLOS Pathog.* **13:** e1006624

Mewhort HEM, Turnbull JD, Meijndert HC, Ngu JMC & Fedak PWM (2014) Epicardial infarct repair with basic fibroblast growth factor–enhanced CorMatrix-ECM biomaterial attenuates postischemic cardiac remodeling. *J. Thorac. Cardiovasc. Surg.* **147:** 1650–1659

Mewhort HEM, Turnbull JD, Satriano A, Chow K, Flewitt JA, Andrei AC, Guzzardi DG, Svystonyuk DA, White JA & Fedak PWM (2016) Epicardial infarct repair with bioinductive extracellular matrix promotes vasculogenesis and myocardial recovery. *J. Hear. Lung Transplant.* **35:** 661–670

Meyer M (2019) Processing of collagen based biomaterials and the resulting materials properties. *Biomed. Eng. Online* **18:** 1–74

Michaud K, Basso C, d'Amati G, Giordano C, Kholová I, Preston SD, Rizzo S,

Sabatasso S, Sheppard MN, Vink A & van der Wal AC (2020) Diagnosis of myocardial infarction at autopsy: AECVP reappraisal in the light of the current clinical classification. *Virchows Arch.* **476:** 179–194

Miyagi Y, Chiu LLY, Cimini M, Weisel RD, Radisic M & Li RK (2011) Biodegradable collagen patch with covalently immobilized VEGF for myocardial repair. *Biomaterials* **32:** 1280–1290

Mohamed TMA, Ang YS, Radzinsky E, Zhou P, Huang Y, Elfenbein A, Foley A, Magnitsky S & Srivastava D (2018) Regulation of Cell Cycle to Stimulate Adult Cardiomyocyte Proliferation and Cardiac Regeneration. *Cell* **173**:104-116

Mondalek FG, Lawrence BJ, Kropp BP, Grady BP, Fung KM, Madihally S V. & Lin HK (2008) The incorporation of poly(lactic-co-glycolic) acid nanoparticles into porcine small intestinal submucosa biomaterials. *Biomaterials* **29:** 1159–1166

Mongiat M, Andreuzzi E, Tarticchio G & Paulitti A (2016) Extracellular matrix, a hard player in angiogenesis. *Int. J. Mol. Sci.* **17:**1822

Mony MP & Anilkumar T V. (2020) Controlled cross-linking of porcine cholecyst extracellular matrix for preparing tissue engineering scaffold. *J. Biomed. Mater. Res. - Part B Appl. Biomater.* **108:** 1057–1067

Moroni F & Mirabella T (2014) Decellularized matrices for cardiovascular tissue engineering *Am J Stem Cells*. **3**:1-20.

Mosala Nezhad Z, Poncelet A, de Kerchove L, Gianello P, Fervaille C & El Khoury G (2016) Small intestinal submucosa extracellular matrix (CorMatrix®) in cardiovascular surgery: a systematic review. *Interact. Cardiovasc. Thorac. Surg.* **22:** 839–850

Movasaghi Z, Rehman S & Rehman IU (2008) Fourier transform infrared (FTIR) spectroscopy of biological tissues. *Appl. Spectrosc. Rev.* **43:** 134–179

Muhamed J, Rajan A, Surendran A, Jaleel A & Anilkumar T V. (2017) Comparative profiling of extractable proteins in extracellular matrices of porcine cholecyst and

jejunum intended for preparation of tissue engineering scaffolds. *J. Biomed. Mater. Res. - Part B Appl. Biomater.* **105:** 489–496

Muhamed J, Revi D, Rajan A & Anilkumar T V. (2015a) Comparative local immunogenic potential of scaffolds prepared from porcine cholecyst, jejunum, and urinary bladder in rat subcutaneous model. *J. Biomed. Mater. Res. - Part B Appl. Biomater.* **103:** 1302–1311

Muhamed J, Revi D, Rajan A, Geetha S & Anilkumar T V. (2015b) Biocompatibility and Immunophenotypic Characterization of a Porcine Cholecyst–derived Scaffold Implanted in Rats. *Toxicol. Pathol.* **43:** 536–545

Mythili S & Malathi N (2015) Diagnostic markers of acute myocardial infarction. *Biomed. Reports* **3:** 743–748

Nair RS, Ameer JM, Alison MR & Anilkumar T V. (2017) A gold nanoparticle coated porcine cholecyst-derived bioscaffold for cardiac tissue engineering. *Colloids Surfaces B Biointerfaces* **157:** 130–137

Navaee F, Renaud P & Braschler T (2020) Highly efficient cardiac differentiation and maintenance by thrombin-coagulated fibrin hydrogels enriched with decellularized porcine heart extracellular matrix. *bioRxiv***:** 2020.01.30.927319

O'Rourke SA, Dunne A & Monaghan MG (2019) The Role of Macrophages in the Infarcted Myocardium: Orchestrators of ECM Remodeling. *Front. Cardiovasc. Med.* **6:** 101

Pasotti M, Prati F & Arbustini E (2006) The pathology of myocardial infarction in the pre- and post-interventional era. *Heart* **92:** 1552–1556

Pattar SS, Hassanabad AF & Fedak PW (2019) Acellular extracellular matrix bioscaffolds for cardiac repair and regeneration. *Front. Cell Dev. Biol.* **7:** 1–10

Patten V, Chabaesele I, Sishi B & Van Vuuren D (2017) Cardiomyocyte differentiation: Experience and observations from 2 laboratories. *SA Hear.* **14:** 96–107

Pittenger MF & Martin BJ (2004) Mesenchymal stem cells and their potential as cardiac therapeutics. *Circ. Res.* **95:** 9–20

Prabhu SD & Frangogiannis NG (2016) The biological basis for cardiac repair after myocardial infarction. *Circ. Res.* **119:** 91–112

Prasad T, Shabeena EA, Vinod D, Kumary T V. & Anil Kumar PR (2015) Characterization and in vitro evaluation of electrospun chitosan/polycaprolactone blend fibrous mat for skin tissue engineering. *J. Mater. Sci. Mater. Med.* **26:** 28

Prasath Mani M, Jaganathan SK, Prabhakaran P, Nageswaran G & Pandiyaraj Krishnasamy N (2019) Fabrication and characterization of polyurethane patch loaded with palmarosa and cobalt nitrate for cardiac tissue engineering. *Int. J. Polym. Anal. Charact.* **24:** 399–411

van Putten S, Shafieyan Y & Hinz B (2016) Mechanical control of cardiac myofibroblasts. *J. Mol. Cell. Cardiol.* **93:** 133–142

Qian Q, Qian H, Zhang X, Zhu W, Yan Y, Ye S, Peng X, Li W, Xu Z, Sun L & Xu W (2012) 5-Azacytidine Induces Cardiac Differentiation of Human Umbilical Cord-Derived Mesenchymal Stem Cells by Activating Extracellular Regulated Kinase. *Stem Cells Dev.* **21:** 67–75

Radisic M (2015) Biomaterials for cardiac tissue engineering. *Biomed. Mater.* **10:** 030301

Raj R, Anilkumar T V. & Rajan A (2018) Preparation and characterization of cholecystic extracellular matrix powder forms for biomedical applications. *Biomed. Phys. Eng. Express* **4:**47008

Raj R, Sobhan PK, Pratheesh K V. & Anilkumar T V. (2020) A cholecystic extracellular matrix-based hybrid hydrogel for skeletal muscle tissue engineering. *J. Biomed. Mater. Res. Part A* **108:** 1922-33

Rebouças J de S, Santos-Magalhães NS & Formiga FR (2016) Cardiac regeneration using growth factors: Advances and challenges. *Arq. Bras. Cardiol.* **107:** 271–

275

Reddy DN, Al-Rajab AJ & Reddy GR (2018) Biomedical and Pharmaceutical Applications of Inductively Coupled Plasma-Mass Spectrometry (ICP-MS). In *Drug Discovery - Concepts to Market* InTech

Reddy K, Khaliq A & Henning RJ (2015) Recent advances in the diagnosis and treatment of acute myocardial infarction. *World J. Cardiol.* **7:** 243–76

Redfors B, Shao Y & Omerovic E (2012) Myocardial infarct size and area at risk assessment in mice. *Exp Clin Cardiol*.**17**: 268–272.

Reis LA, Chiu LLY, Feric N, Fu L & Radisic M (2016) Biomaterials in myocardial tissue engineering. *J. Tissue Eng. Regen. Med.* **10:** 11–28

Ren J, Xu Q, Chen X, Li W, Guo K, Zhao Y, Wang Q, Zhang Z, Peng H & Li YG (2017) Superaligned Carbon Nanotubes Guide Oriented Cell Growth and Promote Electrophysiological Homogeneity for Synthetic Cardiac Tissues. *Adv. Mater.* **29**: 201702713

Revi D, Vineetha VP, Muhamed J, Rajan A & Anilkumar TV (2013) Porcine cholecyst-derived scaffold promotes full-thickness wound healing in rabbit. *J. Tissue Eng.* **4:** 2041731413518060

Rice SB, Chan C, Brown SC, Eschbach P, Han L, Ensor DS, Stefaniak AB, Bonevich J, Vladár AE, Walker ARH, Zheng J, Starnes C, Stromberg A, Ye J & Grulke EA (2013) Particle size distributions by transmission electron microscopy: an interlaboratory comparison case study. *Metrologia* **50:** 663

Rieckmann M, Delgobo M, Gaal C, Büchner L, Steinau P, Reshef D, Gil-Cruz C, ter Horst EN, Kircher M, Reiter T, Heinze KG, Niessen HWM, Krijnen PAJ, van der Laan AM, Piek JJ, Koch C, Wester HJ, Lapa C, Bauer WR, Ludewig B, et al (2019) Myocardial infarction triggers cardioprotective antigen-specific T helper cell responses. *J. Clin. Invest.* **129:** 4922–4936

Robinson KA, Li J, Mathison M, Redkar A, Cui J, Chronos NAF, Matheny RG &

Badylak SF (2005) Extracellular matrix scaffold for cardiac repair. *Circulation* **112:** 135-43

Rodrigues ICP, Kaasi A, Maciel Filho R, Jardini AL & Gabriel LP (2018) Cardiac tissue engineering: current state-of-the-art materials, cells and tissue formation. *Einstein (Sao Paulo).* **16:** eRB4538

Rusu M, Hilse K, Schuh A, Martin L, Slabu I, Stoppe C & Liehn EA (2019) Biomechanical assessment of remote and postinfarction scar remodeling following myocardial infarction. *Sci. Rep.* **9:** 16744

Saberi A, Jabbari F, Zarrintaj P, Saeb MR & Mozafari M (2019) Electrically Conductive Materials: Opportunities and Challenges in Tissue Engineering. *Biomolecules*. **9**: 9090448

Sadeghizadeh M, Esmaeili R, Sadeghpour A, Darbandi-Azar A, Majidzadeh-A K, Vajhi A & Sadeghizadeh M (2017) Echocardiographic assessment of myocardial infarction: comparison of a rat model in two strains. *Iran. J. Vet. Res.* **18:** 30–35

Sadek H & Olson EN (2020) Toward the Goal of Human Heart Regeneration. *Cell Stem Cell* **26:** 7–16

Santoro M, Shah SR, Walker JL & Mikos AG (2016) Poly(lactic acid) nanofibrous scaffolds for tissue engineering. *Adv. Drug Deliv. Rev.* **107:** 206–212

Saravanan S, Sareen N, Abu-El-Rub E, Ashour H, Sequiera GL, Ammar HI, Gopinath V, Shamaa AA, Sayed SSE, Moudgil M, Vadivelu J & Dhingra S (2018) Graphene Oxide-Gold Nanosheets Containing Chitosan Scaffold Improves Ventricular Contractility and Function After Implantation into Infarcted Heart. *Sci. Rep.* **8:** 15069

Sarig U, Sarig H, de-Berardinis E, Chaw S-Y, Nguyen EBV, Ramanujam VS, Thang VD, Al-Haddawi M, Liao S, Seliktar D, Kofidis T, Boey FYC, Venkatraman SS & Machluf M (2016) Natural myocardial ECM patch drives cardiac progenitor based restoration even after scarring. *Acta Biomater.* **44:** 209–220

Sattar Y & Chhabra L (2020) Electrocardiogram StatPearls Publishing

Schipke J, Brandenberger C, Rajces A, Manninger M, Alogna A, Post H & Mühlfeld C (2017) Assessment of cardiac fibrosis: a morphometric method comparison for collagen quantification. *J Appl Physiol* **122:** 1019–1030

Schulz R, Görge PM, Görbe A, Ferdinandy P, Lampe PD, Leybaert L, Schulz PR, Institut G & Direktor J-L (2015) Connexin 43 is an emerging therapeutic target in ischemia/ reperfusion injury, cardioprotection and neuroprotection HHS Public Access. *Pharmacol Ther* **153:** 90–106

Schwach V & Passier R (2019) Native cardiac environment and its impact on engineering cardiac tissue. *Biomater. Sci.* **7:** 3566–3580

Scimeca M, Bischetti S, Lamsira HK, Bonfiglio R & Bonanno E (2018) Energy dispersive X-ray (EDX) microanalysis: A powerful tool in biomedical research and diagnosis. *Eur. J. Histochem.* **62:** 89–99

Senyo SE, Lee RT & Kühn B (2014) Cardiac regeneration based on mechanisms of cardiomyocyte proliferation and differentiation. *Stem Cell Res.* **13**:532-541

Shevach M, Fleischer S, Shapira A & Dvir T (2014) Gold nanoparticle-decellularized matrix hybrids for cardiac tissue engineering. *Nano Lett.* **14:** 5792–5796

Shimizu T, Yamato M, Isoi Y, Akutsu T, Setomaru T, Abe K, Kikuchi A, Umezu M & Okano T (2002) Fabrication of Pulsatile Cardiac Tissue Grafts Using a Novel 3-Dimensional Cell Sheet Manipulation Technique and Temperature-Responsive Cell Culture Surfaces. *Circ. Res.* **90:** e40

Siddiqi S & Sussman MA (2014) The Heart: Mostly Postmitotic or Mostly Premitotic? Myocyte Cell Cycle, Senescence, and Quiescence. *Can. J. Cardiol.* **30:** 1270–1278

Solazzo M, O'Brien FJ, Nicolosi V & Monaghan MG (2019) The rationale and emergence of electroconductive biomaterial scaffolds in cardiac tissue engineering. *APL Bioeng.* **3:** 041501

Stefanon I, Valero-Muñoz M, Fernandes AA, Ribeiro RF, Rodríguez C, Miana M, Martínez-González J, Spalenza JS, Lahera V, Vassallo PF & Cachofeiro V (2013) Left and Right Ventricle Late Remodeling Following Myocardial Infarction in Rats. *PLoS One* **8:** e64986

Sun Q, Zhang Z & Sun Z (2014) The potential and challenges of using stem cells for cardiovascular repair and regeneration. *Genes Dis.* **1:** 113–119

Supokawej A, Kheolamai P, Nartprayut K, U-pratya Y, Manochantr S, Chayosumrit M & Issaragrisil S (2013) Cardiogenic and myogenic gene expression in mesenchymal stem cells after 5-azacytidine treatment. *Turkish J. Hematol.* **30:** 115–121

Tee R, Lokmic Z, Morrison WA & Dilley RJ (2010) Strategies in cardiac tissue engineering. *ANZ J. Surg.* **80:** 683–693

Thakker R & Yang P (2014) Mesenchymal stem cell therapy for cardiac repair. *Curr. Treat. Options Cardiovasc. Med.* **16:** 323

Thygesen K, Alpert JS, Jaffe AS, Chaitman BR, Bax JJ, Morrow DA, White HD, Corbett S, Chettibi M, Hayrapetyan H, Roithinger FX, Aliyev F, Sujayeva V, Claeys MJ, Smajić E, Kala P, Iversen KK, Hefny E El, Marandi T, Porela P, et al (2018) Fourth Universal Definition of Myocardial Infarction (2018)

Thygesen K, Alpert JS, Jaffe AS, Simoons ML, Chaitman BR & White HD (2012) Third universal definition of myocardial infarction. *Nat. Rev. Cardiol.* **9:** 620–633

Toepfer CN, Sikkel MB, Caorsi V, Vydyanath A, Torre I, Copeland O, Lyon AR, Marston SB, Luther PK, Macleod KT, West TG & Ferenczi MA (2016) A post-MI power struggle: Adaptations in cardiac power occur at the sarcomere level alongside MyBP-C and RLC phosphorylation. *Am. J. Physiol. - Hear. Circ. Physiol.* **311:** H465–H475

Turkevich J, Stevenson PC & Hillier J (1951) A study of the nucleation and growth processes in the synthesis of colloidal gold. *Discuss. Faraday Soc.* **11:** 55–75

Turner NJ, Pezzone MA, Brown BN & Badylak SF (2013) Quantitative multispectral imaging of Herovici's polychrome for the assessment of collagen content and tissue remodelling. *J. Tissue Eng. Regen. Med.* **7:** 139–148

Tzahor E & Poss KD (2017) Cardiac regeneration strategies: Staying young at heart. *Science* **356:** 1035–1039

Uchinaka A, Yoshida M, Tanaka K, Hamada Y, Mori S, Maeno Y, Miyagawa S, Sawa Y, Nagata K, Yamamoto H & Kawaguchi N (2018) Overexpression of collagen type III in injured myocardium prevents cardiac systolic dysfunction by changing the balance of collagen distribution. *J. Thorac. Cardiovasc. Surg.* **156:** 217-226.e3

Ullah I, Subbarao RB & Rho GJ (2015) Human mesenchymal stem cells - Current trends and future prospective. *Biosci. Rep.* **35:** 191

Venkata G, Srikanth N, Prakash P, Tripathy NK & Nityanand S (2009) www.pubstemcell.com. **5:** 26-33

Venugopal JR, Prabhakaran MP, Mukherjee S, Ravichandran R, Dan K & Ramakrishna S (2012) Biomaterial strategies for alleviation of myocardial infarction. *J. R. Soc. Interface* **9:** 1–19

Vogel B, Siebert H, Hofmann U & Frantz S (2015) Determination of collagen content within picrosirius red stained paraffin-embedded tissue sections using fluorescence microscopy. *MethodsX* **2:** 124–134

Voucharas C, Lazou A, Triposkiadis F & Tsilimingas N (2011) Remote preconditioning in normal and hypertrophic rat hearts **6:** 1749-8090

Vunjak Novakovic G, Eschenhagen T & Mummery C (2014) Myocardial tissue engineering: In vitro models. *Cold Spring Harb. Perspect. Med.* **4:** a014076

Walker BW, Lara RP, Yu CH, Sani ES, Kimball W, Joyce S & Annabi N (2019) Engineering a naturally-derived adhesive and conductive cardiopatch. *Biomaterials* **207:** 89–101

Wang Z, Wang Z, Lu WW, Zhen W, Yang D & Peng S (2017) Novel biomaterial strategies for controlled growth factor delivery for biomedical applications. *NPG Asia Mater.* **9:** e435–e435

Weinberger F, Mannhardt I & Eschenhagen T (2017) Engineering Cardiac Muscle Tissue: A Maturating Field of Research. *Circ. Res.* **120:** 1487–1500

Wen Z, Mai Z, Zhang H, Chen Y, Geng D, Zhou S & Wang J (2012) Local activation of cardiac stem cells for post-myocardial infarction cardiac repair. *J. Cell. Mol. Med.* **16:** 2549–2563

Wilhelm MJ (2015) Long-term outcome following heart transplantation: current perspective. *J. Thorac. Dis.* **7:** 549–51

Wollert KC & Drexler H (2005) Clinical applications of stem cells for the heart. *Circ. Res.* **96:** 151–63

Wu W qiang, Peng S, Song Z yuan & Lin S (2019) Collagen biomaterial for the treatment of myocardial infarction: an update on cardiac tissue engineering and myocardial regeneration. *Drug Deliv. Transl. Res.* **9:** 920–934

Xu W, Zhang X, Qian H, Zhu W, Sun X, Hu J, Zhou H & Chen Y (2004) Mesenchymal stem cells from adult human bone marrow differentiate into a cardiomyocyte phenotype in vitro. *Exp. Biol. Med.* **229:** 623–631

Ye G & Qiu X (2017) Conductive biomaterials in cardiac tissue engineering. *Biotarget* **1:** 9–9

Zhan XS, El-Ashram S, Luo DZ, Luo HN, Wang BY, Chen SF, Bai YS, Chen ZS, Liu CY & Ji HQ (2019) A comparative study of biological characteristics and transcriptome profiles of mesenchymal stem cells from different canine tissues. *Int. J. Mol. Sci.* **20:** 1485

Zimmermann WH, Melnychenko I & Eschenhagen T (2004) Engineered heart tissue for regeneration of diseased hearts. *Biomaterials* **25:** 1639–1647

Zimmermann WH, Melnychenko I, Wasmeier G, Didié M, Naito H, Nixdorff U, Hess

A, Budinsky L, Brune K, Michaelis B, Dhein S, Schwoerer A, Ehmke H & Eschenhagen T (2006) Engineered heart tissue grafts improve systolic and diastolic function in infarcted rat hearts. *Nat. Med.* **12:** 452–458

LIST OF PUBLICATIONS & PATENTS

- **Nair, R.S**., Ameer, J.M., Alison, M.R. & Anilkumar, T.V. A gold nanoparticle coated porcine cholecyst-derived bioscaffold for cardiac tissue engineering. Colloids and surfaces. B, Biointerfaces 157, 130-137 (2017)

- Patent application filed: **Reshma Sukumaran Nair**, Praveen Kunjan Sobhan and Thapasimuthu Vijayamma Anilkumar "A process for developing uniform surface topography maintained cardiac patch from porcine cholecyst derived extracellular matrix" (Application no. 20194104242, dated 18-10-2019)

- **Book chapter accepted**: Fabrication of a conductive scaffold from porcine cholecystic extracellular matrix, **Reshma S. Nair** and T. V. Anilkumar, Protocols in Tissue Scaffolds Research, Springer Publisher, 2021

CONFERENCE PRESENTATIONS

Poster presentations

1. **Reshma Sukumaran Nair** & Anilkumar TV "Gold nanoparticle loaded porcine cholecystic extracellular matrix: a potential bioscaffold for cardiac tissue engineering" at the 10th World Biomaterials Congress, Montreal, Canada from 17-21st May 2016. **(DBT Travel Grant, 2016)**

2. **Reshma S. Nair**, Sachin J. Shenoy & Thapasimuthu V. Anilkumar "Cholecyst Derived Extracellular Matrix Graft-Assisted Healing of Experimental Myocardial Infarction in a Rat Model" at the 31st Kerala Science Congress, Kollam from 2-3rd February 2019.

3. **Reshma S. Nair**, Sachin J. Shenoy &TV Anilkumar "Porcine cholecyst derived scaffold as a cardiac-patch for myocardial repair" at the Global Congress and Expo on Biomaterials May 13-14, 2019 | Kuala Lumpur, Malaysia **(Moderated the conference)**.

4. **Reshma S. Nair** & TV Anilkumar "Fabrication and in vitro evaluation of cardiac-patch prototypes for tissue engineering application" DST-INSPIRE Review Meet held at GITAM, Bengaluru, June 14th 2019

5. Sachin J. Shenoy, **Reshma S. Nair** & Thapasimuthu V. Anilkumar "A refined protocol for myocardial infarction induction by coronary artery ligation in Sprague Dawley rats", 9th International Conference of LASA India, Laboratory animals in biomedical research–the way forward November 22-23, 2019

Oral presentations

1. **Reshma S Nair**, Sachin J Shenoy, Praveen K Sobhan, Surya Ramachandran, Mukund A Prabhu and Anilkumar TV "Porcine cholecyst derived extracellular matrix-scaffold as a potential cardiac-patch for myocardial repair" at 'Targeting Metabolism in Non-Communicable Diseases' organised by Department of Biochemistry, SCTIMST on 2nd August 2019 **(2nd best oral presentation award)**

2. **Reshma S Nair**, Sachin J Shenoy, Praveen K Sobhan, Surya Ramachandran, Mukund A Prabhu and Anilkumar TV "Porcine cholecyst derived extracellular matrix-scaffold as a potential cardiac-patch for myocardial repair" at 32nd Kerala Science Congress held at Palakkad from 25-27th January 2020.